THE DEVELOPMENT AND PROPERTIES

OF GLASS-CERAMIC FIBRES

BY

RONALD WILLIAM JONES, B.Sc. (hons), M.Sc.

This thesis is submitted for the degree of Doctor of Philosophy in Physics. The thesis was submitted to THE UNIVERSITY OF WARWICK.

The research work reported in this thesis was conducted in the Department of Mechanical and Production Engineering, LIVERPOOL POLYTECHNIC.

December 1977.

TABLE OF CONTENTS.

FIGURES

PLATES

ACKNOWLEDGEMENTS.

The author wishes to thank Dr. P.W. McMillan for his invaluable guidance throughout this investigation and Dr. D. Clegg who helped greatly with computational problems.
He also wishes to express his gratitude to the Science Research Council whose financial support enabled this work to take place and Liverpool Polytechnic for laboratory facilities.
Finally, the author thanks his wife for much help and patience without which this thesis would not have been completed.

SUMMARY.

Fibres were produced from glasses with the following compositions:

A = 25% Li_2O 74% SiO_2 1% P_2O_5

B = 29% Li_2O 68% SiO_2 1% P_2O_5 1% ZnO 1% K_2O

by drawing the fibres from a single tip platinum bushing. The fibres, in the form of tows, were then subjected to a series of heat treatments in which the nucleation and crystallization temperatures and times were varied. The tensile strength and elastic modulus was determined for each sample of fibres and use was made of microscopy and X-ray diffraction to determine the microstructure resulting from the subsequent heat treatments. The data obtained from the tests performed in this investigation required a statistical analysis because of the variance in any one measured parameter. This is often found to be the case when investigating small volumes of material such as fibres. A model was proposed, for each composition, relating the strength to crytallization time and an attempt was made to justify each model on the basis of the empirical data obtained and indirect evidence arising from the statistical interpretation of this data.

The strength of crystallized fibres produced from composition A. decreased with crystallization time. This was explained by assuming that the strength controlling flaws were introduced by the appearance of a surface crystal layer and that the flaw size was proportional to the thickness of the layer. Evidence was produced to reinforce this argument. Two proposals, regarding the elastic modulus, were tested and it was found that observed moduli could best be described by considering the fibre to be a composite cylinder with an outer annulus of lithium disilicate surrounding a core of glass.

Glass B. fibres did not behave in the same way as A. after crystallization except at high crystallization temperature. In general the strength would decrease then increase again slightly before finally decreasing. This behaviour was explained by assuming that the mean intercrystal spacing controlled flaw size until the depth of the surface crystal layer became large enough to dominate.

Some research is described in which an attempt is made to inhibit surface nucleation/crystallization by using a vapour phase ion-exchange treatment. This work remains incomplete but there was some indication that it would be successful in allowing higher strengths to be achieved in glass-ceramic fibres after prolonged crystallization.

1. INTRODUCTION.

The past twenty years has seen a rapid development in fibre reinforcement of materials. This research has produced not only a new range of fibres with high strength and stiffness but also fibres which are compatible with metallic and ceramic as well as the more common polymeric matrices.

In principle, the reinforcement of metals would appear to be potentially useful but in practice the fabrication route often involves the application of high temperatures which encourage interfacial reactions between fibre and matrix thus degrading the useful properties of the fibre. Siliceous materials have the advantage of relative inertness to metals but to date they have been exploited, almost entirely, as vitreous fibres which have relatively low elastic moduli and refractoriness. By inducing controlled crystallization in vitreous materials it is possible to increase the above properties and gain further advantages such as thermal expansion coefficients which match the metallic matrix. It was the purpose of this research to investigate if such fibres could be produced from lithia/silica glasses and to attempt to relate mechanical properties to the microstructure of the resulting fibres.

1.1 Synopsis of the Research Programme.

Many potential glasses were examined for their ability to be drawn into continuous fibre from a single tip platinum bushing. Eventually two compositions were selected for further investigation, these being:

(a) 25% Li_2O 74% SiO_2 1% P_2O_5

(b) 29% Li_2O 68% SiO_2 1% P_2O_5 1% ZnO 1% K_2O

The fibres produced in this way were subjected to various heat treatments in which temperature and time were varied. This

brought about the crystallization of the fibres. Both the tensile strength and elastic modulus of each sample of fibre was measured and the fibres microstructure investigated using electron microscopy and X-ray diffraction. Whilst the elastic modulus always increased with degree of crystallinity the strength decreased. The nature of this decrease appeared to be different for each composition and an attempt was made to explain this behaviour in terms of microstructural parameters. This research indicated that it would not be possible to obtain polycrystalline fibres with a higher strength than the parent glass fibres. It also became obvious that the strength decreased more rapidly in fibres possessing surface crystallinity. In the final part of this research attention was turned to supressing surface crystallinity. The technique employed consisted of an ion-exchange, at the fibre surface, using a vapour containing the exchanging ion. Although this work is incomplete the results indicate that the techniqe is promising.

2. Nucleation and Crystal Growth

2.1 Nucleation

Research carried out in the field of glass-ceramics falls into two broad categories. One aspect is fundamental research attempting to establish physical models in order to explain such processes as nucleation, crystallization and the microstructure/property relationships of the materials. The other research employs an empirical approach. By observing how composition and heat treatment effect physical properties it is often possible to optimize those properties and obtain a commercially useful material. It could be argued that the fundamental approach is not necessary if empirical studies produce good materials, however, glass-ceramics are complex materials and the possible combinations of composition, heat-treatment temperature and time present an enormous number of variables.

The fundamental research worker attempts to discover which factors affect each process and the results of this work can be used by the empiricist to narrow the field of his investigations. Despite the formidable amount of research that has been carried out in both areas the interaction between theory and empiricism is still in its early stages. The reason for this is the complexity of the crystallization process in glasses. Often the equilibrium phases expected to crystallize from a glass do not appear since kinetic as well as thermodynamic considerations play an important role, also the high viscosity of the glass enables metastable phases to exist almost indefinitely without transition to a more stable phase.

The major emphasis in this thesis is placed on the empirical relationship between microstructural parameters and the mechanical strength of glass-ceramic fibres but it was important to consider which factors influence the microstructure. For this reason some consideration is given in this chapter to reviewing the relevant research which has attempted to explain nucleation

and crystallization in lithia-silica glasses in terms of classical nucleation and crystallization theories.

The classical theory of nucleation recognizes that systems do not in general undergo transition from metastable to a stable phase simultaneously and homogeneously, throughout the material. In particular, the crystallization of a solid from a condensed phase requires that atoms undergo local ordering into stable nuclei possessing a similar crystal structure to the stable phase. During the early stage of formation these small clusters of atoms or "embryos" have a high surface to volume ratio and thus are unstable since the increase in surface energy γ caused by their growth exceeds the volume free energy change ΔG_V associated with the transition from a less to more stable phase. For a spherical embryo of radius r the net free energy change ΔG is given by

$$\Delta G = 4\pi r^2 \gamma + \frac{4}{3}\pi r^3 \Delta G_V \qquad (2.1)$$

As the embryo increases in size the change in surface energy becomes small compared to the volume free energy change and the free energy change then becomes negative. Hence a critical radius r^* exists greater than which the embryo becomes stable.

It can be shown that this critical radius r^* is given by:

$$r^* = -\frac{2\gamma}{\Delta G_V} \qquad (2.2)$$

and

$$\Delta G^* = \frac{16\pi \gamma^3}{3(\Delta G_V)^2} \qquad (2.3)$$

where ΔG^* is the free energy change at radius r^*. In a condensed phase such as a glass the formation of a nucleus also involves the formation of a phase boundary. The rate of growth of the nucleus will depend on two processes taking place at this boundary

(i) Transport of atoms to the boundary

(ii) Rate of reaction at the boundary

The equation generally used to describe the rate of growth of a nucleus I in terms of these two processes is:

$$I = \left(\frac{N_s^* \; k \; T}{h}\right) \; n \exp\left(-\frac{\Delta G^*}{kT}\right) \quad \exp\left(-\frac{Q}{kt}\right) \qquad (2.4)$$

where N_s^* = number of atoms adjacent to the interface

Q = free energy for diffusion across interface

N = number of molecules per unit volume.

The difference in temperatures Tm - T is the under-cooling ΔT. When ΔT is small the first exponential term controls the rate of growth and so the rate is dependent on the volume free energy difference between crystalline and amorphous phase. At large under-cooling, however, the rate is controlled by the transport to the growing nucleus. Thus a maximum exists in the nucleation rate as a function of undercooling as shown in figure 2.1. This process is known as homogeneous nucleation.

If foreign surfaces are present in the glass such as container walls, dust particles, colloidal suspensions or other crystalline phases the rate of nucleation can be accelerated. These extraneous surfaces have no effect on the volume energy change between the two phases neither do they affect transport rate but they can lower the interfacial energy between the nucleus and surrounding glass. The effect is to reduce the degree of undercooling required to initiate nucleation.

Many attempts have been made to apply classical nucleation theory to "real materials" such as glasses, but, problems have been encountered owing to the complexity of the nucleation mechanisms in glasses even with relatively simple compositions and there appears to be little correlation between theory and experimental observation in more complex glasses.

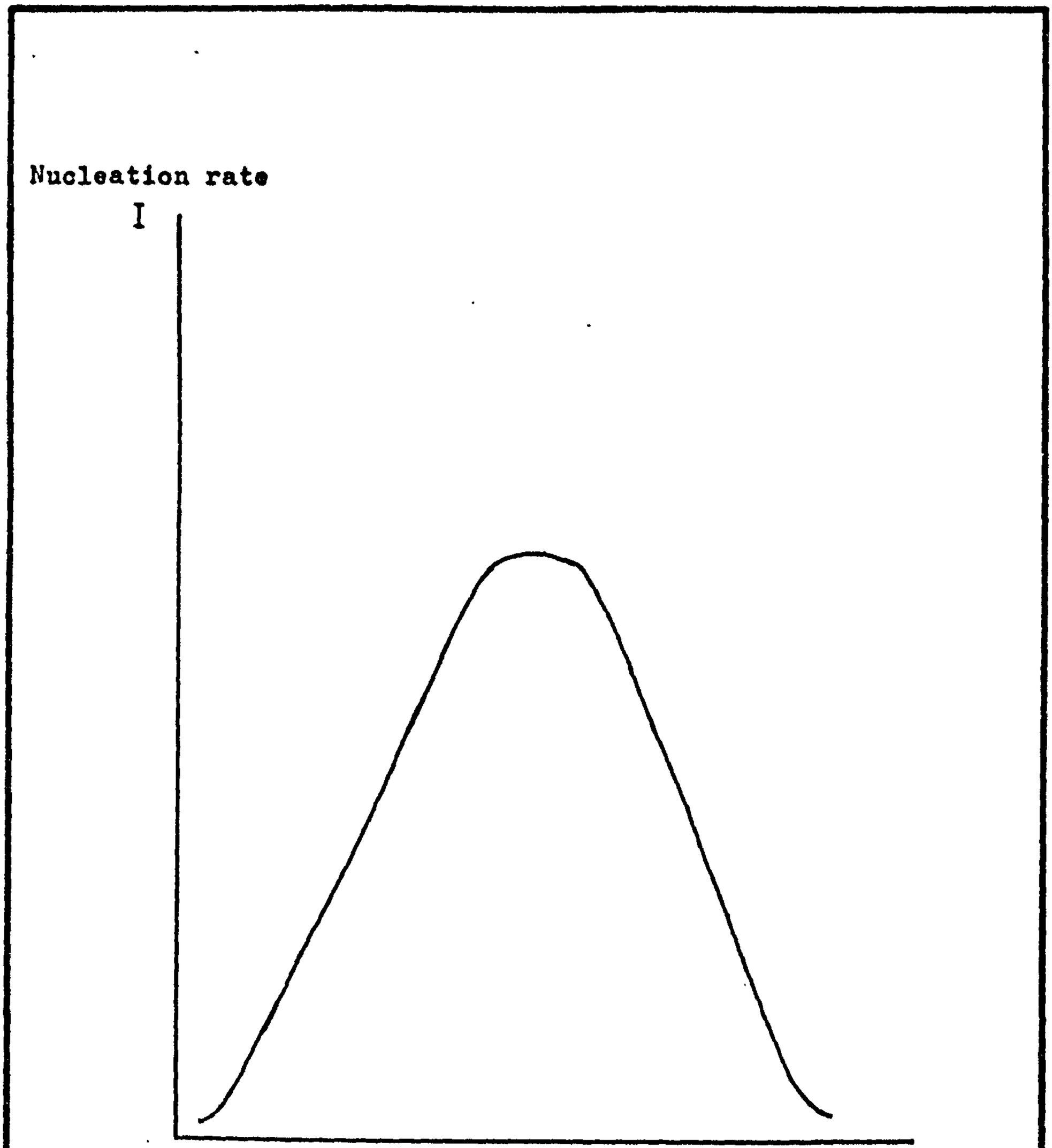

FIG 2-1

2.2 Nucleation in Lithia/Silica Glasses

One such attempt to apply classical nucleation theory to lithia/silica glass was made by Ito et al [1] who claimed that a rate equation similar to equation 2.4 was appropriate to their results. Although they show some evidence that the rate is controlled by a transport process at large undercoolings, it is inferred that the rate factor close to the equilibrium temperature is the volume free energy difference between lithium disilicate and the glass but no direct evidence is given. The number of nuclei in each specimen was measured by crystallizing the samples at a temperature much higher than the nucleation temperature. This was done in order to grow crystals large enough to be seen by optical microscopy. Such measurements should be treated cautiously since many nuclei disappear at the higher crystallization temperature. Likewise there is some doubt as to the accuracy of their calculated value of nucleus/glass interfacial energy since their calculation involved the assumption of an enthalpy of transformation between glass and crystal.

Hench and Frieman[2] suspected that lithium disilicate was hetergeneously nucleated in these glasses. They concluded that lithium metasilicate first appeared then a diffusional rearrangement of Li^+ ions brought about the transformation from meta- to disilicate. Since this investigation there has been no further evidence to support this idea. A vigorous attempt was made by Matusita and Tashiro[3, 4, 5] to apply classical nucleation theory to this system. Part of their work consisted of varying the viscosity of the glass at a given temperature by the addition of various oxides in the hope of showing that growth was transport controlled at large ΔT since the nucleation rate would then be expected to be greater the lower the viscosity. Their results, displayed as nucleation rate vs cationic radius, show some relationship between nucleation rate and viscosity but several oxides were found to form exceptions to this rule. To establish the validity of

the nucleation rate equation (4) accurate knowledge of the glass viscosity is needed over a wide temperature range. Unfortunately many of their values were extrapolated or interpolated from measurements made well outside of the temperature range of interest and this may account for the large discrepancy in their calculated rates. Another factor is the assumption that transport or diffusion of ions is controlled only by the glass viscosity. Slight compositional changes may have a pronounced effect on ionic mobility without changing the viscosity appreciably[6]. They also studied nucleation and crystallization in potassium and sodium dislicate glasses and compared their results with those for lithium disilicate glass, again trying to fit the measured rates to a classical nucleation model. Here they proposed that viscosity and therefore transport differences of ions in these glasses could not account for the vastly different rates but that the volume free energy change for the crystalline phase accompanying crystallization was responsible for the difference. This appears to conflict with their previous findings.

In general, glass-ceramics produced by homogeneous nucleation have poor mechanical properties which makes them commercially unattractive. Better materials have been made by employing heterogeneous nucleation to yield a more controlled and desirable microstructure. As mentioned previously, nuclei can form on foreign surfaces withing the glass and one effective method of introducing such surfaces is by dispersing a colloidal suspection of metal atoms in the glass prior to crystallization. Rindone[7] crystallized lithia/silica glasses using a fine suspension of colloidal platinum and discovered that there was an optimum concentration of platinum needed for maximum nucleation rate. It is also possible to obtain suspensions of other metals in glass such as Ag, Au and Cu[8, 9, 10] but the metal has to be reduced from the metal ion in order to form metallic particles. This reduction process can be effected using X-rays or ultra-violet radiation

and commercial use has been made of this process to cause preferential crystallization within the body of a glass; these materials are termed photo-ceramics. The most effective method, however, of achieving a high density of nuclei is to introduce phosphorous pentoxide into the glass.

The exact role played by this oxide is not fully understood. For instance Tomozawa et al[11] found it the exception to the rule obeyed by most other oxides in that it increased nucleation rate appreciably without causing a proportional change in glass viscosity. Doremus and Turkalo[12] examined several lithia/silica glasses containing P_2O_5 and report a higher nucleation density in glasses with P_2O_5. They suggest that the oxide reduces the interfacial energy between nucleus and glass but produce no experimental to verify this. Other workers report similar results but many of these investigations have been carried out using glasses known to undergo phase separation. Phase separation adds a further complexity to the understanding of nucleation since the constituents of the glass are now inhomogeneously distributed. Classical nucleation theory relies on the system remaining compositionally homogeneous which reinforces the idea that it is not strictly applicable to such systems. However, in reviewing the work carried out on these glasses some ideas are developed which may lead to a more comprehensive theory of nucleation at a later date. Some of this work is now outlined.

Tomozawa[11] proposes that phase separation directly effects the nucleation rate of lithium disilicate and the mechanism put forward is that during the formation of silica-rich droplets a narrow zone around the particle becomes depleted in silica owing to the increase of P_2O_5 in this region. The net effect is to give an interface with a low energy. Such a zone could then act as a site for nucleation. The assumed silica concentration profile is shown across a droplet in figure 2.2.Whilst this

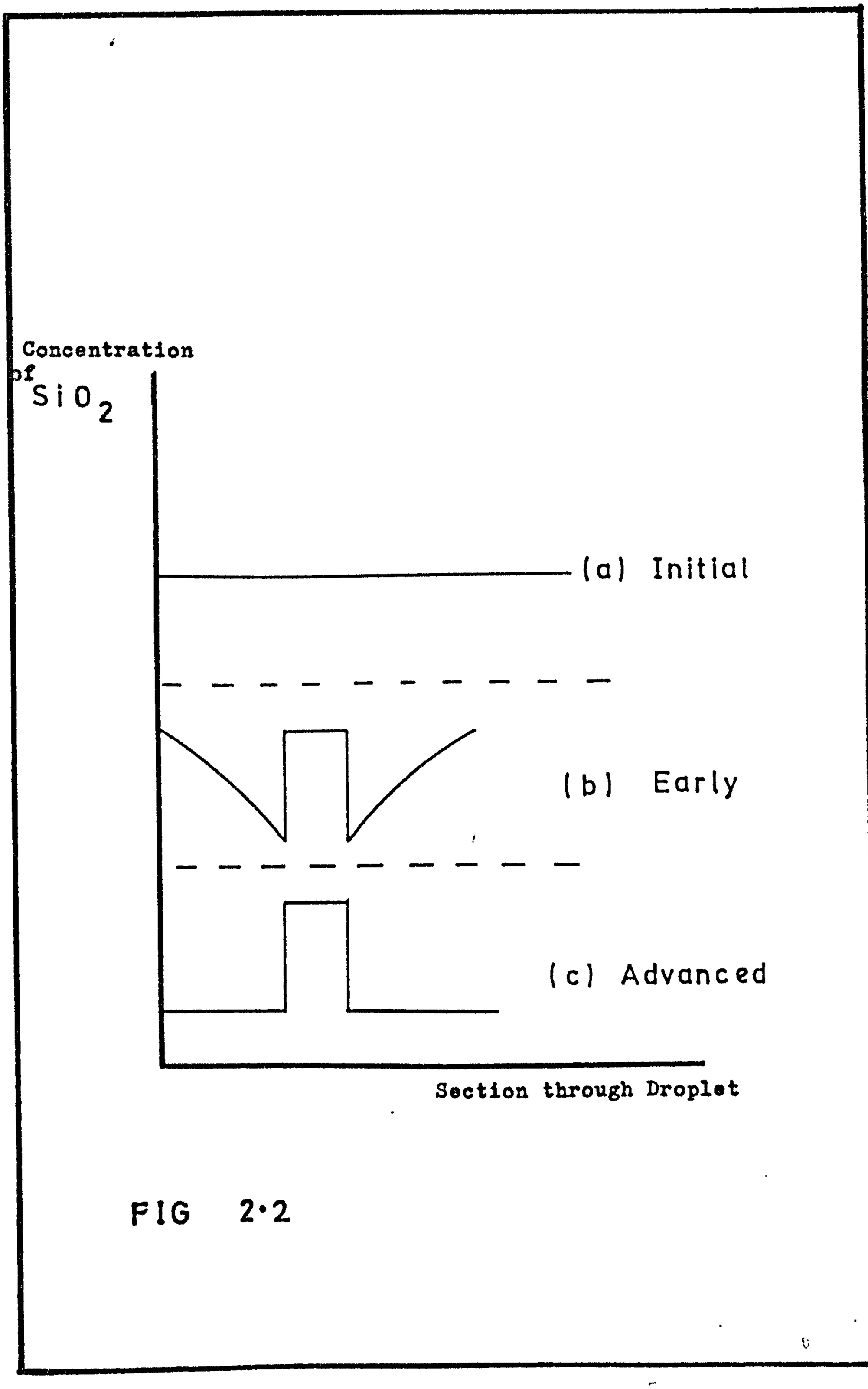
Concentration of SiO_2
(a) Initial
(b) Early
(c) Advanced
Section through Droplet

FIG 2·2

hypothesis is interesting and plausible, Tomozawa produces no direct evidence to verify its validity. This view is also supported by Plumat[13] but again without direct experimental evidence. Strong objections to this proposition are raised by McMillan[14, 15] et al who have made exhaustive studies of a wide range of glasses containing P_2O_5. They attempted to relate nucleation rate to various parameters representative of the degree of phase separation

(i) number fraction of discrete phase

(ii) volume fraction of discrete phase

(iii) surface area of discrete phase

but did not find any correlation. To date there is no further evidence to support either view but a point can be made against the reasoning of Tomozawa since he assumes that if phase separation does not affect nucleation then classical nucleation theory should predict the rate accurately. As mentioned previously it is unlikely that such a simple theory should apply to a system in which the constituents are inhomogeneously distributed.

2.3 Crystal Growth

Once the nuclei have attained the critical radius further growth can take place. At the optimum nucleation temperature atomic mobility in condensed systems, such as glasses, is so low that the growth rate would be imperceptibly slow. Thus for practical reasons crystallization is usually carried out at a higher temperature. As with nucleation the crystal growth rate shows a maximum with temperature since the driving force for growth increases with degree of undercooling but atomic mobility decreases. Several models have been developed to describe crystal growth and the corresponding rate equations derived. The common basis of these models is the assumption that a crystal face grows by the succesful collision of atoms or ions at certain sites on the surface but the hypotheses vary in the manner in which this is achieved. Some consideration is given here to

the development of a simple model which is often applied to condensed systems.

The driving force for crystallization is the free energy difference between glass and crystalline phase ΔG.

$$\Delta G = \Delta S_f \, (Tm - T) \qquad (2.5)$$

where ΔS_f = the entropy of transformation

$$= \frac{-\Delta H_f}{Tm}$$

and ΔH_f = the latent heat of transformation.

This thermodynamic driving force gives the relative number of succesful jumps of atoms from the melt to the crystal so the rate of crystallization U should be given by the gradient of this driving force divided by the force required to move an atom through the glass of viscosity η. Assuming the diameter of an atom to be d an expression can be derived thus

$$U = \frac{\Delta H_f \, (T_m - T)}{3\pi \, \lambda^2 \eta \, Tm} \qquad (2.6)$$

where λ = the thickness of the transition layer between the crystal and glass and λ is usually taken to have the same order as d.

This equation, however, does not give accurate growth rates for real systems, since it does not account for the fact that only a fraction of the atoms arriving at the surface do so at singularities suitable for growth and also it is necessary to assume a value for λ since this quantity is difficult to measure.

Another model termed "transition state" theory has been applied to glasses. The assumption here is that an atom or molecule must acquire a minimum activation energy in order to cross the glass/crystal interface. Using the Stokes-Einstein equation to relate diffusion coefficient D to glass viscosity η

$$D = \frac{kT}{3\pi\eta\lambda} \qquad (2.7)$$

and thus an expression for growth rate can be derived:

$$U = \frac{\left[1 - \exp\left(\frac{\Delta G}{kT}\right)\right] kT}{3\pi \lambda^2 \eta} \qquad (2.8)$$

This equation is more appropriate to glasses but when $\frac{\Delta G}{kT}$ is small, equation 2.8 transforms to equation 2.6. Modifications made to equation 2.8 for specific systems usually involve attempts to describe the growth interface, thus determining λ more accurately and also to use an accommodation coefficient to give the fraction of atoms which arrive at the correct singularity for growth.

The usual procedure for applying such rate equations to glasses is to measure the size of crystals in the glass after various crystallization times for a series of temperatures. Early studies employed optical microscopy which meant that crystals needed to be large before they could be detected thus no information was available for the early stages of growth. Electron microscopy has now enabled this information to be obtained but the results rarely fit theory closely. There are two possible sources of error in this practice. Firstly rate equations do not allow for a temperature rise at the growth interface as the latent heat of fusion is evolved. This is only a problem if the growth rate and therefore heat evolution is so rapid that the heat cannot be conducted away rapidly enough. This is also a function of size and geometry but Doremus[16] has shown that growth rates greater than 10^{-6} m/sec in glasses can cause a significant temperature rise at the interface. Some alkali/silicate glasses do crystallize faster than this and thus some consideration should be given to this effect. A temperature gradient at the interface can also dictate the growth morphology since the degree of undercooling is now reduced close to the crystal and a protrusion from the face will then be in a region of

greater undercooling and higher growth rate. This can give rise to dendritic morphology. A second error can arise from the use of viscosity values taken from experiments carried out on the bulk glass at temperatures other than the range suitable for crystal growth. This was the explanation given by Ito[1] for the fact that he was unable to fit theoretical rate equations to observed rates in lithia/silica glasses. Thus, at best, it is only possible at present to generalize about some of the factors affecting growth in glasses and it does not appear to be possible to develop an all-embracing theory. In fact the assumption that such rate equations apply to complex glasses could be incorrect even if all the parameters were determined accurately since the growth rate is controlled essentially by the nature of the interface and it is in this region where the ionic distribution is likely to be different from the rest of the glass. Ions showing a tendency to lower interfacial energy will tend to segregate to the interface changing many of the properties in this zone. Matusita and Tashiro[4, 5] point out that additions of phosphorous and titanium increase growth rate but this cannot be accounted for by the corresponding increase in ionic mobility since there is little variation in bulk viscosity. Phosphorous pentoxide does have an effect on phase separation in lithia silica glasses. However, the effect of phase separation on growth rate is a matter of some controversy. Filipovich and Kalina[17] found no correlation between growth rate and phase separation yet McMillan[15] and co-workers suggest the opposite. They found that phase separation slowed down the growth of lithium disilicate and proposed that the silica rich droplets impede the crystal growth front. This would account for the fact that phase separated glasses generally have a high density of small crystals in the resulting microstructure after crystallization. What is not readily explainable is the fact that phase separated glasses containing P_2O_5 yield smaller crystals in the microstructure.

McMillan et al[15] have suggested that P_2O_5 may lower the interfacial energy between the discrete and continuous phase encouraging a good dispersion. Another effect in phase separated glasses was noticed by Tomozowa[11] who claims that an incubation period was required at the crystallization temperature before crystal growth proceded. This was thought to be the time required for phase separation to complete but no such effect was discovered by Scherer and Uhlmann[18] in their investigations. More recent work has been carried out by Hautojarvi, Lemusoksa and Kompa[19] and James et al[20] who have used positron annihilation to study crystallization in these glasses. Lemosoksa and Kompa reinforce the argument that phase separation influences crystal growth rate. James et al have shown that this technique is sensitive and reproducible certainly for studies of lithia/silica glasses.

Finally some consideration should be given to crystal morphology. Many workers have reported that in $Li_2O\ 2SiO_2$ glasses after prolonged growth the disilicate crystals appear as a cluster and often this is referred to as a spherulite although there are few analogies that can be made between these spherulites and their counterpart in a polymeric material. James and Keown[21] used transmission electron microscopy to investigate this system and discovered that the cluster formation could be accounted for by crystal branching from non-faceted parts of an original crystal; this would then be the centre of the cluster. A twinning mechanism is proposed as the cause of branching. After prolonged crystallization these clusters adopt an ellipsoidal shape which agrees with observations made by Tomozawa[11]. Investigating a similar glass but with 1% P_2O_5 present they claim to observe phase separation but find it has little effect on the final morphology of the crystal cluster although it does produce less faceted crystals in the early growth stage. The work of Hautojarvi, Lehmusoksa and Kompa[19] conflicts with the above findings. They develop an empirical equation which shows the volume fraction of crystallinity V(t) to be related to time by

a power law:

$$V(t) = Vo\,[1 - \exp(-k\,t^{n})] \qquad (2.9)$$

where Vo = saturation volume fraction of crystallinity at a given temperature

k = a constant

n = a constant.

The exponent n was found to depend on growth morphology and thus fibrous growth denotes n = 1 whereas equiaxed growth, n = 3. Using electron microscopy as a method of confirming their observations they find that, in the phase separated glass, crystals were equiaxed and a value of n = 2.9 was appropriate to their results whilst the non phase separating glass gave rise to elongated crystals and n = 1.5 was the exponent.

In this work both elongated, equiaxed and oblate clusters were noticed in the fibre microstructure but this will be amplified in the discussion.

Summarizing the state of the art: it appears that classical models of nucleation and crystal growth are not entirely suitable for glasses particularly those containing small additions of constituents such as P_2O_5 which appear to have an effect on nucleation and growth. This is possibly due to segregation of P^{5+} ions at the growth interface causing a lowering of interfacial energy but there is no direct evidence to verify this. From a practical point of view, however, glasses undergoing phase separation and containing P_2O_5 do give microstructures which give the material some desirable mechanical properties as will be discussed in more detail in the next chapter.

3. The Strength of Ceramics

3.1 Fracture of Ceramics

Ceramic materials have rarely been used in engineering applications, in which they would be subjected to tensile loads. However, much interest is now being shown in utilizing their combination of high strength and refractoriness in many highly stressed components. The inherent drawback in using ceramics is related to the fact that they are brittle and as such their strength is governed by the size of pre-existing flaws. Because of the statistical nature of the flaw size distribution, ceramics exhibit a variance in strength determined by the flaw distribution and so it is difficult to asign a strength which can be used reliably in design calculations. The approach being taken to give a better understanding of these materials is two-fold

(i) Fracture mechanics

(ii) Statistical analysis.

Fracture mechanics attempts to establish fracture criteria by relating mechanical parameters such as the stress field at a crack tip or energy released as a crack grows to the structure and properties of materials whilst the statistical analysis aims at providing reliable strength data to enable components of complex geometry to be designed for applications where they are subjected to high loads. To some extent these approaches over-lap and recent research is directed towards an all encompasing theory but this is only in its early stages. In this chapter some consideration is given to the fracture of brittle materials in general followed by consideration of this for glass-ceramics and the lithia/silica system in particular. Unfortunately little attempt seems to have been made to apply modern fracture mechanics to these materials and thus present knowledge isbased mainly on empirical observations with speculative ideas about

the factors controlling strength. At the turn of the century there was little known about the reasons why materials fracture and it was not until 1920 that A. A. Griffith[22] published a paper that was to revolutionize the understanding of fracture. Griffith derived a criterion for the extension of an isolated crack in a solid, subject to an applied load. The criterion was formulated in terms of fundamental energy theorems of classical mechanics and the first law of thermodynamics. He considered crack growth to be a reversible system and sought the conditions which minimized the free energy of the system so the crack was in equilibrium.

Now the energy balance can be written as

$$U = (- W_L + U_E) + U_S \qquad (3.1)$$

where U = the free energy of the system

W_L = the work done by the applied load

U_E = the stored strain energy

U_S = the surface energy of the fracture faces

Thus at equilibrium for the free energy to be a minimum $\frac{dU}{dc} = 0$. This was a criterion for predicting fracture since if the left hand side of equation 3.1 is negative the crack will extend whilst if positive it will close up. Griffith then analysed particular systems of loading and crack geometry. Using the analysis of Inglis[23] for the stress distribution around a narrow elliptical crack with a remotely applied uniform load he derived the term U_E and took the term U_S to be the fracture area multiplied by the surface free energy per unit area. The energy U had a maximum at the equilibrium crack length showing that the crack was unstable in this situation and would therefore grow; the critical condition being

$$6_c = \sqrt{\frac{2\gamma E}{\pi C}} \qquad (3.2)$$

where 6_c = critical stress

C = the crack length

E = the elastic modulus of the material.

The above form of the Griffith equation is the best known and is often used as a fracture criterion for brittle materials but it should be remembered that it is derived for the specific situation where a narrow elliptical crack is stressed normally by a remotely applied force. If the Griffith energy criterion is applied to a different situation such as that in the classical Obreimoff's experiment[24] a different result may be derived for crack stability; for instance in the latter case the crack is stable and will only propagate if the wedge continues to push along the cleavage plane. Examining many materials Griffith decided that the measurable strength was always one or two orders of magnitude lower than the theoretical strength calculated from the cohesive bonding forces. He attributed this lowering of strength to the existence of microscopic flaws on the surface or in the body of the material which are now commonly referred to as Griffith flaws. This hypothesis he tested by carrying out tests on glass fibres and the results showed that

(a) pristine glass fibres have the highest measurable strength

(b) the strength degraded with exposure to the laboratory atmosphere

(c) the thinner the fibre the stronger it was.

Finally he attributed the existence of these flaws to the presence of crystalline regions in the glass. It is only this last conclusion which is now considered the wrong explanation for the nucleation of microflaws but his energy balance concept is still used as a fracture criterion for many brittle ceramic materials.

In the 1950's Irwin[25] made further developments to the study of fracture and is often referred to as the originator of "fracture mechanics" as it is called today. His approach was to consider the material as a continuum and to try to find a materials parameter, analagous to the

Griffith surface energy, which represented the resistance to crack growth including the energy dissipative terms that are associated with the crack tip. An energy G is defined as the energy available per unit area for crack extension and using the first law of thermodynamics G can be expressed in terms of the external work W_L and strain energy U_E as follows

$$G = \frac{dW}{dc} - \frac{dU_E}{dc} \qquad (3.3)$$

for a unit width of crack. Thus G remains independent of the proportionation of energy into surface energy, plastic work etc. The analysis is usually carried out for various conditions of loading such as constant force (dead weight) loading where the applied force remains constant during crack growth whilst in fixed grip loading $dW_L = 0$ since the applied loading suffers zero displacement during crack growth. For the case of a material having a centre crack of length 2C loaded with a force P the specimen will behave like an elastic spring where the elongation U of the specimen is related to the applied force P by Hookes Law

$$U = \varphi P$$

where φ is the compliance of the sample. During this loading the ends of the crack are presumed to be held together to prevent extension. If this constraint is now removed the compliance will increase so

$$dU = \varphi\, dP + d\varphi\, P$$

but at the same time the mechanical energy term will decrease thus these energies can be equated

For Constant force loading $d(-W_L + U_E) \simeq -\frac{1}{2} P^2\, d\varphi$ (3.4)

or Fixed grip loading

So the energy released during crack growth dc is independent of loading and we can write

$$G = \frac{1}{2} P^2 \frac{d\varphi}{dc} \qquad (3.5)$$

For fracture to occur the surface energy and other dissipative energy

terms must be provided by the release of strain energy. If we define an effective energy for fracture as γ_e to include all these terms then fracture occurs when $G > 2\gamma_e$. This now gives a critical fracture condition and G_c the critical strain energy release rate must be a materials property. Often the quantity is expressed for a particular mode of crack opening; the most common being mode I where the crack walls separate normally under the action of tensile forces with the suffix G_{IC}. For a central through crack in a remotely loaded body an equation similar to the Griffith relationship can be obtained

$$6_c = \frac{1}{A}\left(\frac{E\,G_{IC}}{C}\right)^{\frac{1}{2}} \qquad (3.6)$$

where A = a constant depending on loading geometry, crack configuration etc.

G_{IC} = critical strain energy release rate also $G_{IC} = 2\gamma_e$.

The important distinction that must be made between G and G_{IC} is that G is derived from solid mechanics whereas G_{IC} is a materials property.

A further fracture criterion can be established, this time not in terms of energy but in relationship to the stress field ahead of the crack tip. This work was also pioneered by Irwin. The stress at any point ahead of a crack 6_{ij} can be written in terms of the remotely applied stress 6. A coordinate system often chosen is polar coordinates

$$6_{ij} = 6\sqrt{c}\ \frac{f(\theta)}{\sqrt{2r}} \qquad (3.7)$$

(r, θ) define the coordinates of 6_{ij}. Assuming the material exhibits perfectly linear elastic behaviour it is possible to derive 6_{ij} for various crack configurations and when this is done it is found that the stress intensification at any point (r, θ) compared to the remote stress 6 depends on $6\sqrt{c}$ so it is possible to define a stress intensity factor K as

$$K = 6\,Y\sqrt{c} \qquad (3.8)$$

where Y again depends on the geometry of loading and crack configuration. Thus fracture should occur at some critical value of K which causes a critical displacement at the crack tip equivalent to bond rupture. For the most common mode I fracture this value is called K_{IC} and again is a materials property whereas K is derived by solid mechanics. Thus K_{IC} and G_{IC} should bear some relationship and it can be shown that

$$G_{IC} = \frac{K_{IC}^2}{E} = 2\gamma_e \quad \text{(for plane stress conditions)} \qquad (3.9)$$

$$G_{IC} = \frac{K_{IC}^2 (1 - \upsilon^2)}{E} = 2\gamma_E \quad \text{(for plane strain conditions)} \qquad (3.10)$$

The conditions of plane stress and strain have not been discussed so far, however, a simple definition will suffice here.

(i) Plane stress: this is the condition found at the free surface intersected by a crack. Because no force can act perpendicular to a free surface the stress field at the crack tip will be biaxial tension.

(ii) Plane strain: this is the condition existing within the body and corresponds to a triaxial tension at the crack tip.

The transition between plane stress and strain is gradual in a material exhibiting plasticity but the transition is sharp in a brittle material and plane stress exists only close to the surface. Both the strain energy release rate and stress intensity factor criteria for fracture were derived using linear elastic fracture mechanics in which it is assumed that the material close to the crack obeys Hookes Law. This assumption is quite erroneous for many materials which exhibit some degree of plasticity and included in this category are some ceramics, particularly at elevated temperatures. Several developments have taken place since the fifties in order to derive better fracture criteria for such material including

(i) Crack opening displacement

and (ii) J integral approach

but for brittle materials at ambient temperatures there appears to be little need to seek such sophistications since the stress intensity approach is still powerful. In the next section some of the microstructural parameters which effect K_{IC} will be discussed.

3.11 Microstructural Parameters Affecting K_{IC}

The application of fracture mechanics is potentially useful not merely as a way of understanding the fracture processes in existing materials but also as a means of improving their performance and developing new materials; for instance strength enhancement can be achieved by employing fabrication controls to reduce flaw size and maintain K_{IC} at an optimum value.

The primary microstructural variables in a ceramic or glass-ceramic are

(i) grain size

(ii) volume fraction of phase present

(iii) grain morphology

(iv) pore size and morphology

(v) impurity distribution.

At present there are few conclusive theories relating K_{IC} precisely to the variation in the above parameters but it is possible to make some observations and general remarks about their dependence.

Grain size variation in ceramics is the most difficult effect to understand. Research workers report that K_{IC} can increase[26], decrease[27] or be unaffected[28] by increasing grain size.

It would appear that any such relationship may be singular to particular materials and that no generalizations can be made. However, if variation in grain size causes the fracture mode to become predominantly transgranular this can increase K_{IC}.

There is little experimental evidence to show a relationship between

K_{IC} and percentage crystallinity but it would be expected that K_{IC} should increase with degree of crystallinity since K_{IC} for a vitreous phase will be lower than for a crystalline phase. Grain morphology has been shown to have a more pronounced effect on K_{IC}[29]. If the aspect ratio of the crystal is high and the crystal interface is sufficiently weak the crack during fracture can deflect along the crystal/metrix interface absorbing energy as would be the case in a fibre reinforced material. This leads to a higher value of K_{IC}. Porosity can increase or decrease K_{IC} but this depends on the size of the pores compared to the mean grain diameter. Large pores reduce K_{IC} slightly whereas small intergranualr pores can impede crack propagation and increases K_{IC}[30].

Finally impurities can segregate at grain boundaries encouraging intergranular fracture decreasing K_{IC} but if the impurity takes the form of a second phase dispersed in the material it can induce local tensile strains in its vicinity which can induce microcracking at the tip of the crack front; this multiple fracture increase K_{IC}[31].

One very important consideration is that factors which help increase K_{IC} may, however, lower the fracture strength by introducing large inherent flaws in the material. The nature of flaws in ceramics is thus of prime importance and is now given some consideration.

3.12 Flaw Size and Configuration

There are few materials which can be produced in a flaw free state but even where this is possible they can only be produced in small volumes such as fibres or whiskers.

Flaws may arise in many ways, the best known of which is surface damage caused by abrasion with another surface or dust particles in the atmosphere. This type of flaw is usually treated as a semi-ellipitcal surface crack and is capable of being analysed. The method used to measure the depths of such flaws is invariably microscopy and some investigations

of glasses have shown reasonable correspondence between the measured flaw size and that predicted from strength measurements[32]. The nature and configuration of internal flaws in polycrystalline materials is more complex and little agreement exists in the literature as to the source of fracture initiating flaws in such materials. To cover the field of ceramics in general would be inappropriate in this thesis so the discussion is now confined to the type of flaws which may exist in glass-ceramics.

Essentially a glass-ceramic can be considered as discontinuous crystalline phase in a continuous vitreous matrix. Since the crystalline phase grows within the vitreous phase any volume change on crystallization may give rise to strain incompatibility and resulting stresses around the growing crystal. Such stresses can give rise to the nucleation of microcracks at the glass/crystal interface. Volume changes can be considerable and if crystallization is rapid the vitreous phase may not be able to relieve such residual stress by viscous flow.

Similar flaws can occur if the crystalline and vitreous phases have different coefficients of expansion particularly if the expansion coefficient of the crystalline phase is lower than that of the matrix. If flaws do not initiate by either of the above mechanisms they can arise when the body is stressed if the crystalline and vitreous phases have differing shear moduli. Provided such residual stress is in existence an applied stress well below the expected critical value can still initiate flaws. Apart from flaw initiation the existence of a dispersed crystalline phase can affect the propagation of a growing crack. The second phase can act as a dispersion of obstacles to the crack front. Several treatments of this problem[33,34] have been undertaken analogous to the line tension experienced by a dislocation attempting to pass pinning sites. If the crystalline phase is considered totally impenetrable expressions can be derived which relate K_{IC} to the size and spacing of the dispersion. If

d represents the mean diameter of second phase particles and D their mean spacing it can be shown that the effective surface energy γ_e increases with the ratio $\frac{d}{D}$. Where the second phase is penetrable Davidge and Green[35] have shown that a travelling crack will pass through the second phase particles provided the matrix has a higher coefficient of expansion than the second phase but will circumvent the particles if the expansion coefficients are reversed.

Cracks can initiate in the crystalline phase itself if it has well defined cleavage planes. The values measured for K_{IC} on single crystals are generally lower than K_{IC} for the bulk poly crystalline material so a crack initiating within the crystal will propagate until it reaches the grain boundary and then stop unless the stress is increased to achieve K_{IC} for the polycrystalline material as would be measured typically in fracture toughness determination for the bulk materials.

Much of the research into factors governing the strength of glass-ceramics has centered on trying to establish relationships between observed fracture stress and parameters controlling the size of flaws within the material. The basis of most analyses is the Griffith relationship. Little work has been carried out, to date, in trying to obtain reliable fracture mechanics parameters such as G_{IC} and K_{IC}. The two obvious factors which may influence flaw size in these materials are

(i) mean grain diameter

(ii) mean intercrystal spacing.

Tashiro[36] investigated two glass-ceramics based on the lithia/silica system and found that the material crystallizing with lithium disilicate, as the only detectable phase, exhibited the following relationship

$$6 \propto \frac{1}{d^{\frac{1}{2}}}$$

d = mean grain diameter

$6'$ = fracture stress

and their results are shown graphically in figure 3.1. The second glass-ceramic contained lithium disilicate and a quartz phase. This material did not obey the above relationship. Tashiro proposes that the strength controlling flaws in this glass ceramic originate in the vitreous phase and since this material exhibited a relatively low volume fraction of crystallinity microcracks would be expected to be larger than the mean grain diameter. Such hypotheses are difficult to test since little is known about the properties of the residual glassy phase. Several workers (37, 38) believe that the zone ahead of a growing crack in a glass experiences plastic deformation which would require the expenditure of strain energy during fracture. Thus if a predictive model of glass-ceramic strength is sought information would be required about the mechanical nature of the residual vitreous phase.

McMillan[39, 40, 41] and co-workers have investigated several materials and also relate strength to microstructural parameters. One composition[39] showed a strength maximum with crystallization temperature as illustrated in fig. 3.2. The fall off in strength with higher temperatures is attributed to the appearance of silica in the material which would create thermal stresses on cooling owing to the difference in expansion coefficients. The appearance of silica would also account for the decrease in elastic modulus at higher temperatures. Two[40] compositions were tested in which surface crystallization was known to take place. The existence of surface crystals was thought to influence flaw size in the material. Later work by Hing and McMillan[41] attempts to establish a relationship between strength and intercrystal spacing. Since the mean intercrystal spacing was a difficult quantity to measure directly it was estimated indirectly from volume fraction measurements using a relationship of the type

$$\lambda = \bar{L}\left(\frac{1 - V_c}{V_c}\right) \qquad (3.11)$$

and their results are shown graphically in figure 3.1. The second glass-ceramic contained lithium disilicate and a quartz phase. This material did not obey the above relationship. Tashiro proposes that the strength controlling flaws in this glass ceramic originate in the vitreous phase and since this material exhibited a relatively low volume fraction of crystallinity microcracks would be expected to be larger than the mean grain diameter. Such hypotheses are difficult to test since little is known about the properties of the residual glassy phase. Several workers (37, 38) believe that the zone ahead of a growing crack in a glass experiences plastic deformation which would require the expenditure of strain energy during fracture. Thus if a predictive model of glass-ceramic strength is sought information would be required about the mechanical nature of the residual vitreous phase.

McMillan[39, 40, 41] and co-workers have investigated several materials and also relate strength to microstructural parameters. One composition[39] showed a strength maximum with crystallization temperature as illustrated in fig. 3.2. The fall off in strength with higher temperatures is attributed to the appearance of silica in the material which would create thermal stresses on cooling owing to the difference in expansion coefficients. The appearance of silica would also account for the decrease in elastic modulus at higher temperatures. Two[40] compositions were tested in which surface crystallization was known to take place. The existence of surface crystals was thought to influence flaw size in the material. Later work by Hing and McMillan[41] attempts to establish a relationship between strength and intercrystal spacing. Since the mean intercrystal spacing was a difficult quantity to measure directly it was estimated indirectly from volume fraction measurements using a relationship of the type

$$\lambda = \bar{L}\left(\frac{1 - V_c}{V_c}\right) \qquad (3.11)$$

FIG 3·1 RELATION BETWEEN MODULUS OF RUPTURE AND GRAIN SIZE.

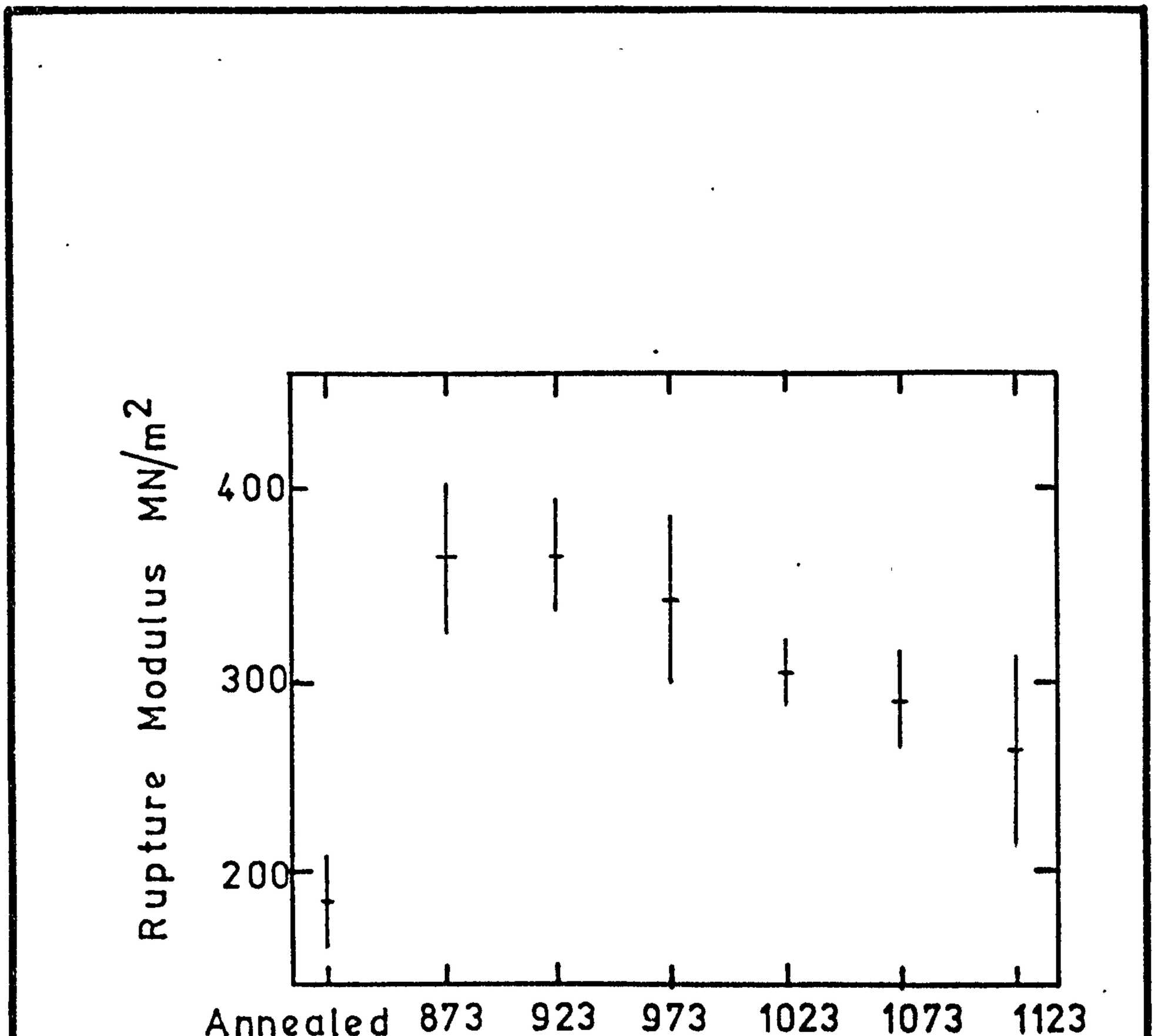

FIG 3·2 VARIATION OF MEAN RUPTURE MODULUS WITH HEAT-TREATMENT CONDITIONS.

λ = mean free path between crystals

L = mean crystal diameter

V_c = volume fraction of crystallinity.

Their results are plotted in figure 3.3. During the early stages of crystallization strength appears to be independant of mean free path but after a critical value the decrease in mean free path corresponds to increasing strength. An effective surface energy calculated from the gradient of this graph was higher than that theoretically predicted and they suggest that the crystalline phase may present a dispersion of obstacles to a propagating crack. If this were the case a relationship of the type

$$\gamma_e \propto \frac{1}{\lambda}$$

would be expected but this was not obeyed by their results. Micrographic examination, however, showed a rough transgranular surface and it is thus possible that the crack will be deflected along the (010) cleavage planes in the randomly oriented lithium disilicate crystals thus requiring extra energy for crack propagation. To some extent their results agree with the work of Hench and Frieman[42] who obtained strength data using diametral compression tests and plotted this against volume fraction of crystallinity as shown in figure 3.4. They conclude that during the early stages of crystallization it is the intercrystal spacing which again controls the flaw size in the material. The eventual decrease in strength is accounted for by the formation of microcracks due to volume contraction on prolonged crystallization. With regard to elastic modulus Hench and Frieman found an almost linear relationship between modulus and volume fraction of lithium disilicate present as shown in figure 3.5. Some recent work[43] has been carried out to obtain the K_{IC} for a glass-ceramic by fracture toughness testing of a precracked specimen and to compare this

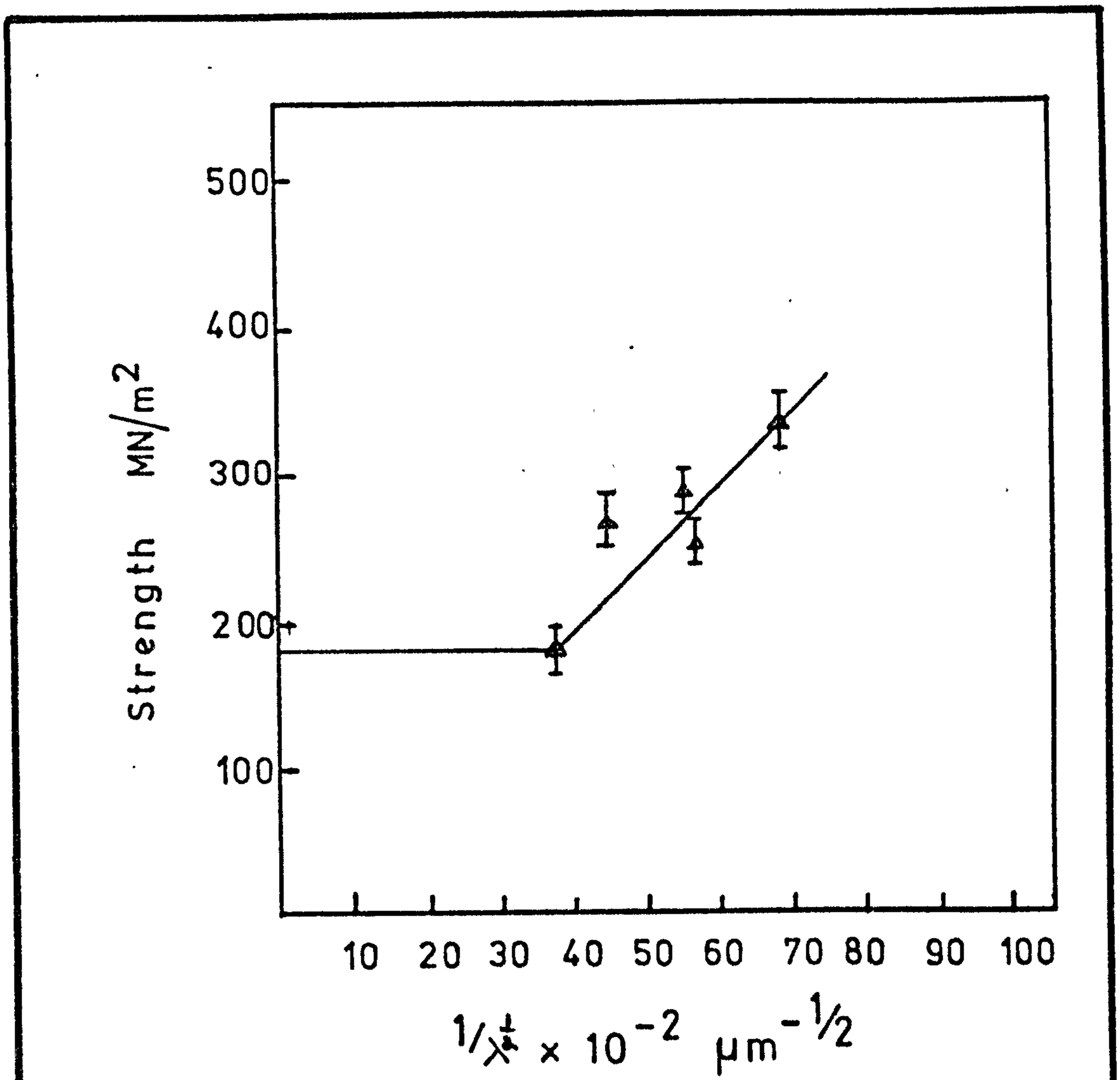

FIG 3·3 RELATION BETWEEN STRENGTH AND THE RECIPROCAL OF THE SQUARE ROOT OF THE MEAN FREE PATH.

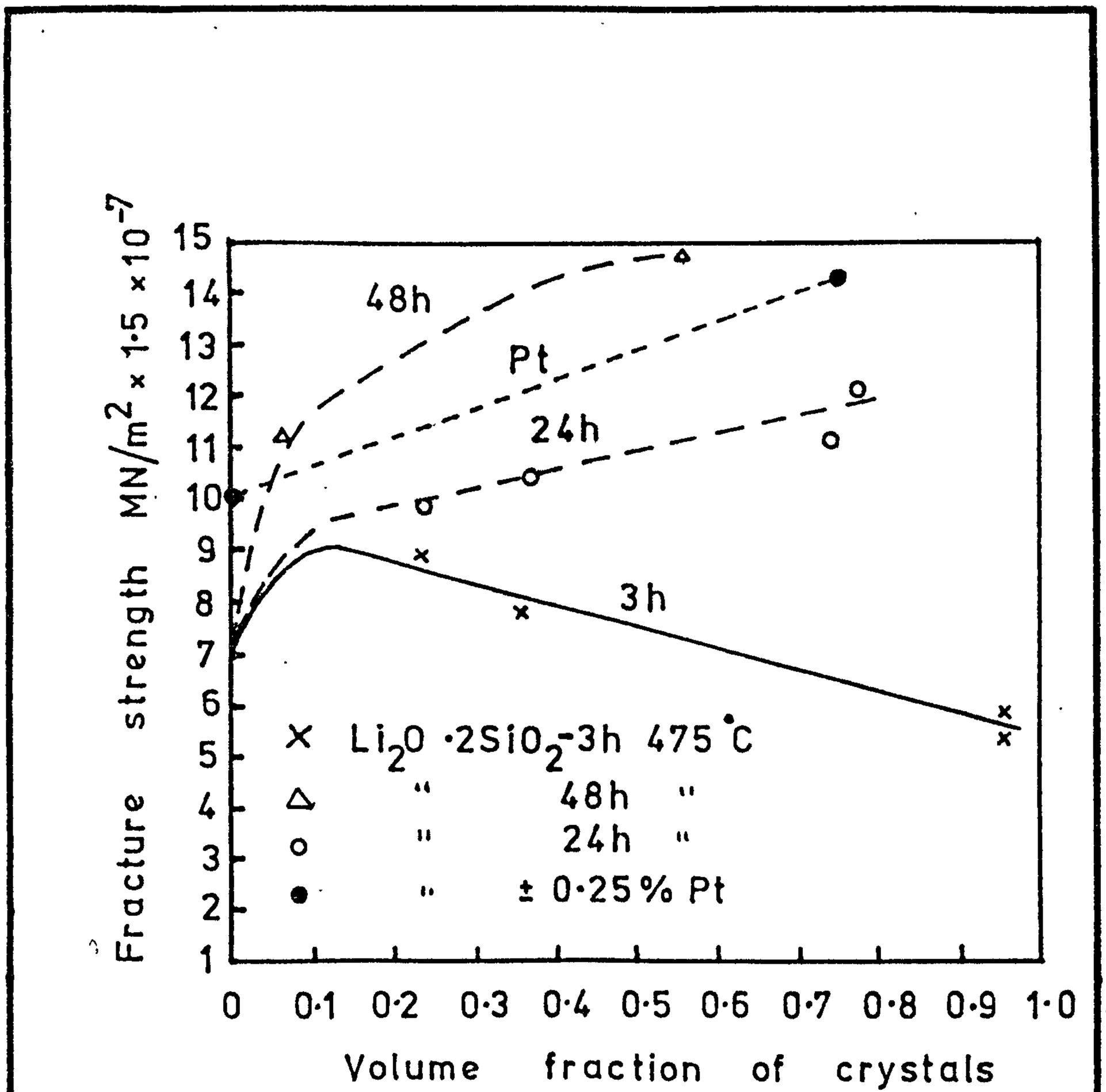

FIG 3·4 FRACTURE STRENGTH OF Li_2O -$2SiO_2$ AS A FUNCTION OF VOLUME FRACTION OF CRYSTALS.

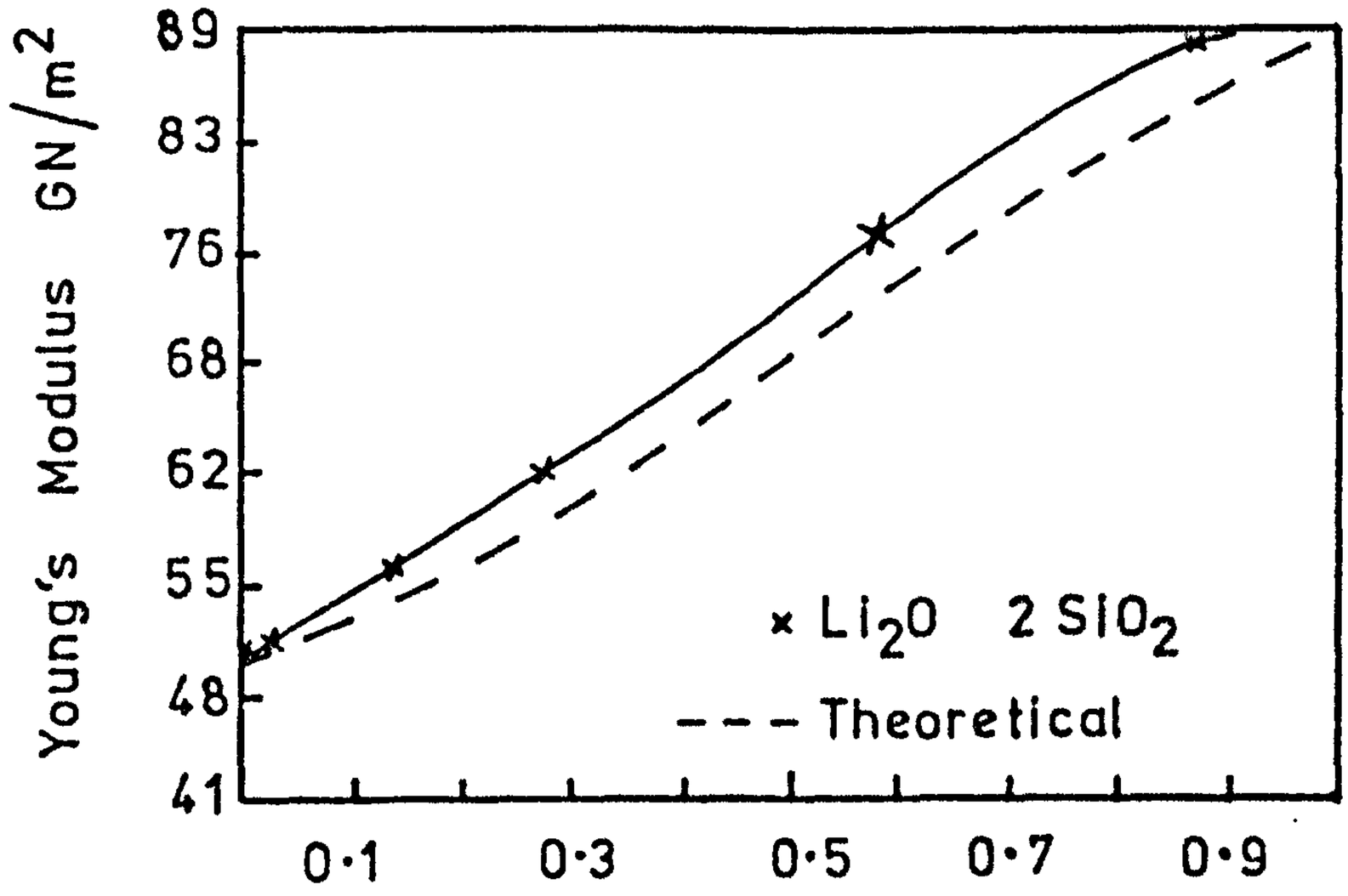

FIG 3·5 DEPENDENCE OF YOUNG'S MODULUS OF $Li_2O-2SiO_2$ GLASS - CERAMIC ON VOLUME FRACTION OF CRYSTALS.

with the K_{IC} calculated from strength measurements using the fracture initiating flaw size obtained by microscopy. The glass-ceramic used was Corning 9606 and the results showed good agreement between the two values obtained implying that K_{IC} in these materials is independent of the critical flaw characteristics at the fracture origin. If these findings are correct it would appear that the improvement of glass-ceramics will be best effected by control of the inherent flaw size in the materials and that improvements in K_{IC} will stem from the production of glass-ceramics containing inherently strong crystalline phases regardless of their microstructural distribution.

3.13 Flaw Size Distribution

Parallel with the development of fracture mechanics has been the statistical analysis of materials strength. It is a well know fact that ceramics exhibit large variations in strength amongst nominally identical specimens. This poses a problem to the designer wishing to use such materials as to which strength value he should use if his design is to have a low probability of failure. The analysis of such a problem is aided by the application of statistics and thus much interest has been shown in the development of fracture statistics in recent years.

The pioneer of this approach , W. Weibull[44], discovered that the distribution of materials strengths could be closely approximated by a particular distribution curve known nowqdays as the Weibull distribution. His assumptions were that the material behaves in a similar way to a chain with a weakest link in that the stressed chain will eventually break at this link so the material will fracture when the critical stress for the largest flaw is reached, also that the stress component normal to the crack or flaw plane contributes to failure. This analysis had no real physical basis but was merely a fit to observable data by a particular

distribution function. In recent years refinement of this analysis has taken place and attempts have been made to relate strength distribution to the flaw size distribution in the material but Weibull statistics still form the basis for much of this work.

Essentially when a material is stressed to fracture one or more of the larger flaws is caused to propagate thus the distribution of fracture strengths must be related to the large flaw-size extreme of the flaw population and thus strength statistics are based firmly on extreme value distributions of which the Weibull distribution is a particular case. Since it forms the basis for much of the work in this field the Weibull distribution will now be discussed more fully.

Weibull assumed that a body of volume V contained a statistical distribution of non interacting flaws so the occurence of a single critical flaw in this volume would lead to fracture. Now if the probability that this flaw does not occur in V is given by P(V) and also does not occur in volume V' is P(V') then

$$P(V + V') = P(V)\, P(V') \tag{3.12}$$

taking logarithms and differentiating gives

$$\frac{d}{dV} \ln P(V + V') = \frac{d}{dV} \ln P(V) \tag{3.13}$$

and thus

$$\frac{d}{dV} \ln P(V) = A \tag{3.14}$$

where A is a constant. Integrating the above equation and introducing the boundary conditions $P(0) = 1$ and $P(\infty) = 0$ gives

$$P(V) = \exp [- AV] \tag{3.15}$$

so the probability of occurence $P'(V) = 1 - P(V)$ is

$$P'(V) = 1 - \exp [- AV] \tag{3.16}$$

This shows that the probability of occurrence of the flaw increases with material volume. P (V) can thus be related to the fracture probability P(S) since the occurrence of the flaw results in fracture. Weibull extended this analysis to derive an expression for the relationship between fracture stress and probability by assuming the constant A, called the "risk of rupture", was a function of the stress distribution 6 and of the weakest element 6_u

$$\text{so} \qquad A(6)\ V = \int_v \left(\frac{6 - 6_u}{6_o}\right)^m \frac{dV}{V_o} \qquad (3.17)$$

where m, 6_o and 6_u are considered materials constants for a constant flaw population. Equating this now to the fracture probability gives:

$$P(S) = 1 - \exp\left[-\int_v \left(\frac{6 - 6_u}{6_o}\right)^m \frac{dV}{V_o}\right] \qquad (3.18)$$

The equation can now be arranged for various stress distribution for instance in the case of a homogeneous tensile stress field

$$P(S) = 1 - \exp\left[-\frac{V}{V_o}\left(\frac{6 - 6_u}{6_o}\right)^m\right] \qquad (3.19)$$

and this is the familiar three parameter Weibull distribution that is often used for ceramics. Weibull showed that this distribution had wide applicability[44] particularly when the stress state considered is uniaxial tension and the analysis is useful in enabling size effect calculations to be performed thus allowing test data from small specimens to be used in the design of longer components.

The method of implementing such statistics for a set of strength data is usually to rank the strength values in ascending order and to assign a failure probability to each value. If the sample is large P(S) is given by

$$P(S_j) = \frac{j}{N + 1} \qquad (3.20)$$

where $P(S_j)$ = probability of failure of j th specimen

N = total number of specimens

but a more sophisticated treatment can be used for smaller N values thus

$$P(S_j) = \frac{j - 0.3}{N + 0.4} \tag{3.21}$$

Equation 3.19 is then written in the form

$$\text{In In } (1 - P(S))^{-1} = \text{In } \frac{V}{V_o} + m \text{ In } \left(\frac{6 - 6_u}{6_o}\right) \tag{3.22}$$

6_o is usually taken as the arithmetic mean stress for most calculations but is more strictly the stress at which the probability of failure is 0.63 per unit volume of material. Equation 3.22 can be plotted to give a straight line by optimizing the value 6_u and the value gives the best straight line fit is taken as correct. Physically 6_u represents a threshold stress below which it is assumed the material will have zero probability of fracture. This suggests a flaw limit in the material; a point which is a matter of some conjecture. The gradient of the graph, m, is called the Weibull modulus and is representative of the variance of strength values. A ceramic such as silicon nitride will have a high $m \sim 11$ whereas glass may have an m value as low as 2. m also reflects the variance of flaw sizes within a material. A simpler two parameter distribution can be used if it is thought reasonable to assume $6_u = 0$. In certain cases such as the strength distribution of fibres it is possible here to find fibres with flaws of similar size to the fibre diameter and therefore an unmeasurably low strength. This situation enables the simpler 2-parameter distribution to be used. Other procedures for fitting a Weibull distribution to data have been developed including plotting on special Weibull paper, the maximum likelihood method[45] and a non linear least squares method[46] and undoubtedly there are sets of data which are suited more to one method than another but essentially if the strength distribution can be truly described by such a distribution a good fit should be obtained. If the fit is poor there can be several reasons for this. Firstly the Weibull

distribution is only one of three possible extreme value distributions. It is infact the asymptotic extreme value distribution for a bounded population and two more distributions exist for distributions unbounded at the extreme thus the most appropriate distribution must also represent the distribution of flaw size at the upper extreme. The extreme value distributions for unbounded populations are different in the rate at which the population decreases towards an asymptotic value. Again these distributions can be expressed as linear equations and an attempt made to obtain a better fit.

Secondly it is possible to plot strength data to a Weibull function and obtain two straight lines of differing gradient. This does not necessarily indicate that the Weibull distribution is incorrect but it is possible that the data comprise a bimodal Weibull distribution. Evidence for this form of distribution and double gradient has been found by Snowden[47] and Scott and Gaddipati[48] for strength measurements made on optical fibres. It is reported that both an increase or decrease in m at higher stress has been observed but distributions characterized by an increase in m at higher stress is more common and readily explicable from a physical basis. Doubtless the other form of distribution exists but the observations can only be explained if it is assumed that neither distribution extends over the entire experimental range of stresses[49]. In glass fibres several types of flaws can give rise to the bimodal Weibull distribution for fibre strength. Very low strength fibres have been shown to have foreign particles embedded in their surfaces. These particles, up to 10 μm diameter, have been identified as various refractory oxides probably caused by furnace contamination. This type of heterogeneity is most likely to contribute to the low strength high variability region. Also random surface abrasion is likely to cause low strength and high variability. Flaws which cause failure at high stress and exhibit low strength variability are probably intrinsic flaws characteristic of the

glass surface structure and thus limit the upper strength. Little work has been carried out, however, to elucidate the nature of these intrinsic flaws. It is claimed in this work that some of the glass-ceramics fibre strength data are best described by a bimodal Weibull distribution and some conjectural sources of strength controlling flaws are given.

2.14 The Combining of Statistics and Fracture Mechanics

The succesful combination of these two approaches is still in its early stages but by understanding the statistics of flaw size more precisely it will be possible to utilize fracture mechanics data to better advantage. The analysis which has been most extensively developed is for an unbounded population of flaws. It is possible to show that[50] the probability that flaws, in a volume V, are larger than C_1 is

$$P = 1 - \exp\left[-\frac{V}{V_o}\left(\frac{C^1}{C_1}\right)^{z-1}\right] \qquad (3.23)$$

where c_1 = flaw size limit

V_o = unit volume

V = volume of specimen

C = flaw size in V.

The flaw size distribution can now be changed into a fracture probability by using the relationship

$$K_1 = Y\ 6\ \sqrt{C}$$

hence the probability that the stress intensity factor is less than K_{IC} when subjected to a homogeneous tensile stress 6 is given by:

$$P = 1 - \exp\left[-\frac{V}{V_o}\left(C^1\ \frac{6^2Y^2}{K_1^2}\right)^{z-1}\right] \qquad (3.24)$$

and since fracture occurs at K_{IC} the probability that fracture occurs at a stress less than 6_c is

$$P(6) = 1 - \exp\left[-\frac{V}{V_o}\left(\frac{\sqrt{C^1}\ 6_c Y}{K_{IC}}\right)^{2z-2}\right] \qquad (3.25)$$

This result is similar to Weibull with $2z - 2 = m$ showing that the Weibull distribution gives a good description of a body with a large number of spatially random flaws, themselves having an extreme value distribution if the body is subjected to a homogeneous tensile load. Another important development coming from this combined analysis is a more representative size effect correction. For instance if a body is subjected to a uniform tensile stress then it can be shown that K_I for surface flaws is larger than for internal flaws by $\simeq \sqrt{2}$. This enables the specimen to be divided into surface and volume elements. Equations have been developed[50] which give the probability of fracture in terms of surface and volume flaw distributions and it appears that surface cracks significantly increase fracture particularly for materials with a high Weibull Modulus m. The analysis described above assumes the flaws fit a Cauchy distribution but other extreme value distributions may be more appropriate in which case a similar analysis can be carried out and the appropriate equation derived for size effect correction.

4. Mixed Alkali Effect, Ion Exchange and Diffusion in Glasses

4.1 Introduction

Throughout this investigation it was suspected that low strength in glass ceramic fibres was invariably caused by preferential crystallization of the fibre surface rather than the interior. It was thus thought desirable to find some way of supressing surface crystallization. Firstly surface crystallization is likely to occur in most glass systems when there is no effective means of nucleation in the material. This is because surface flaws can act as nucleation sites. Also ions which lower surface energy will segregate to the surface and again increase nucleation rate. Thus nucleation will be preferred on the surface and crystallization will then follow this. To supress nucleation at the surface the rate must be reduced in some way such as increasing the activation energy for ionic transport. In this work it was realised that reduction in nucleation velocity by changing the transport properties of the surface atoms would be the best method to pursue. It was decided then to alter the surface glass composition to this end. The easiest way was to ion exchange K^+ for Li^+ at the glass surface in order to produce a "mixed alkali" glass which possesses a much reduced atomic Li^+ mobility compared to the single alkali glass. In the following sections there is a review of relevant papers dealing with mixed alkali effect, ion exchange and diffusion.

4.2 Mixed Alkali Effect

When a second alkali oxide is added to a glass marked property changes come about commonly referred to as the "mixed alkali effect". The properties effected by the introduction of the second alkali ion are

1. electrical conductivity
2. dielectric loss
3. viscosity

4. chemical durability

5. alkali diffusion

6. internal friction

These property changes are more than one would expect from the compositional changes and an example of this effect on electrical resistivity can be seen in fig. 4.1[51] As can be seen the position of the maximum is not usually located at the composition where both ions are present in equal proportions also the magnitude of the effect is a function of the size difference of the ions present. The position of minimum conductivity correlates well with the change in mobility of the more mobile ion as can be seen in figure 4.2[52].

Thus if the mobility of the more mobile ions is reduced in such a glass and the development of lithium disilicate nuclei is dependent on the mobility of the Li^+ ion then the presence of a larger cation such as K^+ would be expected to slow the nucleation rate down.

4.3 Ion Exchange

Ion exchange seemed the most logical method of achieving a mixed alkali glass at the surface of the fibres thus some consideration is given here to previous research in this field.

Ion exchange in glasses was used to a large extent in the early sixties as a strengthening mechanism[53,54,55]. The exchange was effected by means of a molten salt bath. This produces a "crowding effect" in the glass surface as shown in fig. 4.3. producing a compressive surface layer. Kistler[54] recorded surface compressive stresses of up to 860 MN/m^2 in microscope cover slips ion exchanged with K^+.

Ion exchange has been employed to strengthen glass-ceramics[56] but here the surface stress is caused by a transformation in crystal structure

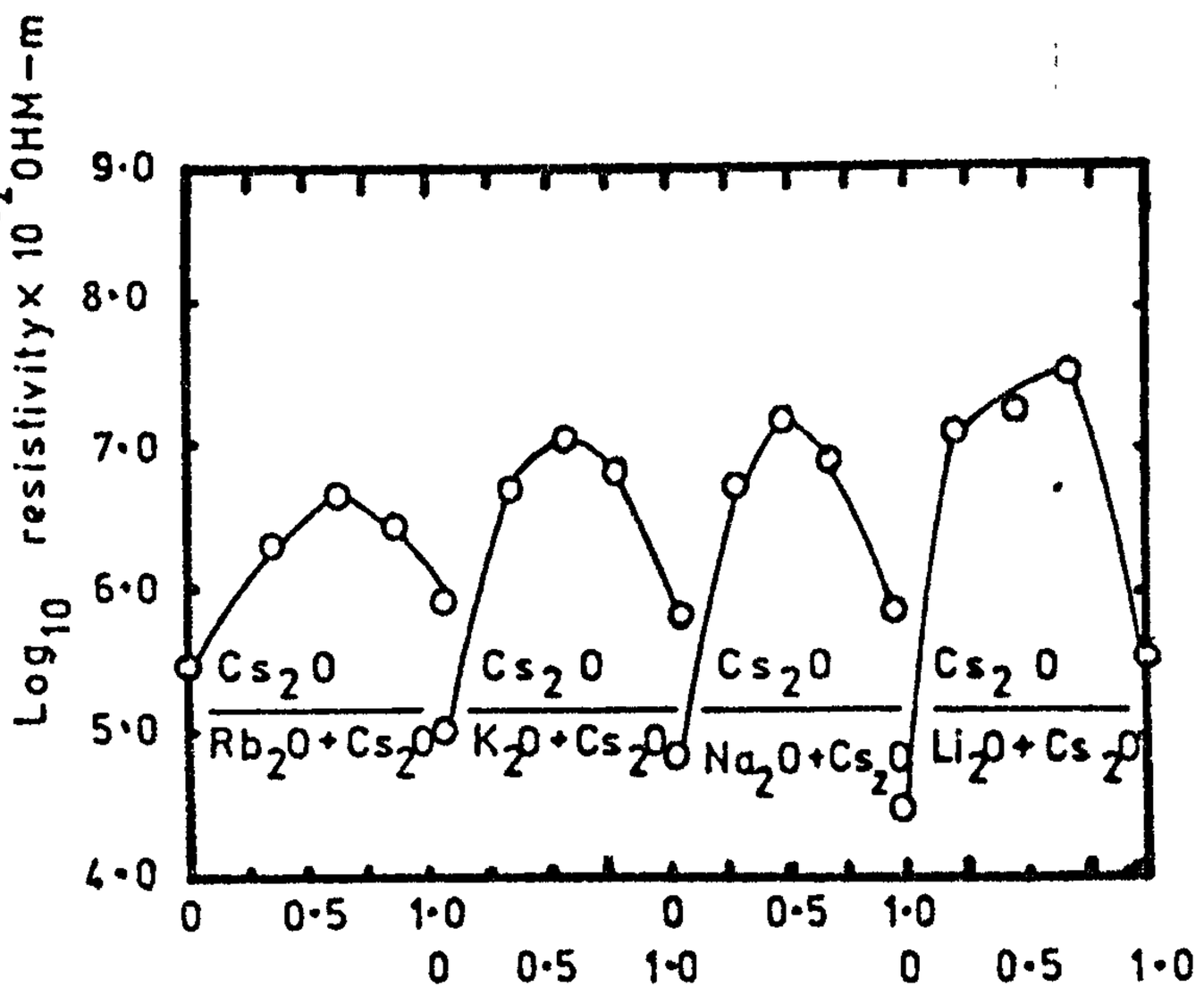

FIG 4·1 Resistivity isotherms at 623 K.

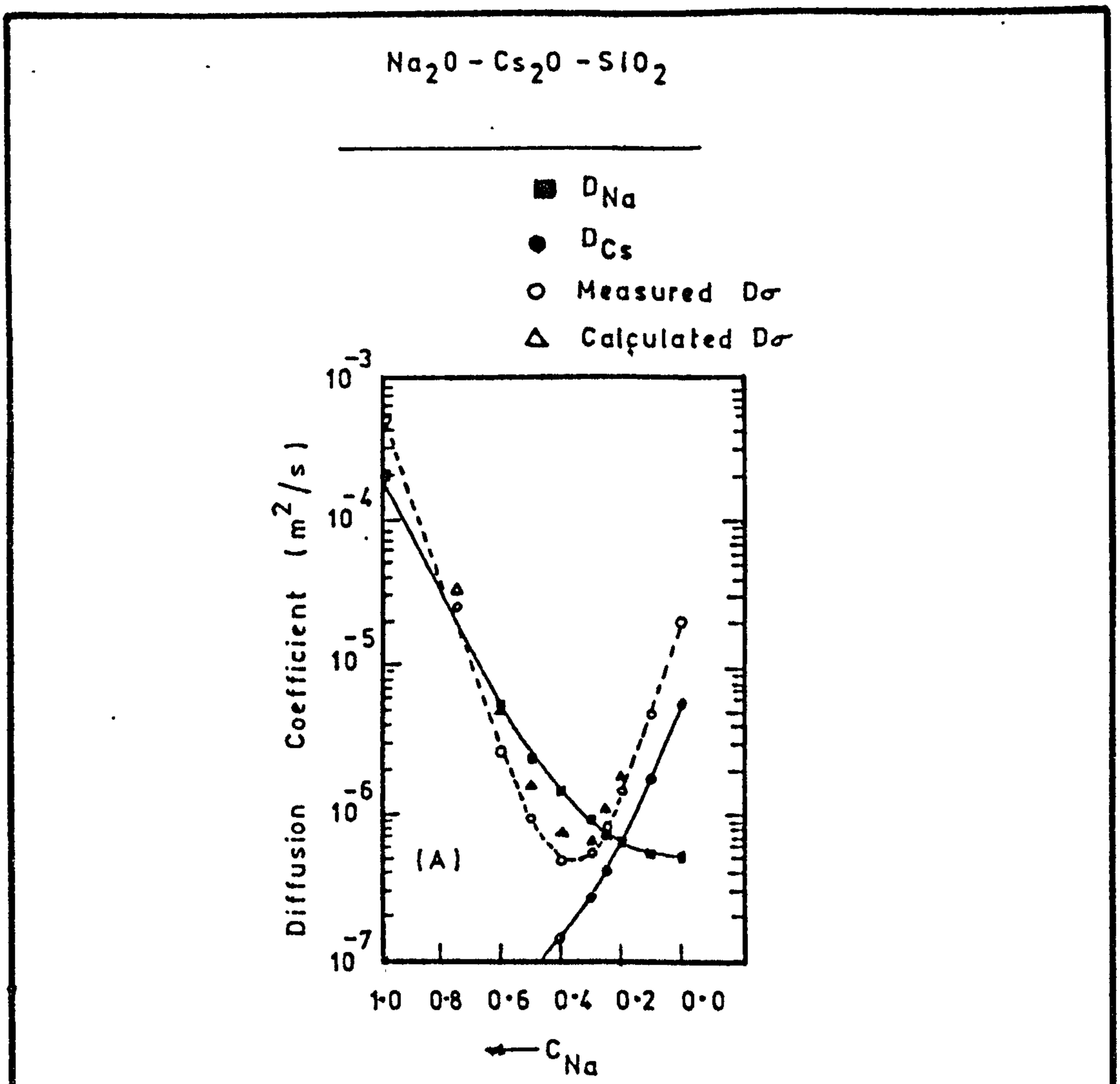

Fig 4·2 Alkali diffusion at 753K

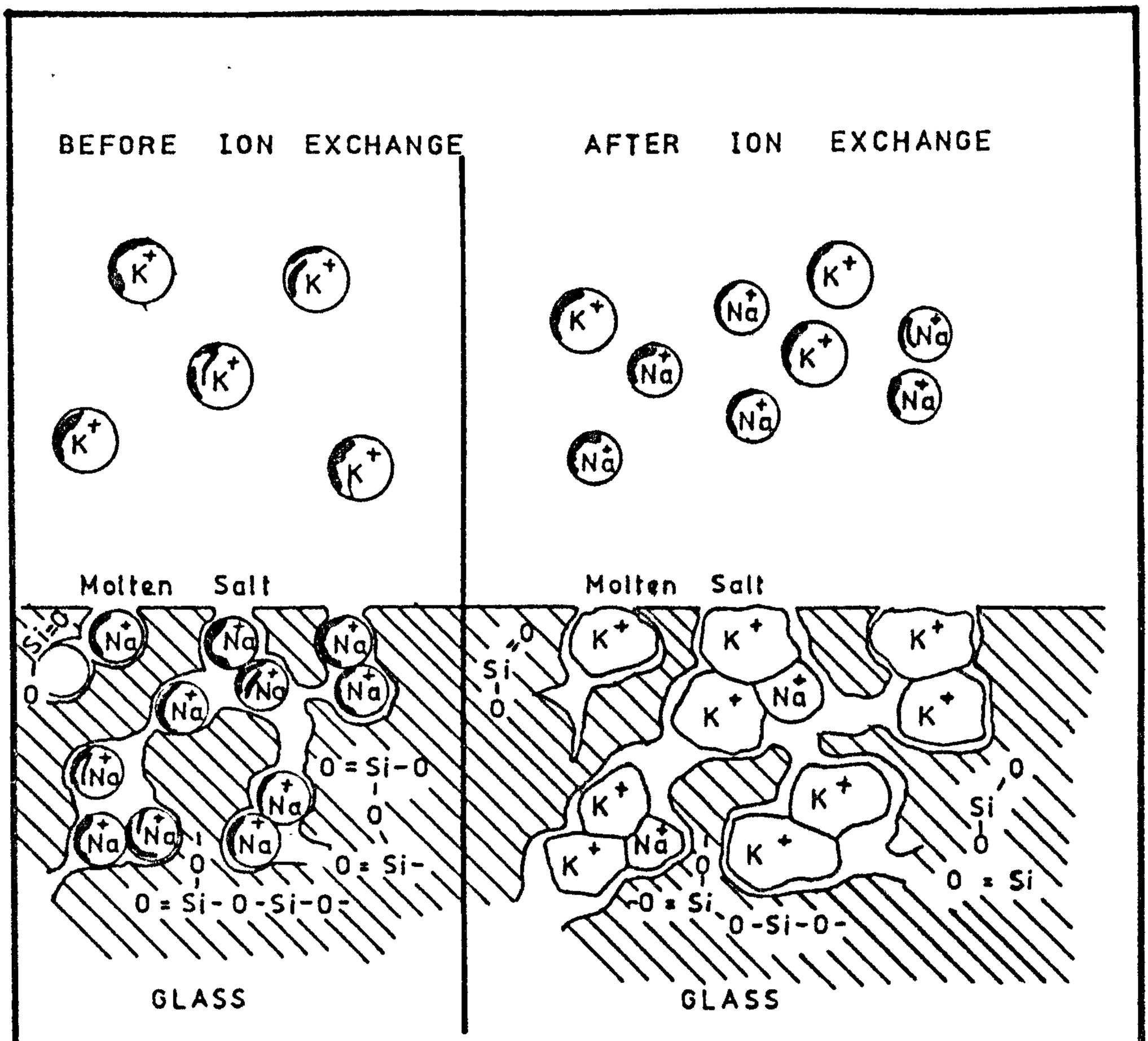

Fig 4·3 Crowding from low - temperature exchange of K^+ for Na^+ ions.

brought about by the presence of the exchanging ion.

Ion exchange is, however, not a simple one for one exchange mechanism. The kinetics of exchange and resulting profile of concentration of exchanging ion through the glass is a function of several variables and has been investigated by many workers. Ion exchange is usually performed by placing the glass in contact with a molten salt of the exchanging ion but an aqueous solution can also be used in certain cases. Thus an equilibrium is established between the ions in the glass and the medium:

$$A_{(g)} + B_{(s)} \rightleftharpoons A_{(s)} + B_{(g)}$$

A,B = cations

s,g = medium and glass.

The distribution of ions is given by a distribution coefficient K which can be derived thermodynamically in terms of the activities of the ions.

If the glass is held in contact with the exchanging medium for some time the exchanged ions at the surface will diffuse into the glass and establish a concentration profile. This diffusion process can be described by a diffusion equation of the form

$$\frac{\partial c}{\partial t} = \frac{\partial}{\partial x} \left(D \frac{\partial c}{\partial x}\right) \qquad (4.1)$$

to which many solutions have been derived[57] for D = a constant or D = a function of concentration. The main problem in the case of ionic diffusion in glass is the derivation of the correct diffusion coefficient. The tracer diffusion coefficient has been measured by numerous investigators for various glass systems and ions, but often little agreement is found between their results. It has been suggested[58] that even the presence of atmospheric moisture during diffusion annealing has a profound effect on the results. The diffusion coefficient has also been derived

from conducitivity measurements made on glass; the relationship being given by the Nernst-Einstein equation

$$\sigma = \frac{Z^2F^2DC}{RT} \qquad (4.2)$$

where σ = electrical conductivity

Z = the ionic charge

F = the Faraday

D = the diffusion coefficient

C = ionic concentration

R = the gas constant

T = the absolute temperature

The equation given above does not give an accurate value of diffusion coefficient unless modified by a correlation factor "f" which is a parameter representative of the actual diffusion mechanism involved and which has been the attention of much research[59, 60]. Table 4.1 lists correlation factors for various glass compositions. Phase separation is also known to have an effect on the diffusion of alkali ions in glass. Frischat[60] has modelled diffusion in such glasses by considering two simultaneous diffusion processes to occur and assigning a separate diffusion coefficient to each phase. This enabled him to compute a diffusion profile by superimposing the two processes and his computer curve fit is shown to give good agreement with the experimentally determined concentration values in fig. 4.4. Svanson and Johansson[61] proposed that in Li_2O/SiO_2 glasses Li^+ ions are distributed in the glass in two ways

(a) in Li^+ rich clusters

(b) in the SiO_2 matrix

each having its own activation energy for diffusion. Thus it is possible to obtain the self diffusion coefficient in a single alkali glass despite inhomogeneity, however, the presence to the second alkali ion in the mixed alkali glass will also effect the activation energy necessary for the ion

TABLE 4.1 CORRELATION FACTORS OF VARIOUS GLASS SYSTEMS

System	Alkali content (mol %)	Temperature K	Correlation factor
$Na_2O - SiO_2$	20.0	573 - 973	0.3
	20.0	688	(0.63)
	13.0 - 30.0	623 - 743	0.37-0.52
	33.3	373 - 523	0.25
	33.3	373 - 773	0.5
	10.0 - 33.3	473 - 723	0.15-0.38
	17.4	621 - 719	0.37-0.5
	25.0	623 - 823	0.5
	33.3	1173 - 1673	0.4
	24.0 - 33.3	1173 - 1573	0.28-0.46
$K_2O - SiO_2$	20.0	688	(0.26)
$Na_2O - CaO - SiO_2$	15.5	623 - 1273	0.3-0.5
	16.6	543 - 873	0.40-0.46 (glass)
			0.43-0.65 (crystal)
	10.0 - 16.7	473 - 723	0.2-0.4
$Na_2O - Al_2O_3 - SiO_2$	13.0	573	(0.27-0.8)
	28.6 - 33.3	373 - 523	0.2-13.0
	30.0	373 - 523	0.49-1.3
	30.0 - 33.3	373 - 773	0.5
	11.01 - 15.70	473 - 773	0.34-0.73
	20.0 - 33.3	473 - 773	0.15-0.3
Na_2O $CaO - Al_2O_3 - SiO_2$	5.0 - 20.0	473 - 773	0.17-0.45
Na_2O RO - SiO_2 (R = Li,K,Mg,Ca,Sr, Ba,Zn, Cd,Pb,La)	16.0 - 21.0	473 - 723	0.14-0.33

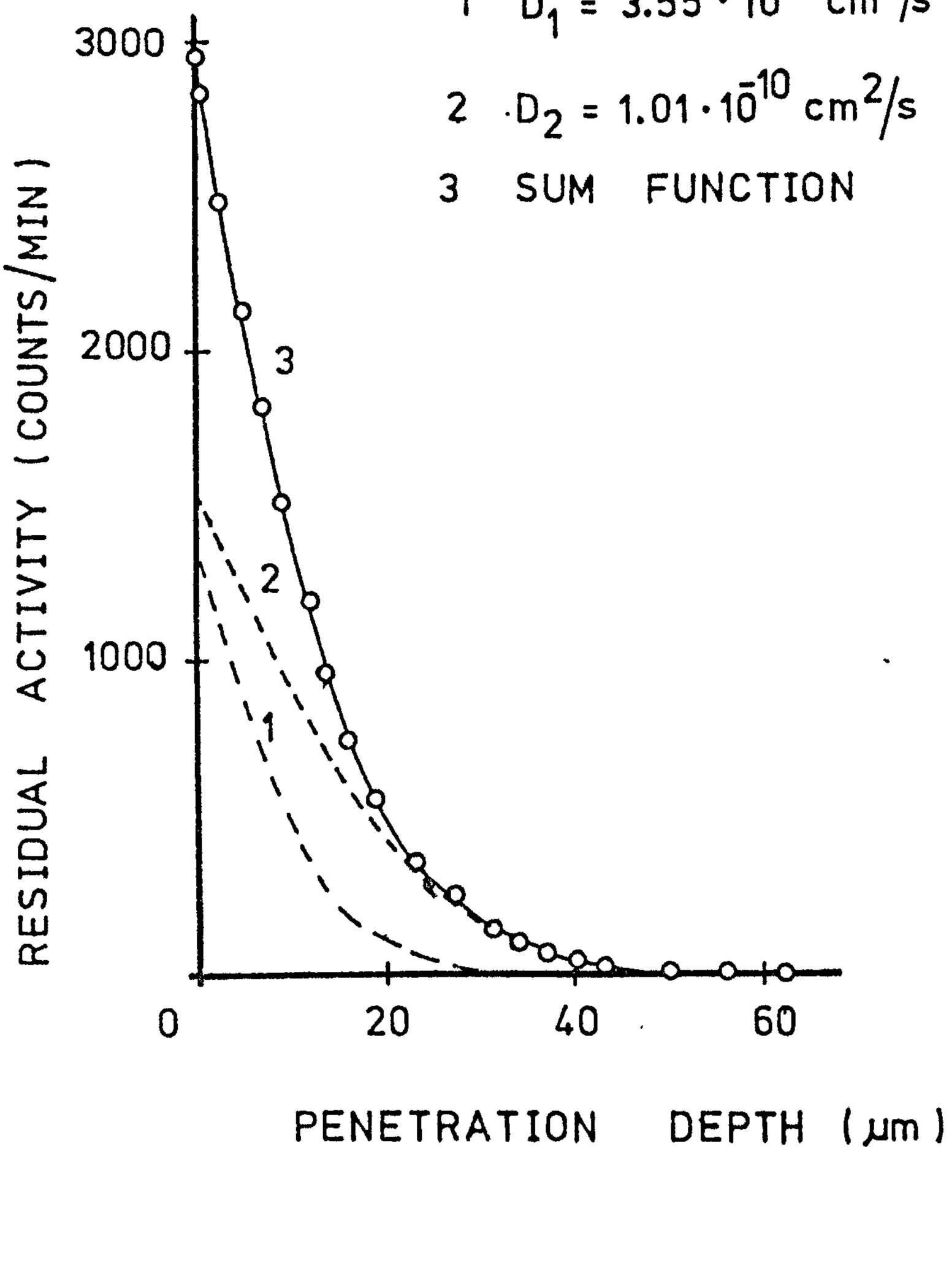

Fig 4·4 Computer least squares fit of the diffusion profile in the phase separated glass assuming two superimposing processes.

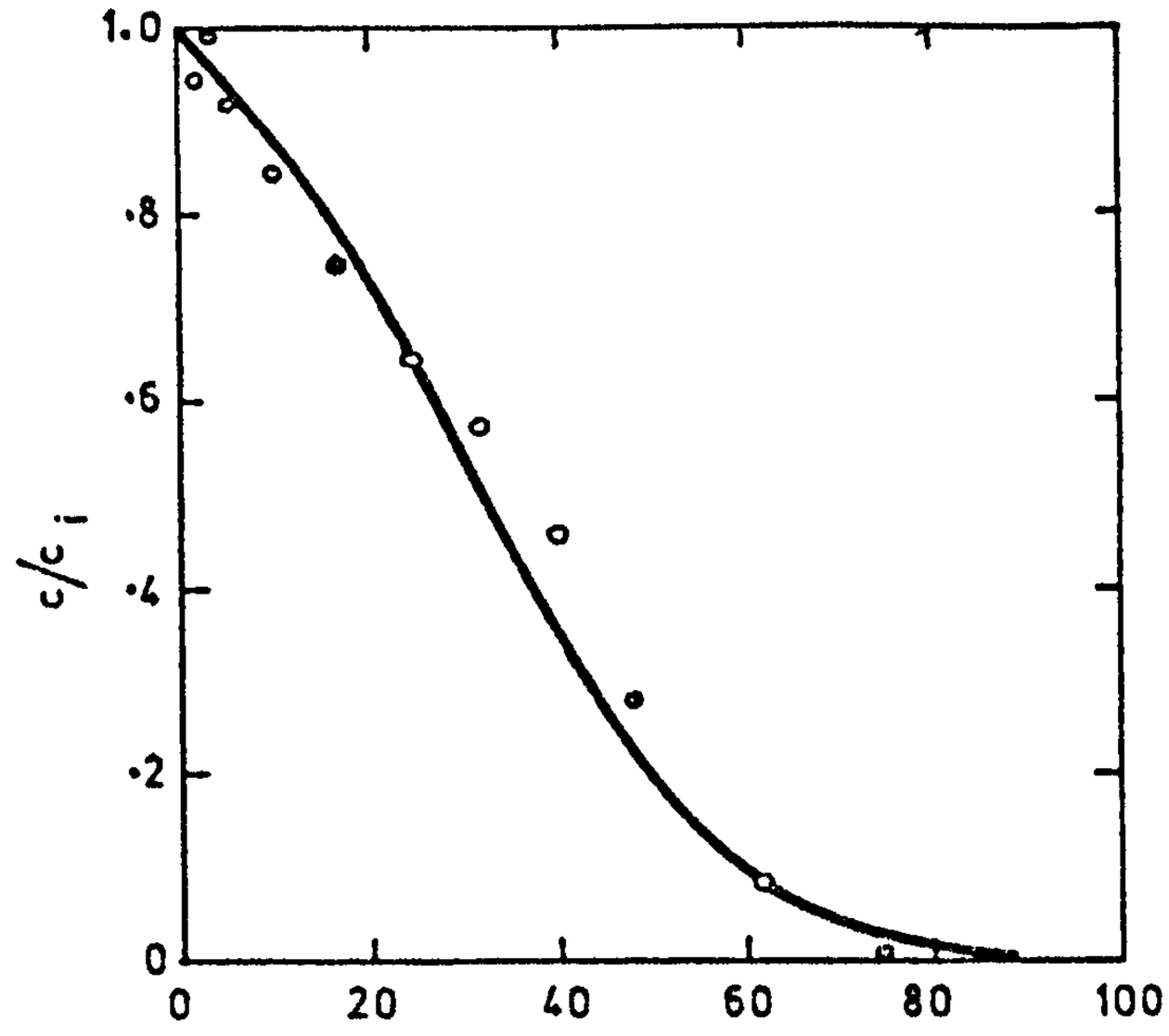

Fig 4·5 Profile of silver that diffused from a silver nitrate melt into a soda-lime glass Line for $D_{Na}/D_{Ag} = 10$.

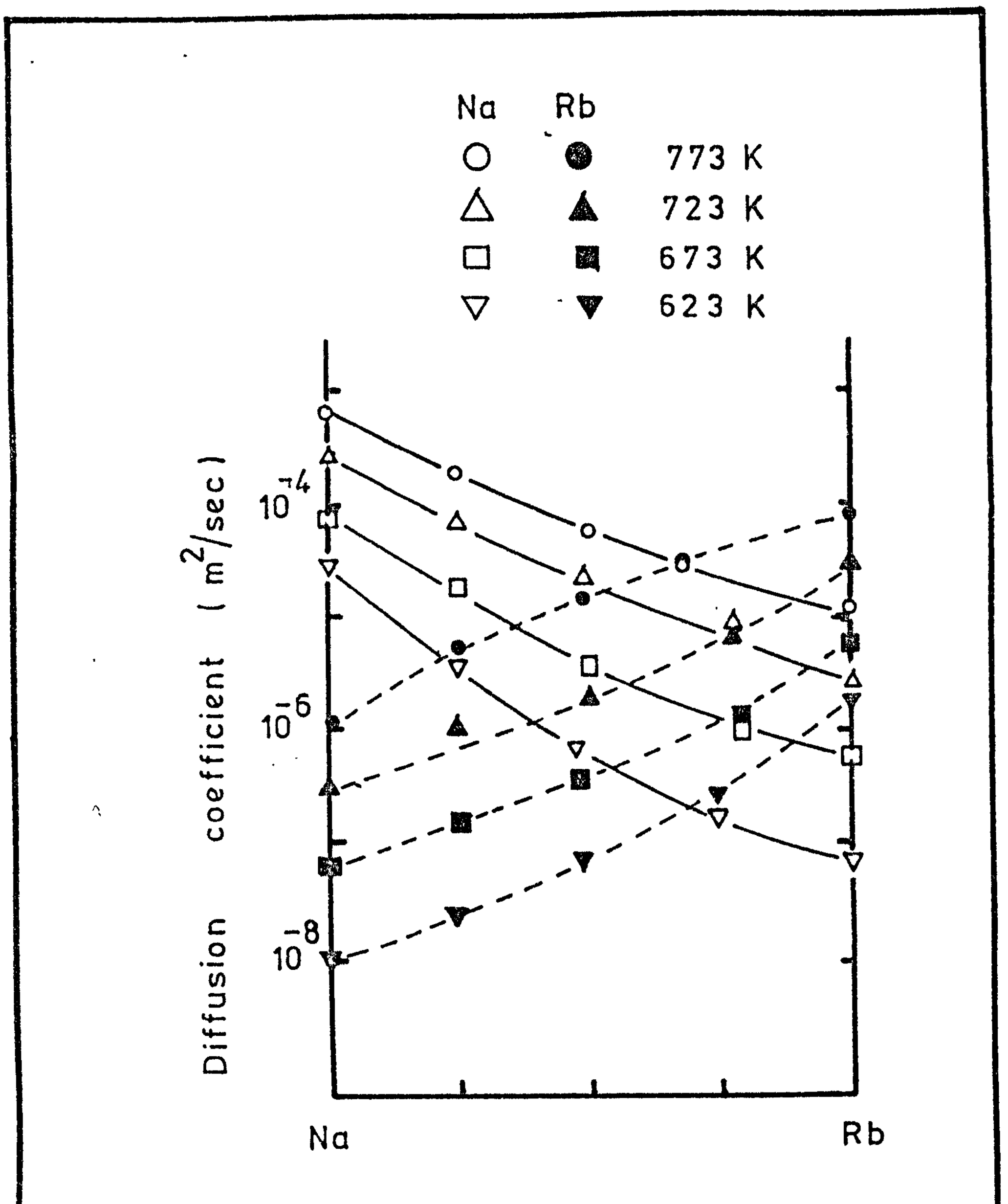

Fig 4·6 Self - diffusion coefficients of Na^+ and Rb^+ ions at various temperatures.

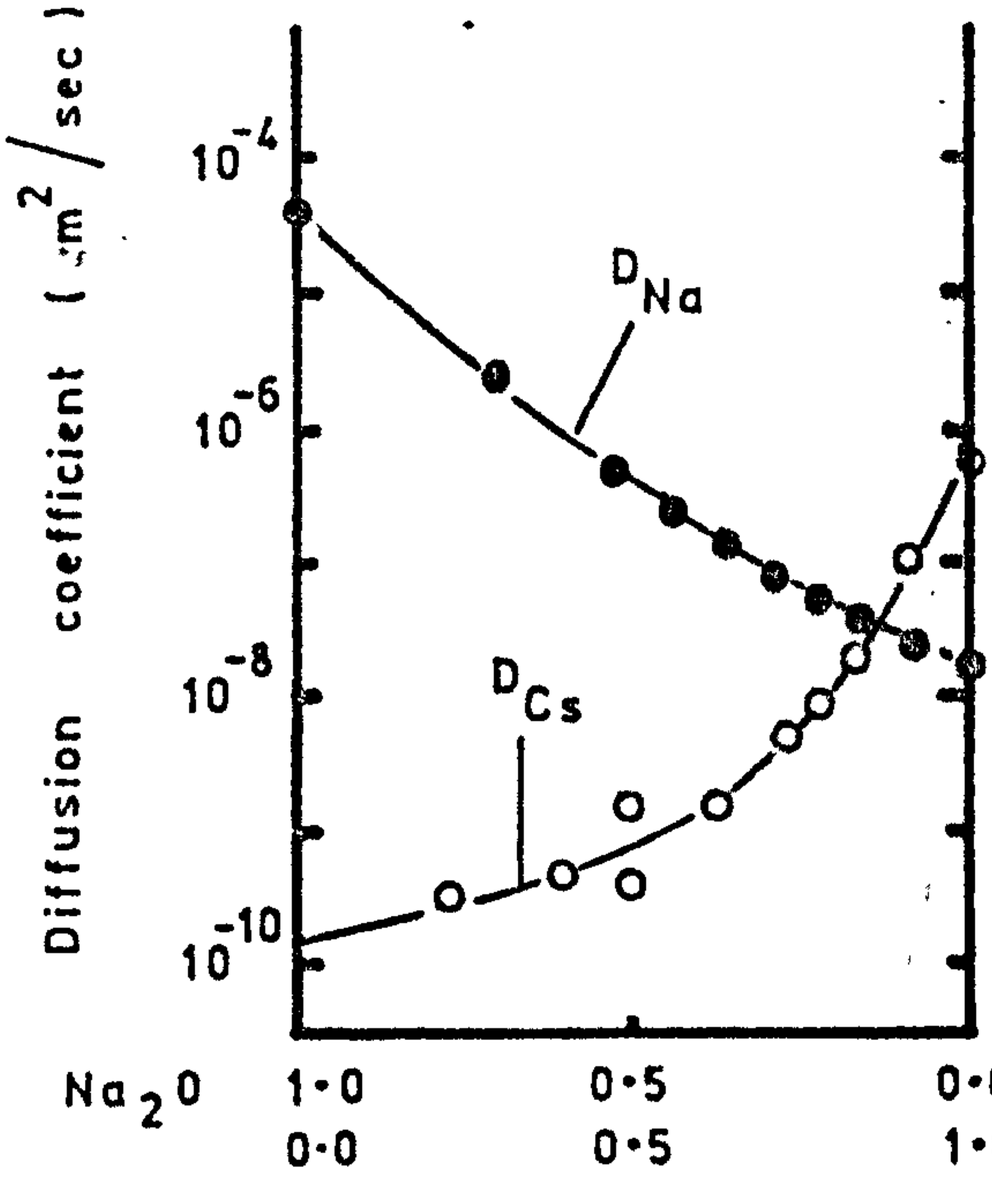

Fig 4·7 Variation of D_{Na} and D_{Cs} at 673 K

to diffuse. Essentially each ion will have a different mobility owing to the size difference. The tendency for the smaller ion to outrun the larger is prevented, however, since to preserve charge neutrality the ionic fluxes must be the same. The mobility of each ion U can be related to its tracer diffusion coefficient by the Einstein equation

$$U = \frac{D}{RT} \tag{4.3}$$

hence an expression for the interdiffusion of ions can be written in terms of their respective self diffusion coefficents which are measurable quantities. So in mixed alkali glass with ions A and B

$$\frac{D_A}{D_B} = \frac{U_A}{U_B} \tag{4.4}$$

Assuming D_A, D_B to be independent of ion concentration Helfferich and Plesset[62,63] solved the diffusion equation for ratios of $\frac{D_A}{D_B} = 10, 5, 2, \frac{1}{2}, \frac{1}{5}, \frac{1}{10}$ and for different specimen geometries. Their results obtained from experiments performed on ion exchange resins showed good agreement with the values expected by solution of the appropriate diffusion equation. Doremus[64] used this data to predict the concentration profile of silver ions in a soda lime glass. The curve shown in figure 4.5 based on a ratio of $\frac{D_{Na}}{D_{Ag}} = 10$ shows a close fit between computed and experimental data. This theory is only a first approximation to the diffusion process in mixed alkali glasses since the ratio $\frac{D_A}{D_B}$ is not always a constant and can be a function of the alkali ion ration $\frac{C_A}{C_B}$. For instance the work of McVay and Day[65] has shown the ratio of $\frac{D_{Na}}{D_{Rb}}$ in $Na_2O/Rb_2O/SiO_2$ glass is certainly not constant over the range of alkali ion ratios and can be seen in fig. 4.6. This has also been shown by Terai[66] fig. 4.7.

The diffusion mechanism in such glasses is thought to be very complex since during ion exchange the structural homogeneity of the glass is lost when diffusion takes place above the transformation temperature.

5. Experimental Procedure

5.1 Glass Batch Preparation

The furnace available for glass batch preparation was a Carbolite box furnace capable of operating continuously at 1750 K and for short periods at 1773 K. This imposed limitations on the glasses which could be prepared and thus the less refractory systems were investigated. All reagents used in batch preparation were "Analar" grade chemicals of known purity. The source of silica was Brazilian quartz which was thermally shocked to reduce it to fragments. It was then acid washed and ground to 240 mesh size in an automatic mortar and pestle. This powder was again washed in dilute acid (HCl) to remove iron and other impurities. Finally the quartz was washed several times with water and dried in a warm air oven. This was then sieved and the material with mesh size smaller than 240 used in glass batch preparation. Typical batch sizes were 250 g. All ingredients were weighed to an accuracy of $\pm$ .005 g then they were charged into a ball mill and milled with alumina balls for periods of up to one day. In certain cases reagents were added in the form of a slurry with water. The slurry would then be dried and further ball milled. This method was particularly suitable for homogeneously dispersing small additions of salts. The batch was then transferred to a 250 ml platinum crucible and introduced into a Carbolite glass melting furnace. Where batches contained carbonates they were preheated at 1123 K to decompose the carbonate slowly. Generally the lithia/silica glass compositions were melted at 1713 K for periods of four hours. Whilst higher temperatures would have been desirable from the point of view of homogeneity chemical analysis of the resulting glasses fired above 1773 K showed loss of lithium. This was thought to be due to volatilization of the oxide during firing. After a four hour firing the crucible was removed from the furnace and the glass poured into iced water in a stainless steel bucket. To ensure homogeneity this glass was further ground and then refired at the same melting temperature for four hours. The glass was stored in

desiccator cabinets. Where flat glass samples were needed, molten glass was pressed between two stainless steel plates.

Samples of each batch were analysed chemically. In the later part of this work the analysis was carried out in the Department of Chemistry (Analytical Services) at Liverpool Polytechnic but many of the earlier batches were analysed by G. Watson Gray (Analysts) Ltd., Dale Street, Liverpool. Some samples were also subjected to X-ray diffraction to ensure that no crystallization had taken place during cooling.

Flat glass samples were always annealed after pressing by transferring the plates quickly to a box furnace heated to the annealing temperature, then left for periods of 4 to 12 hours after which they were cooled slowly at the natural rate of the furnace. Table 6.1 lists the compositions prepared for investigation together with the chemical analysis on the prepared glass.

5.2 Preparation of Fibres

The ability of a glass to be drawn into fibres depends very much on

(a) The viscosity/temperature characteristics

(b) The crystallization velocity at the drawing temperature.

Some insight into the glass's suitability for fibre drawing was gained by simply holding a piece of the glass in a bunsen flame and pulling when hot to produce a fibre. Glasses which would not draw easily were deemed unsuitable for the method of fibre preparation described below and were given no further consideration.

Large quantities of fibre were required for this project so it was decided to use a single tip bushing technique similar to the method employed for fibre production on a commercial scale.

A single tip platinum bushing as shown in figure 5.1 was used for fibre production. The bushing was heated by the passage of a heavy current through the two side lugs. The bushing was encapsulated in refractory cement with

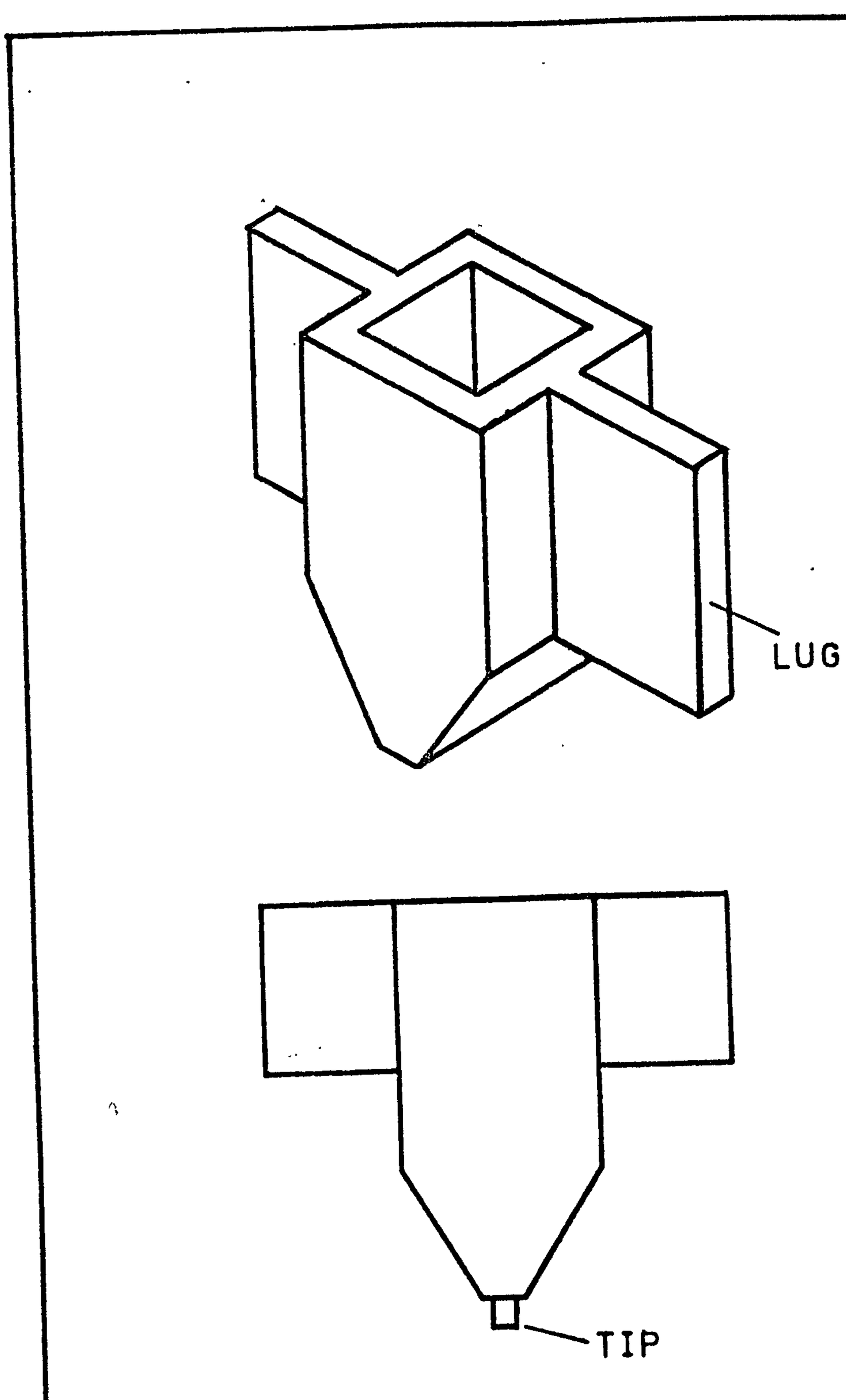

FIG 5·1 Single tip platinum bushing

two thermocouples mounted near to the tip of the bushing. The bushing was supplied by Pilkington Brothers who established the optimum tip dimensions by performing viscosity tests on the two glasses of interest.

The bushing was clamped by the lugs into water cooled copper blocks which in turn were bolted to two air cooled bus bars. The bus bars were connected to a West transformer capable of supplying 3000 A at one of three voltages i.e. 1.1v, 1.5v and 2v. The voltage could be adjusted on the front of the instrument. Fig. 5.2 shows the schematic arrangement of the apparatus and plate 5.1 a photograph of the actual rig. To achieve accurate temperature control the signal from thermocouple T_1 was linked to a West-Guardian proportional controller used to control the supply to the primary coils and thus the current in the secondary coils. When operating directly in proportional mode the controller allowed primary current to flow when the thermocouple was below the set point temperature then cut off as the temperature rose above set point. This is the normal mode of operation if used for instance to control a furnace. This, however, was found to be unsatisfactory since the sudden surge of current from the secondary coils caused the bus bars to jerk sideways due to the magnetic fields associated with such high current. Often this "shock" would cause the fibres to break. To overcome this erratic control the set point control was moved a few degrees above the required temperature then the power control was reduced so that there was just insufficient power to achieve set point. Thus the current was supplied continuously and by adjusting set point and power the bushing could be made to reach a steady temperature within a few degrees of the desired value. Checks were made using a Telsec chart recorder connected to thermocouple T_2 and control better than $\pm$ 2°C was achieved this way.

FIG 5·2 FIBRE DRAWING APPARATUS

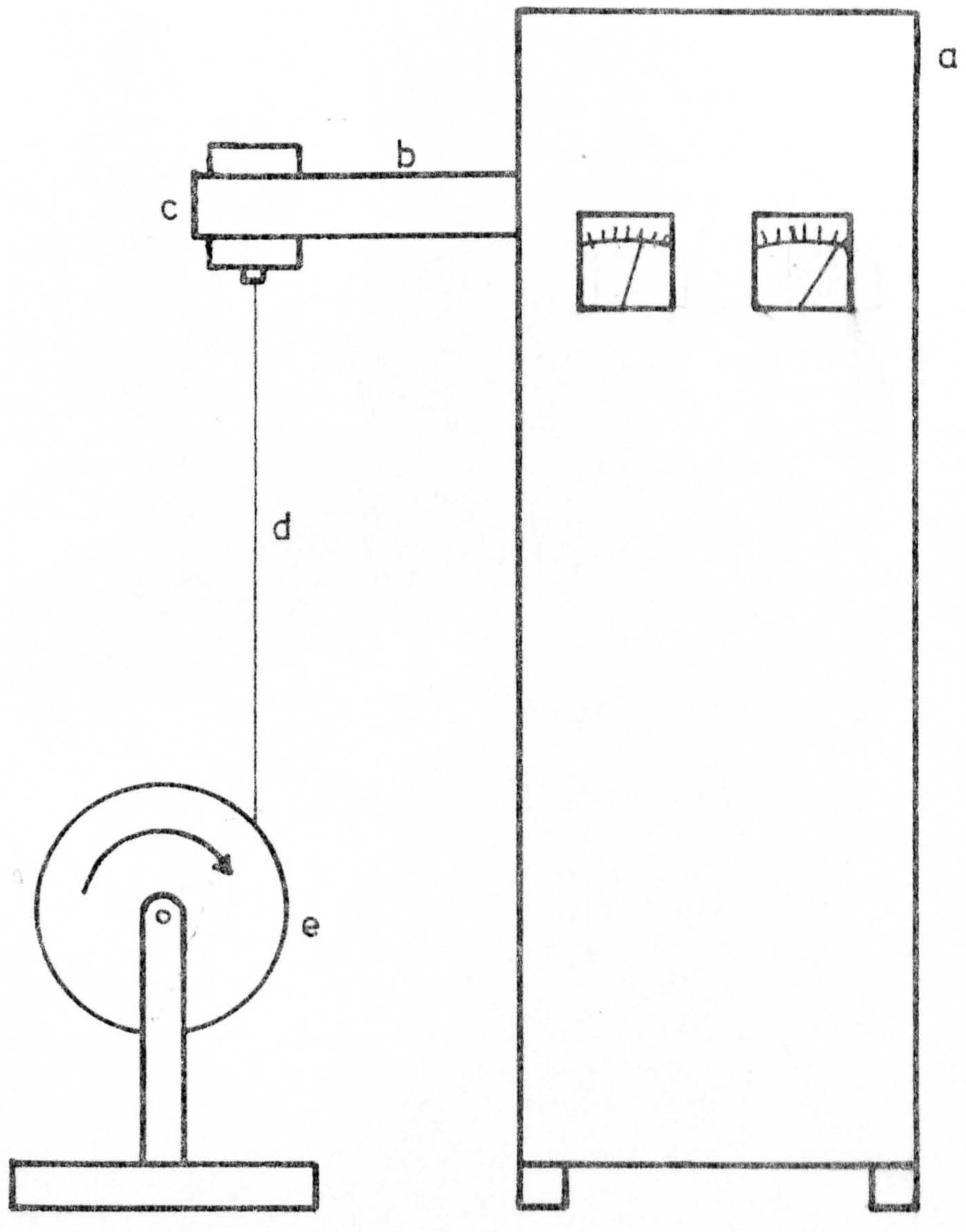

a = 6 KVA TRANSFORMER 3000 A AT 1·1 V

b = AIR COOLED BUS BARS

c = PLATINUM BUSHING ENCASED IN REFRACTORY CEMENT

d = THE GLASS FIBRE

e = ROTATING DRUM

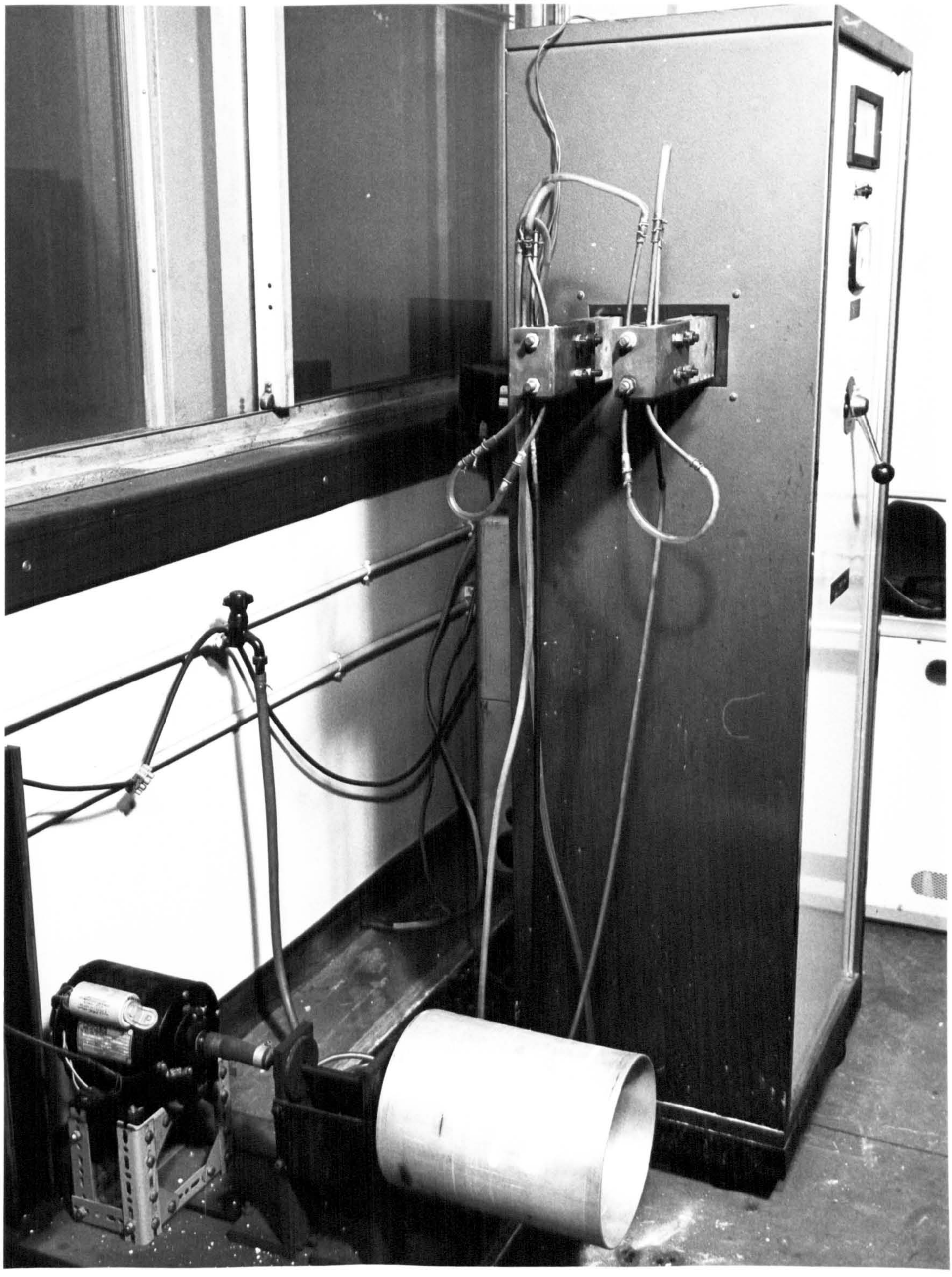

Plate 5.1 Fibre Drawing Apparatus

Glass frit was placed in the bushing which was quickly brought up to the melting point of the glass. The temperature in the bushing was normally raised above the fibre drawing temperature to lower the viscosity of the glass and allow the air bubbles to reach the surface. This generally took about one hour but the batch in the bushing had to be continually replenished because of loss through the tip. When the glass was as bubble free as possible the temperature was reduced to a suitable value for fibre drawing. This was determined simply by trial and error for each glass. The optimum drawing temperature for Glass A was 1653 K and for B 1620 K.

With some glasses, in order to induce flow through the tip, the first fibre would be drawn at a higher temperature than optimum then the temperature would be quickly lowered to the optimum level. To draw the fibre a thin brass rod was used to pull the drop of glass from the tip down towards a rotating drum; Fig. 5.2. This was done by hand and as the glass drop was pulled down it would form a fibre. The fibre was quickly flicked around the drum and friction caused this to lock so that continuous fibre could then be drawn. The drum itself was made of aluminium (210 mm diameter) and rotated by means of a flexible coupling to a 240 v $^{1}/_{4}$ H.P. motor capable of a maximum speed of 1400 r.p.m. A rheostat was included in the motor circuit which gave a rough degree of speed control and speeds were measured by pushing a hand held revolution counter against the drum.

Theoretically the speed of fibre drawing is supposed to have little influence on the fibre diameter, this being governed by

(a) the tip diameter,

(b) the head of glass in the bushing,

(c) the temperature of drawing.

In this investigation, however, the drawing speed was found to have a great influence on the fibre diameter in all cases. This enabled fibres of various thicknesses to be made by simply controlling the speed.

This technique of fibre production was dependent to a large extent on operator skill and practice was required with each glass before successful fibres could be drawn, however, once the skills were developed it was possible to draw fibres continuously on the drum for periods of up to an hour. It was essential throughout this operation to keep a constant head of glass in the bushing and this was achieved by simply topping it up from time to time. Knowing the drum speed the time required to produce a given size of fibre tow could be estimated. The drum was then moved a small distance to enable a further tow to be wound on. It was not necessary to stop the drawing operation to do this. When sufficient tows had been produced the drum was stopped and the fibre tows cut off, placed in plastic bags and stored in desiccators over silica-gel. After adequate quantities of a particular glass fibre had been produced as much molten glass as possible was removed from the bushing then the new glass introduced. This was then allowed to melt with the remnants of the previous glass and then removed again. The operation was repeated several times to flush out the old glass. This method was quite suitable if the compositions of the glasses did not differ greatly but when they did there was a risk of contaminating the new glass. In this case the tip of the bushing was sealed off with wax and concentrated hydrofluoric acid poured in then allowed to stand until all the original glass had dissolved away. The acid was then run off and the bushing cleaned with water. Despite precautions this method often caused damage to the refractory cement surrounding the bushing so it was not used unless essential.

Fibres produced under the above conditions had consistent diameters for a given speed and drawing temperature. The fibre diameter of each batch was measured using a Vickers image shearing eyepiece on a Vickers metallurgical microscope. The magnification of the microscope was 400 times and the eyepiece in this situation gave an accuracy of measurement of $\pm$ 0.10 μm. The eyepiece was calibrated by using a graticule ruled in 10 μm divisions. Fibre diameters and drawing conditions for glasses A and B are given in Table 6.2.

5.3 Fibre Heat Treatment

The fibres were crystallized in a programmed box furnace enabling the rate of increase in temperature to be controlled. The temperature in the furnace was controlled to an accuracy of $\pm$ 1 K up to 823 K. Several arrangements were tried for holding the fibres in the furnace including winding the fibres on a frame to prevent them from touching each other. It was found, however, that this was unnecessary and so the fibres were then heat treated as lightly separated tows about 100 mm in length. These tows were suspended in the centre of the furnace. After heat treatment the fibres were stored in a desiccator.

5.4 Fibre Tensile Testing

A tensile testing machine was designed to enable large batches of fibres to be tested quickly so that a statistical analysis of the strength data could be made. The fibres were mounted by gluing them on cards as shown in fig. 5.3. The gauge length was 58 mm. The cards were punched with holes to enable them to be mounted to the clamps of the machine as shown in fig.5.4. The most suitable adhesive for this purpose was found to be CATACOL 374 FC resin plus CATACOL 368 FC accelerator.

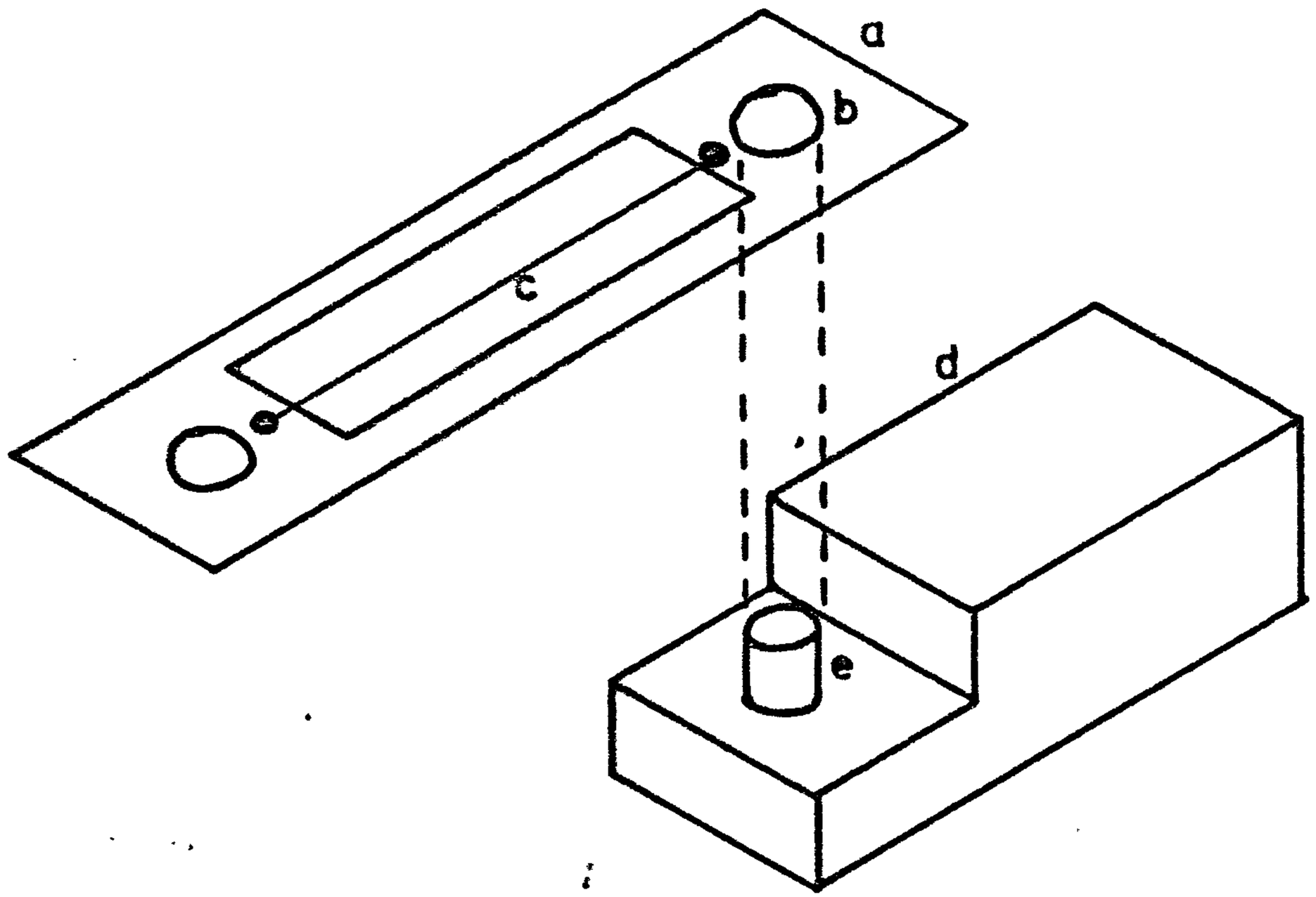

FIG 5·3 FIBRE MOUNTING AND CLAMP

a = CARDBOARD MOUNT

b = HOLE FOR PEG

c = FIBRE GLUED ACROSS CARD

d = SPECIMEN GRIPS

e = PEG FOR APPLYING LOAD

FIG 5·4 TENSILE / TESTING APPARATUS

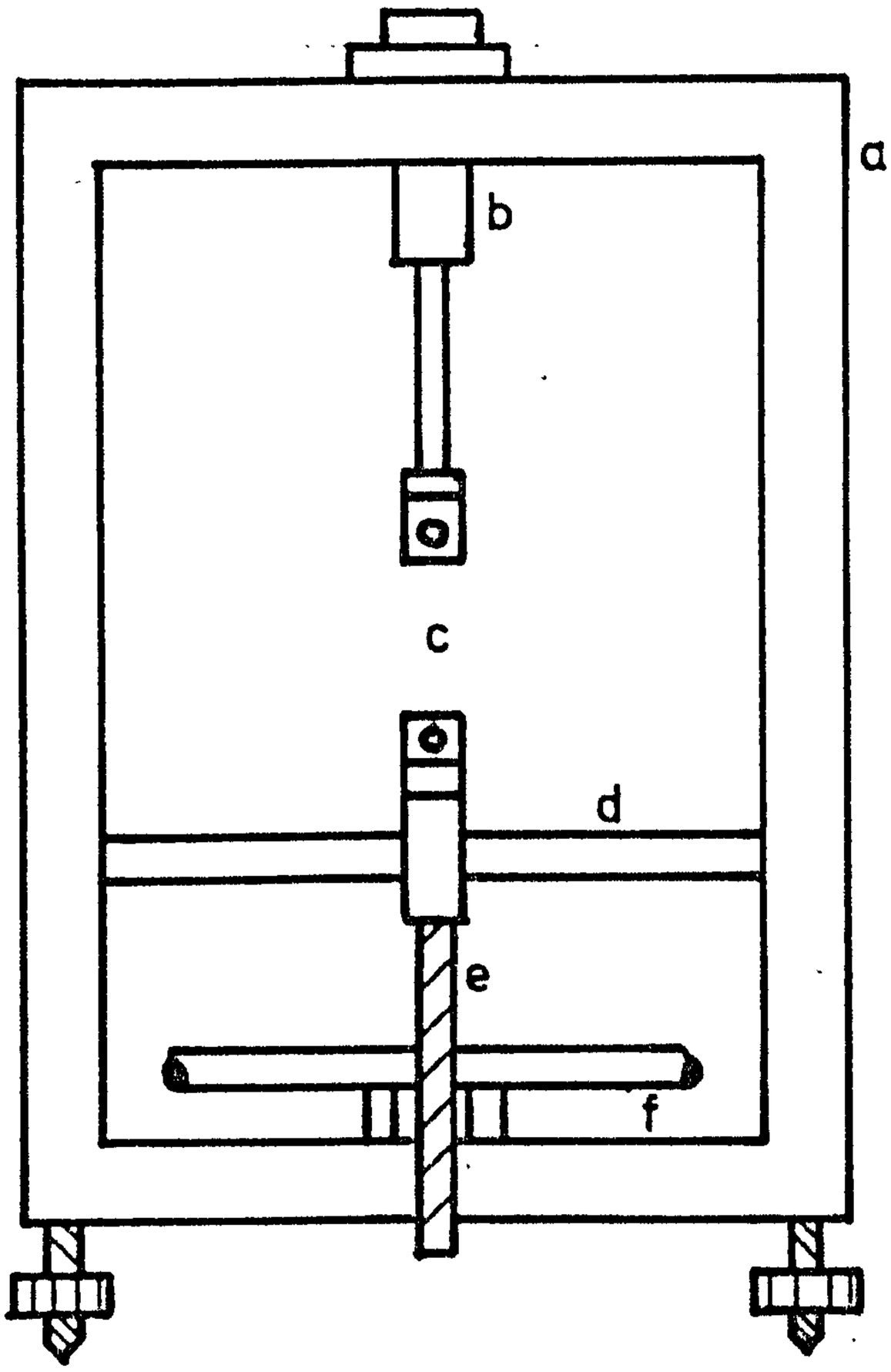

a = FRAME

b = LOAD CELL

c = CLAMPS

d = GUIDE

e = LEAD SCREW

f = WHEEL

The tensile testing machine is shown schematically in fig. 5.4 and plate 5.2. The lower clamp was connected to a drive mechanism giving a strain rate of 0.01 mm per minute, driven by an induction motor. The top clamp was connected to a Schaevitz load cell capable of force measurements up to 10N. This was activated by a CAS 2500 carrier wave amplifier. The load was recorded on a Telsec chart recorder. Once mounted on the clamps the sides of the card were cut away and the fibre loaded to fracture. It was possible to adjust the gain of the transducer amplifier and recorder to record a wide range of loads but because of the variation in breaking load from fibre to fibre it was not possible to select the load range in order to achieve full scale deflection and therefore maximum accuracy of breaking load measurement. Many values, however, fell in the range 0 - 25 g or 0 - 50 g so the instrument was adjusted to give full scale deflection over these ranges. Calibration of the instrument was achieved by hanging weights from the load cell. The scale on the chart paper was ruled in 2 mm divisions from 0 - 200 mm. Whilst this gives a theoretical accuracy of measurement of $\pm$ 1 mm it was possible to estimate to $\pm$ 0.5 mm. To obtain the breaking stress the fibre diameter was measured with an image shearing eyepiece on a metallurgical microscope. Batches of about fifty fibres were tested for each heat treatment.

5.5 Fibre Modulus Testing

A dynamic method was used to measure the elastic modulus since accurate strain measurements are difficult to make on fibres and also expensive. A piece of apparatus was designed and built which vibrated the fibre as a cantilever beam. The apparatus is shown schematically in fig. 5.5 and in plate 5.3. The fibre was glued vertically to the tip of an electromechanical vibrator. The arrangement was enclosed in a bell jar capable of evacuation

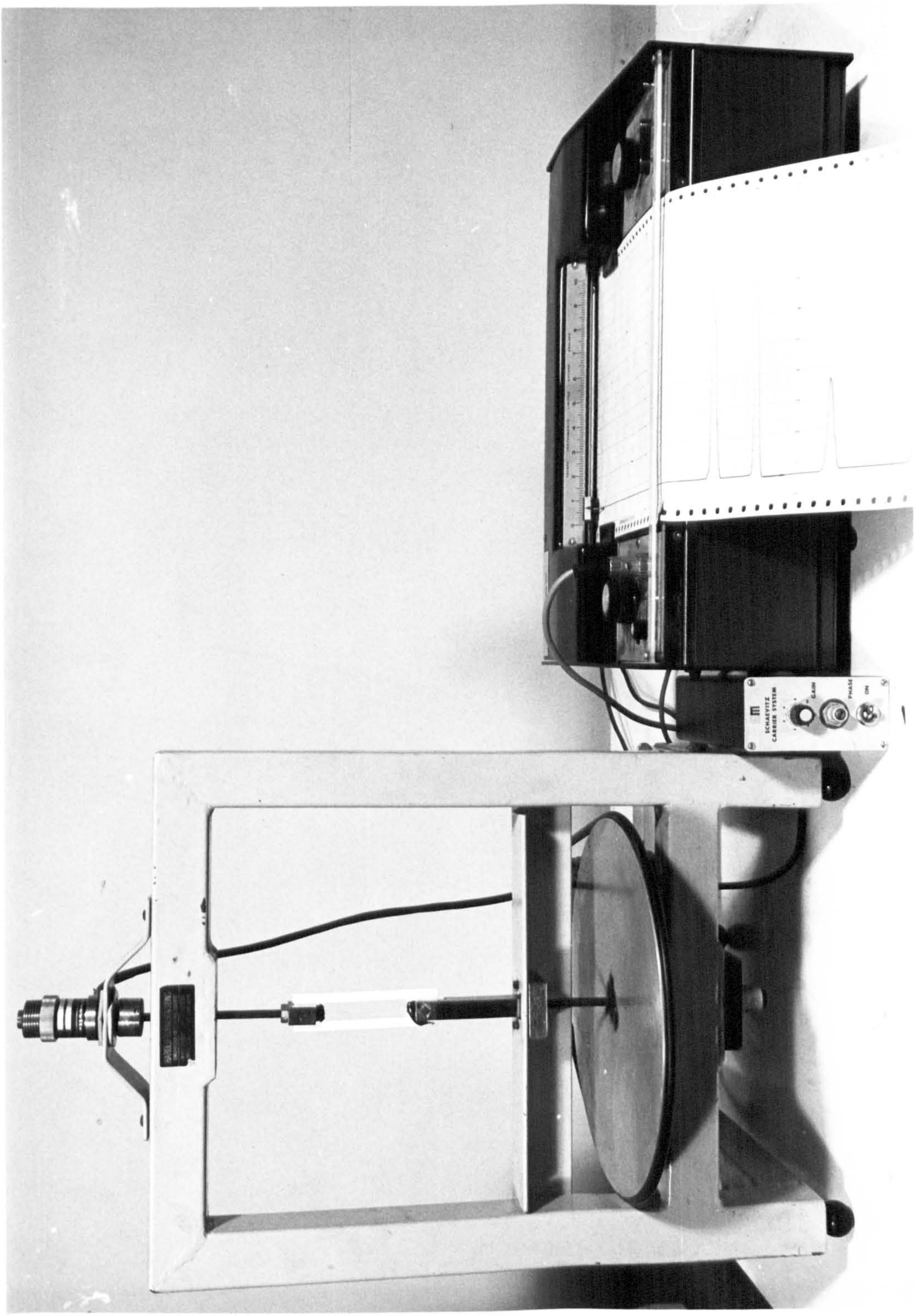

Plate 5.2 Tensile Testing Machine for Fibres

FIG 5·5 ELASTIC MODULUS APPARATUS

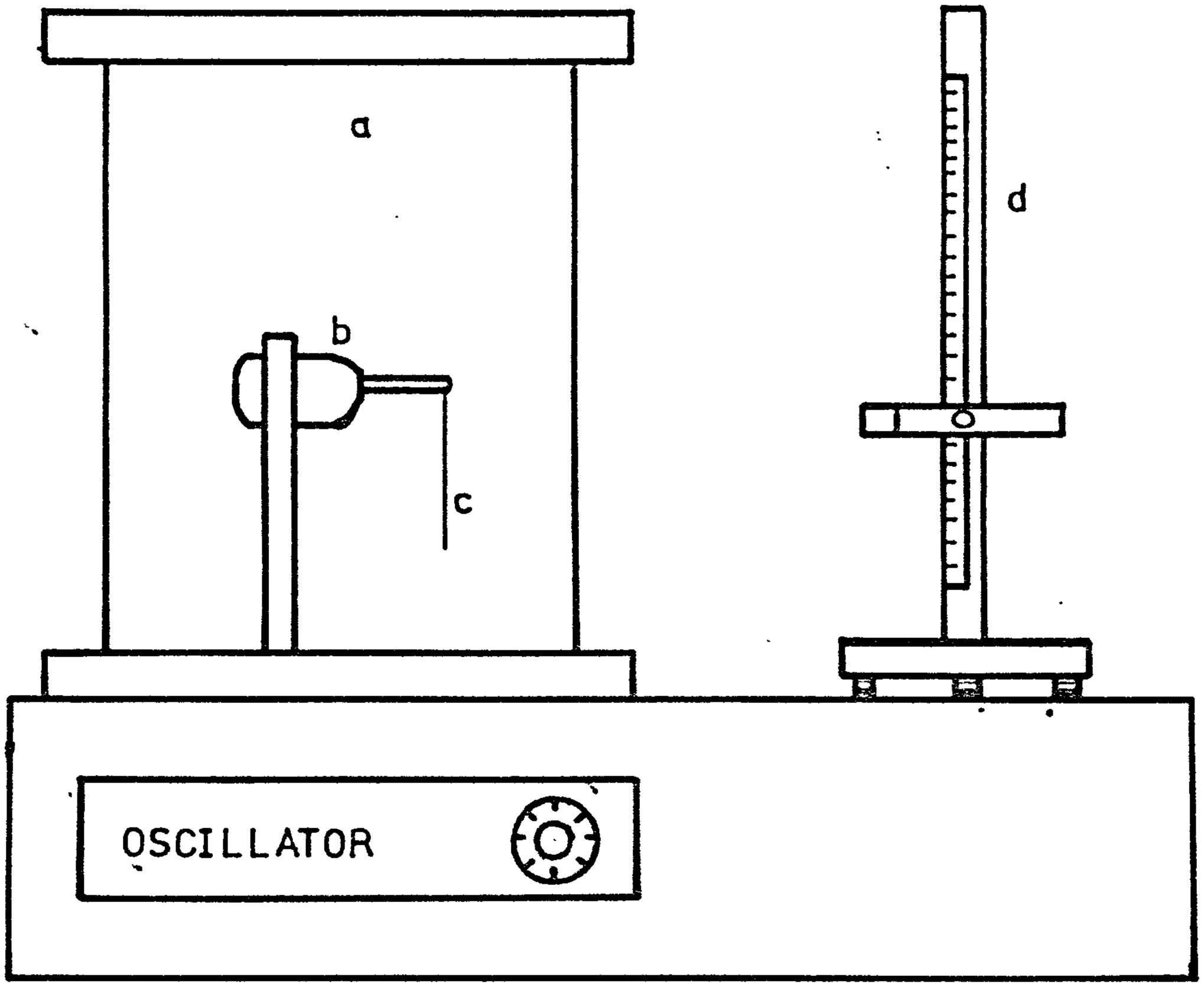

a = EVACUATED BELL JAR

b = VIBRATOR

c = FIBRE ATTACHED TO VIBRATOR

d = CATHETOMETER

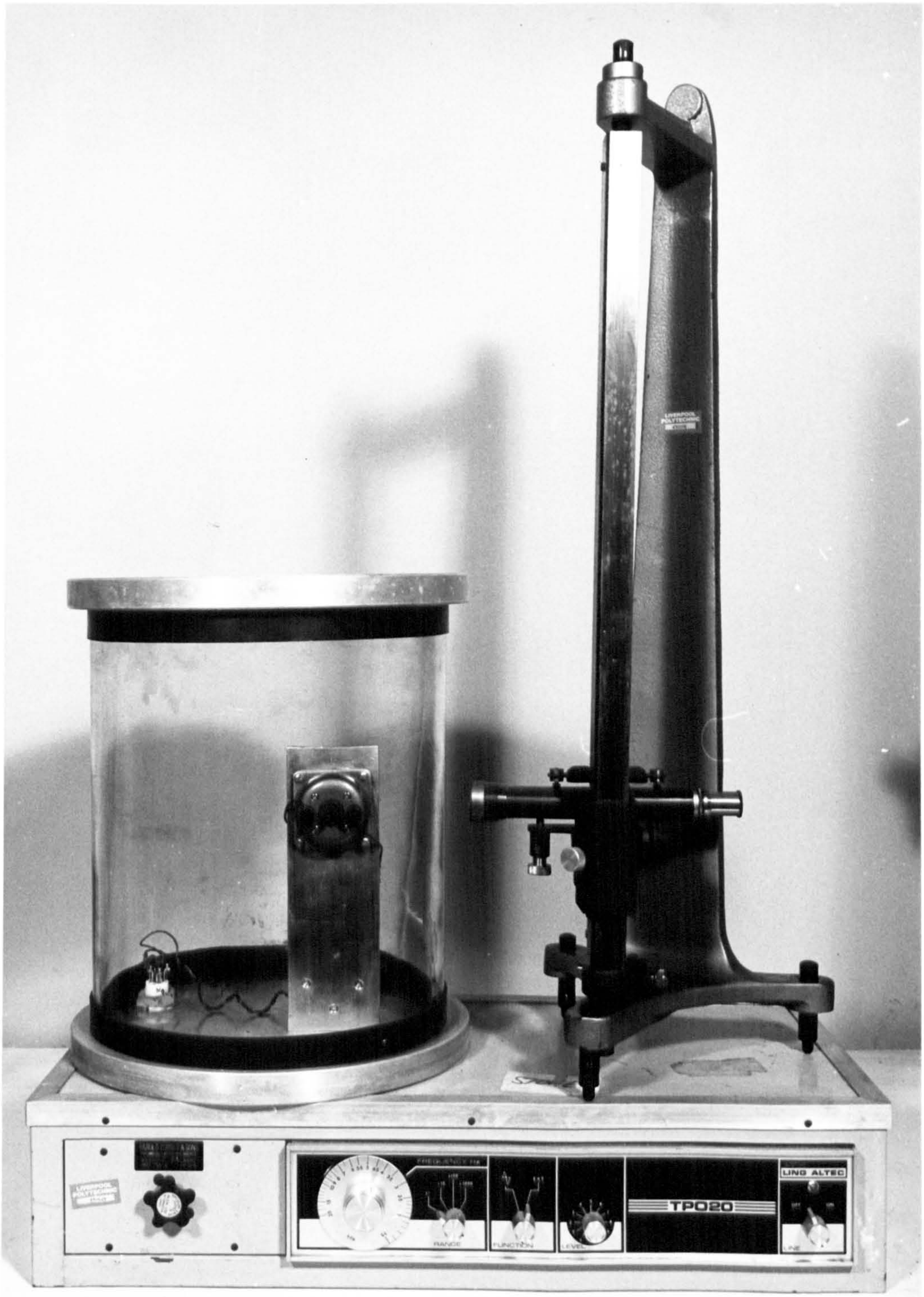

Plate 5.3 Apparatus for the Determination of the Elastic Modulus of the Fibres

to a pressure of 2×10^{-2} Torr. Thus it was possible to eliminate convection and air damping effects. The vibrator was operated by a power oscillator with a frequency range of 1.5 HZ to 25 kHZ. Once evacuated the fibre was vibrated then the frequency increased until the fibre reached resonance. This point could be seen clearly since the fibre adopted a standing wave pattern with clear nodes and antinodes. After noting the frequency of the first harmonic the frequency was increased until the fibre vibrated with the second harmonic. This was repeated for several harmonics to enable a check to be made on the results. The frequency in each case was measured accurately using a timer counter. The fibre length was measured using a cathetometer placed outside the bell jar. The expression relating frequency ω to elastic modulus E at resonance is

$$\omega_n = \beta_n^2 \, l^2 \frac{EIq}{wl^4} \qquad (5.1)$$

where ω_n = the frequency of the n^{th} harmonic

β_n = a constant

I = second moment of area of fibre

l = fibre length

For the fundamental and first four harmonics $\beta_n l$ is

$\beta_n l$	
$\beta_o l$	1.875
$\beta_1 l$	4.694
$\beta_2 l$	7.855
$\beta_3 l$	10.996
$\beta_4 l$	14.137

and the general formula for $\beta_n l$ given by $_n l = (\frac{2n - 1}{2}) \pi \, l$ (5.2)

Apart from the frequency and fibre length the other parameters which had to be determine were the fibre diameter and mass per unit length. The diameter was measured as before using an image shearing eyepiece. The mass per unit length was measured by weighing a known length of fibre. Fibre was wound on the drum for a given time. The drum speed and diameter enabled the number of fibres in the tow to be determined. A measured length of tow was cut and weighed and thus the mass per unit length of fibre W determined:

$$W = \frac{\text{mass of fibres}}{\text{length of fibre tow x number of fibres}}$$

A density gradient column was considered but the toxic nature of the liquids, necessary to determine such high gradients, discouraged its use.

5.6 Examination of Microstructure

It was important to this investigation to try to examine the fibre microstructures resulting from the various heat treatments. Both optical and electron microscopy were used and much time spent in this part of the work, however, the results are somewhat incomplete because of the difficulties experienced in handling fibres of such small dimensions.

The information being sought by microscopy was

1) Crystal size
2) Crystal morphology
3) Intercrystal spacing
4) Volume fraction of crystals

5.6.1 Optical Microscopy

Preliminary investigation with a Vickers Metallurgical microscope (M12a) revealed the limitations of this technique for quantifying microstructural parameters owing to small crystal sizes. For the above reason optical microscopy was limited to simply measuring fibre diameter.

5.6.2 Scanning Electron Microscopy

The scanning electron microscope was the most useful instrument for investigating the structure of these fibres since the specimen preparation was simple.

Many techniques were tried for mounting fibres, and some were better than others. The methods used are outlined below.

(a) Fibres were attached to an aluminium stub in short sections by means of double sided sellotape.

(b) The ends of a short bundle of fibres were embedded in silver DAG; so they were perpendicular to the stub.

(c) Fibres were embeded completely in Metaserv resin then sectioned and a sample of the section glued to the stub with silver DAG.

In each case fibres were coated with gold/palladium to prevent charging. Some fibres were etched in 4% hydrofluoric and others examined without any prior treatment. Attempts were also made to grind and polish fibres encapsulated in resin but often the structure was damaged. The fibres were examined on a Cambridge S4-10 Stereoscan microscope. Fine fibres charged despite the coating. This caused the fibres to move about so many measurements were made on thicker fibres (200-600)μm diameter. A ruled scale was attached to the Stereoscan screen to enable crystal size and spacing to be measured and the volume fraction measured by lineal analysis. Working at high magnification on the Stereoscan it was difficult to calibrate the instruments magnification, but it was thought that the actual value would not be too different from the instrument reading so this value was used in subsequent calculations.

A check was made, however, by comparing fibre diameters measured optically with the measurements made on the Stereoscan.

Where microstructures exhibited low crystal density then the long axis of at least thirty crystals was measured to obtain a mean value. After long crystallisation periods the microstructural features became less clearly defined. These fibres were powdered in a percussion mortar and pestle and a little of the powder mounted and examined. This technique was reasonably accurate for large crystal size but replication and transmission electron microscopy were used for the smaller crystal size found in glass B fibres.

5.6.3 Replication and Transmission Electron Microscopy

Fibres were encapsulated in epoxy resin in both a longitudinal and transverse position. The fibre was then polished on γ-alumina, cleaned and the area around the fibre masked with sellotape. Finally it was shadowed with carbon/platinum. Difficulties were encountered when removing the carbon/platinum replica which often adhered too well to the fibre. Thus only fragments were collected and examined on a JEOL J.E.M. 6A microscope.

During this investigation a Leitz Ultramicrotome and Phillips EM 300 microscope became available but for a limited period of time. Use was made of this facility, however, and some ultrathin sections of encapsulated fibre were examined by transmission microscopy. It was also possible to perform selected area diffraction on the fibres. Here the diffractions rings were measured using a Joyce Loebel III Microdensitometer and thus the interplanar spacings calculated. These were compared with "d" spacings obtained from the Powder Diffraction File for the phases suspected present. This gave an approximate method of phase identification.

5.7 X-ray Diffraction

X-ray diffraction was used to augment the somewhat sparse microscopical data. In particular this technique enabled the volume fraction of lithium disilicate in the fibres to be estimated.

Fibres, after crystallization, were ground and loaded into boro-silicate glass capillary tubes. The tubes were mounted in a Debye-Scherrer camera and irradiated with Cu Kα radiation using a Ni filter. The exposure was 80 mins at 40 KV/15 mA. This radiation was generated by a Raymax tube. The film used in the camera was Ilford Industrial G. All films were developed under as identical conditions as possible. The films were then scanned using a Joyce Loebel Microdensitometer. This enabled an accurate determination of the interplanar spacings to be obtained and also the relative intensities of the lines. This latter measurement was performed by drawing a base line on the microdensitometer trace then measuring the area beneath the peaks using a planimeter. These measurements were carried out on three lines for each film. The area beneath the curves was compared with the areas obtained for a glass considered to be fully crystalline. This glass was 66.6% SiO_2/ 33.3% Li_2O and crystallized at 1023 K for 72 hours.

Also to check the volume fractions of crystallinity measured by this technique a mechanical mixture of 50% by volume $Li_2O.2SiO_2$ was mixed with 50% cristobalite and again the intensity of the peaks was compared with the intensity of the fully crystalline glass-ceramic. This showed a good approximation to a linear relationship between line intensity and volume fraction of $Li_2O.2SiO_2$. The measurements taken from crystallized glass A fibres were accurate owing to the large crystal size giving sharp lines but with glass B it was difficult to separate the lines from the diffuse background. Some line broadening was also noticed for glasses in the very early stages of crystallization.

In general X-ray diffraction studies are difficult to perform on alkali silicates since the "d" lines which could give very positive identification are all at low angles and often fall in the diffuse halo caused by the amorphous phase.

5.8 Ion Exchange Experiments

5.8.1 Preliminary Investigations

Mention was made in Chapter 4 of the fact that mixed alkali glasses would crystallize more slowly than single alkali glasses. The literature, however, did not give much direct evidence of this behaviour so it was decided that a mixed alkali glass of lithium and potassium silicate should be prepared then subjected to similar heat treatment as the fibres. This glass had the composition given in table 6.1 and was called glass C. The glass was prepared from reagents of similar purity to those used in the preparation of glasses A and B. It was then ground and melted in the same way as glasses A and B. After remelting some fragments of glass were then heated at various crystallization temperatures on platinum foil in a programmed box furnace. These samples were then crushed in a percussion mortar, ground and loaded into an x-ray powder camera for x-ray diffraction analysis. The results of the experiment are given in Chapter 6. The problem now was to see if it was possible to produce a mixed alkali layer in the surface of a glass sample. Fibres were difficult to handle so this part of the investigation was carried out on thin rods varying between 0.5 and 2 mm diameter. Rods such as these were found in abundance in the quenching bucket after the molten glass was poured into cold water. These rods were immersed in a crucible containing potassium nitrate. The crucible was then placed in a box furnace and heated until the potassium salt was fused after which it was held at elevated temperature for various time periods to enable ion exchange to take place. The rods were then removed whilst the salt was molten and washed with water then ethanol to remove the encrusted salt. They were then subject to nucleation and crystallization procedures followed by microscopic examination using the scanning electron microscope.

The results are presented in Chapter 6 and a typical micrograph shown in Chapter 7, plate 7.9.

5.9 Ion-Exchange on Fibres

On the basis of the results from the preliminary investigations it was decided that ion exchange was feasible and that a technique should now be sought for ion-exchanging potassium for lithium in the glass surface. The obvious method to try first was molten salt bath treatment which is discussed below.

5.9.1 Molten Salt Bath Treatment

For this investigation it was decided to try ion-exchange on small bundles of glass B fibres about 90 mm in length. Potassium nitrate was fused in an alumina crucible in a small crucible furnace at 610 K. The fibre bundles were then immersed as well as possible in the molten salt.

This technique presented many manipulative problems such as poor wetting of fibres and difficulty in removing the encrusted salt afterwards. Fibres subjected to this treatment were, however, crystallized and small samples were tested after various immersion times in the salt bath. The strength was never improved by this technique compared to fibres crystallized without this treatment but on the contrary the crystallized fibres were often weaker.

Ideally the ion exchange should only take place in the outermost surface layer of the fibre to suppress nucleation otherwise a deep penetration of potassium ions may cause a progressive change in properties establishing volumetric changes and residual stress in the fibre. It was suspected that ion exchange took place too rapidly in a salt bath treatment and also that extra lithium ions may have been leached out into the salt bath leaving a surface layer depleted in lithia. Experimentation was thus turned towards finding a slower ion exchange process and one in which the fibres would have

good contact with the exchanging medium leading to homogeneity of exchange throughout the fibre bundle. Work could have been carried out on a few or even single fibres but such experiments would be impractical since large numbers of fibres were required for testing.

5.9.2 Vapour Phase Ion Exchange

A vapour phase ion exchange was chosen since it was thought that the process would allow more control of ion concentration and temperature than the salt bath.

The apparatus designed to do this is shown in fig. 5.6 and plate 5.4. A porcelain boat of a potassium salt was heated in the side arm C of the apparatus and a monitored flow of argon gas passed over this. The fibres were suspended as a tow in the vertical tube which passed through a programmable tube furnace. All temperatures were monitored by placing thermocouples close to the required zones. Thus the fibres were subjected to the passage of argon gas containing some potassium salt vapour. Both potassium nitrate and chloride were tried. The salt vapour was passed over the fibres and allowed to flow for various periods of time, whilst the fibres were maintained at 673 K. After passage of vapour the fibres were then nucleated at 763 K by raising the temperature of the tube furnace and finally crystallized.

The vapour pressure was given by $\log P = -11.495/T + 3.526 \log T + 20.929$ where P = pressure in mm. Potassium nitrate was used in the early part of the investigation and some results are quoted in Appendix IV. Later work involved the use of potassium chloride.

The vapour of potassium chloride is know to be ion pairs at 973 K whereas lithium chloride vapour exists almost entirely as dimers $(LiCl)_2$. Thus a lithium ion removed from the glass surface should become highly

FIG 5.6 VAPOUR DEPOSITION APPARATUS

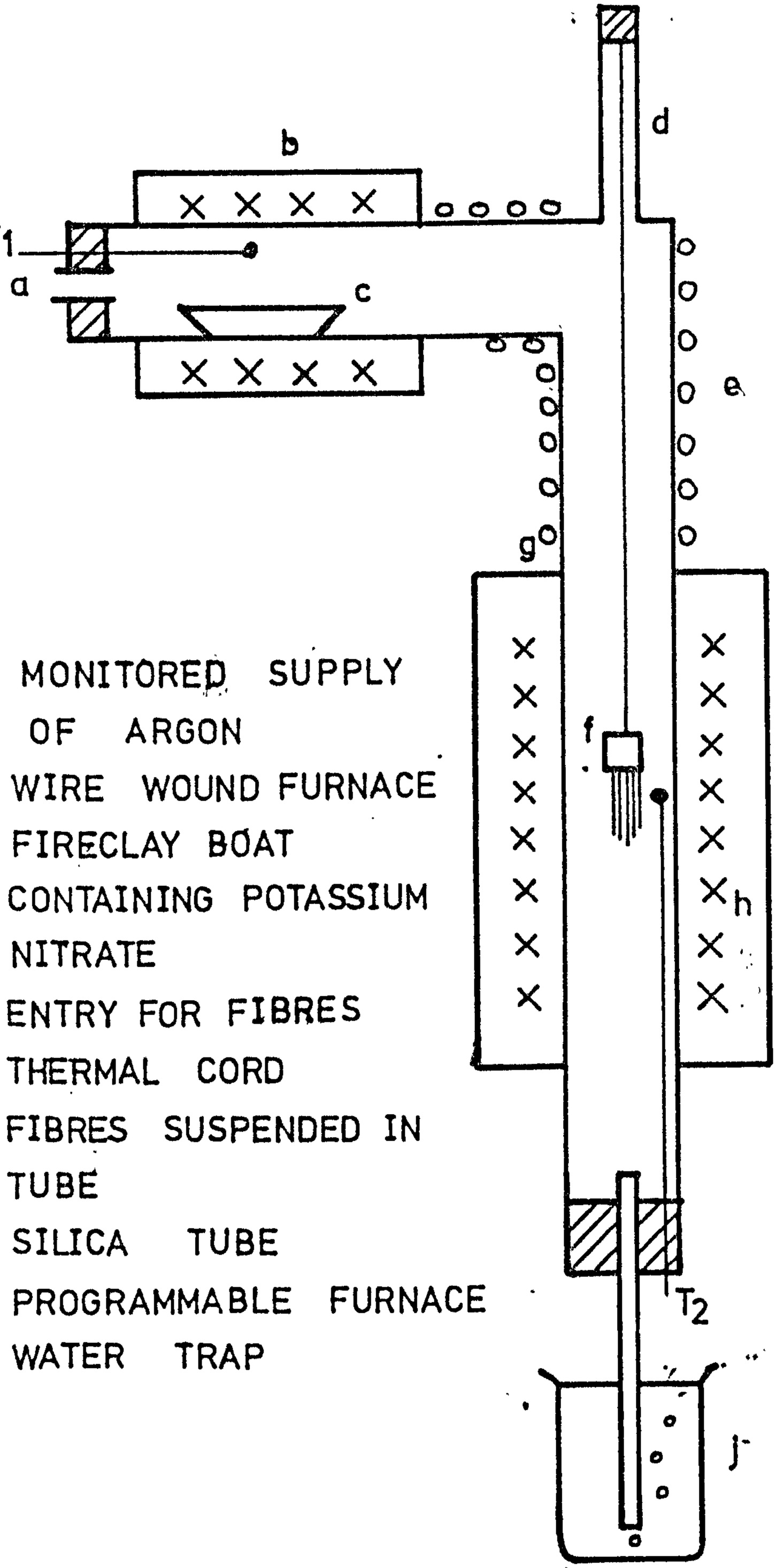

a = MONITORED SUPPLY OF ARGON

b = WIRE WOUND FURNACE

c = FIRECLAY BOAT CONTAINING POTASSIUM NITRATE

d = ENTRY FOR FIBRES

e = THERMAL CORD

f = FIBRES SUSPENDED IN TUBE

g = SILICA TUBE

h = PROGRAMMABLE FURNACE

j = WATER TRAP

T_1 & T_2 = THERMOCOUPLES

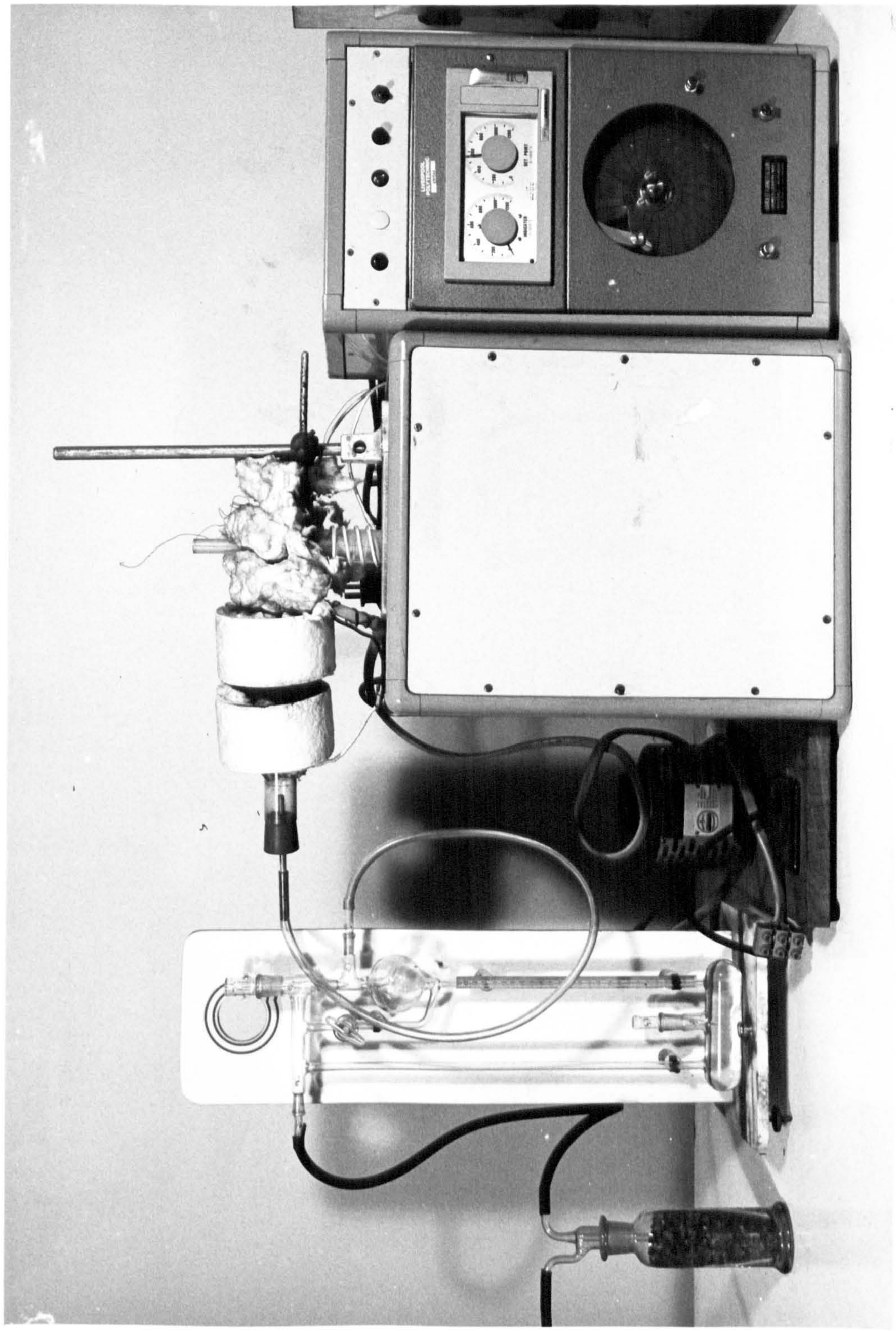

Plate 5.4 Ion Exchange Apparatus

associated and more stable as the halide thus favouring the reaction

$$K^{+}_{(v)} + Li^{+}_{(g)} \rightleftharpoons K^{+}_{(g)} + Li^{+}_{(v)}$$

v = vapour

g = glass

to shift to the right. This shift would also be aided by the continual removal of the lithium halide by the gas flow. Insufficient time did not allow this process to be investigated thoroughly, but some work was carried out to establish

(i) Concentration profiles of K^+ ions in the fibres

(ii) A numerical analysis of the exchange and diffusion process.

Despite much time and effort spent on this part of the investigation the complexity of the process and experimental difficulties caused this area of the investigation to remain incomplete.

5.10 Determination of Diffusion Profiles

Three techniques were employed to try to establish the K^+ ion concentration profiles which were

(i) Electron microprobe analysis

(ii) Radioactive tracer analysis

(iii) Flame photometry

5.10.1 Electron Microprobe Analysis

An electron microprobe analyser in the Metallurgy Department, Liverpool University was used to investigate the K^+ concentration in a specimen of glass ion exchanged in a salt bath, however, K^+ could not be detected in the glass and it was suspected that the analysing crystal was not suitable for detecting the radiation from K^+.

5.10.2 Radioactive Tracer Analysis

This technique is a standard method of measuring diffusion profiles and thus was adopted in this work. Samples of fibres subjected to vapour phase ion exchange were irradiated in a neutron flux of 1.4×10^{16} neutrons/m^2s for eight hours. (Universities Research Reactor, Risley, Warrington). This transforms the ^{39}K to ^{42}K and the isotope ^{42}K has a half life of 12.5 hours. The fibres were then analysed by dissolving away surface layers in dilute hydrofluoric acide and analysing the activity of the solution. Some preliminary experiments showed the fibres to dissolve almost linearly with time in dilute hydrofluoric acid. A fibre bundle would be stirred continually in 3% hydrofluoric acid and aliquots removed after given time periods of analysis. Unfortunately, trace impurities of iron in the glass gave rise to the presence of ^{59}Fe; a highly active isotope with a Y-ray emission capable of masking the spectrum from ^{42}K. The source of the iron was thought to have been impurities in the Brazilian quartz. Hence little reliable information was gained from this investigation.

5.10.3 Flame Photometry

Alkali metals are readily detected by flame photometry provided several important experimental procedures are observed. This technique was employed and found to be more successful than either of the above methods. The wavelength of the lines for lithium and potassium are

$$Li^+ = 670.8 \times 10^{-6}m$$

$$K^+ = 766.5,\ 769.9 \times 10^{-6}m \ *$$

(* the K^+ being an intense doublet). The experimental procedure was similar to the tracer analysis in that a bundle of ion exchanged fibres were dissolved in dilute hydrofluoric acid and aliquots removed at various time intervals. These samples were neutralized with dilute ammonia then sprayed into an

air/propane flame of an EEL flame photometer. A set of working cruves were obtained for the photometer using standard solutions of lithium and potassium salt mixtures. Lack of time did not allow an accurate determination to be made of absolute concentration of ions but it was possible to estimate ionic ratios at various depths within the fibre.

6. Results

6.1 Glass Compositions

Because of the variety of analytical techniques used to determine the composition of the glasses it is not possible to state the accuracy of the mole percentages quoted and therefore it was considered reasonable to quote these values to the nearest decimal place. The results are given for compositions A, B and C in table 6.1.

6.2 Fibre Diameter

The fibre diameter was found to be influenced by the drawing speed and temperature of the molten glass in the bushing and so an attempt was made to determine the relationship between the fibre diameter and the process variables.

Diameter measurements were made using a Vickers image shearing eyepiece in conjunction with a microscope operating at a magnification of X 400. The accuracy of the measurements using this arrangement was found to be: $\pm$ 0.1 μm. Fibres in any one batch showed a variation in diameter and for this reason measurements were carried out on samples of 20 fibres drawn at a particular speed and temperature. The mean and variance of each sample was calculated and these parameters were used to estimate if there was a significant difference between mean diameter of fibres produced under the various conditions. The test used was that for two sample means whose distribution was assumed normal and whose variance was estimated. The statistic

$$t = \frac{\bar{X}_1 - \bar{X}_2}{\frac{S_1^2}{n_1} + \frac{S_2^2}{n_2}}$$

TABLE 6.1

GLASS COMPOSITIONS

GLASS	Li_2O (mol %)		SiO_2 (mol %)		P_2O_5 (mol %)		K_2O (mol %)		ZnO (mol %)	
	EXPECTED	ANALYSED	EXPECTED	ANALYSED	EXPECTED	ANALYSED	EXPECTED	ANALYSED	EXPECTED	ANALYSED
A	25	26.7	74	72.4	1	0.9				
B	29	28.2	68	68.9	1	1.1	1	0.9	1	0.9
C	12.5	11.6	74	75.1	1	1.1	12.5	12.2		

where $\bar{X}_1$, $\bar{X}_2$ = are respective means

S_1^2 , S_2^2 = are estimated variances

n_1 , n_2 = sample sizes

was used to test the null hypothesis that the two samples have the same mean. This statistic has a t distribution with $V = n_1 + n_2 - 2$ degress of freedom. Typically the mean diameters of glass A fibres drawn at 750 and 450 r.p.m. and 1653 K were 25.6 and 28.2 with respective standard deviations of 0.6 and 0.5. The calculated value of t was 14.8 and from tables the value of $|t|$ for a 1% significance level was found to be 2.7. This leads to the rejection of the null hypothesis at the 1% and also the 0.1% significance level and thus these means can be considered different. When any such pairs of observations were tested in this way a significant difference in means was found. It can thus be assumed that the variation of temperature and winding speed affect fibre diameter. These results are summarized in Table 6.2.

6.3 Tensile Strength of the Fibres

Many measurements of fibre tensile strength were made for a wide variety of heat treatments. This large volume of information is presented in Appendix I. The accuracies of the individual measurements were determined using the relationship

$$\frac{\Delta 6}{6} = \frac{\Delta P}{P} + 2\frac{\Delta r}{r} \qquad (6.1)$$

where $\Delta 6$, ΔP and Δr are the absolute accuracies of the load and diameter measurements. Equation (6.1) shows the relative accuracy of each parameter and as can be seen the relative accuracy of the stress depends on the size of the stress. For this reason the relative accuracy is presented in

TABLE 6.2

FIBRE DRAWING CONDITIONS FOR GLASSES A AND B

GLASS	DRAWING TEMPERATURE (K)	MEAN DRUM SPEED (r.p.m.)	MEAN FIBRE DIAMETER (μm)	STANDARD DEVIATION OF DIAMETER (μm)
A	1653	1000	21.1	0.5
		750	25.6	0.6
		450	28.2	0.5
	1635	300	30.7	0.6
B	1620	1000	23.6	0.4
		750	27.3	0.5
		450	32.0	0.5
	1606	300	38.4	0.5

graphical form as a function of stress in figure 6.1 (a, b) for the two stress ranges 100 - 700 and 100 - 1300 MN/m^2. Individual measurements were accurate and did not give rise to the main source of error, in the strength values quoted, which was due to the large variance in values for any particular heat treatment. It was not practical to test very large samples of fibres because of the time involved in such a procedure but the sample size chosen i.e. 50 fibres was sufficiently large to give reasonable confidence limits to the mean strengths. The confidence limits were calculated using the following relationship:

$$\bar{6} \pm 2.01 \frac{S}{\sqrt{n}} \qquad (6.2)$$

where $\bar{6}$ = mean strength

S = estimated standard deviation for the sample

n = sample size.

The value 2.01 is found from 't' tables for 95% confidence limits. The confidence limits are tabulated with strengths in Appendix I.

An implicit assumption was made that the population from which the sample was taken was a normal distribution. Later in the discussion it will be argued that the strength data is best represented by a Weibull extreme value distribution and so it would appear that a dilema exists here. Infact with such a small sample size of fifty variates it is difficult to establish conclusively which distribution is correct. Tests were made to establish the form of the strength data distribution. For instance, the values were plotted on histograms, an example of which is shown in figure 6.2 and likewise relative frequency plots were made see fig. 6.3. The histograms generally appeared to be symmetrical and many sets of data gave a reasonable fit to a straight line on normal relative frequency paper. The Weibull distribution, on the other hand, is a skew distribution. However, the data appeared to fit reasonably well to a two parameter Weibull distribution and in certain cases there was evidence of a bimodal Weibull distribution. At this stage an assumption was made that the

Relative Accuracy of Mean Stress Values

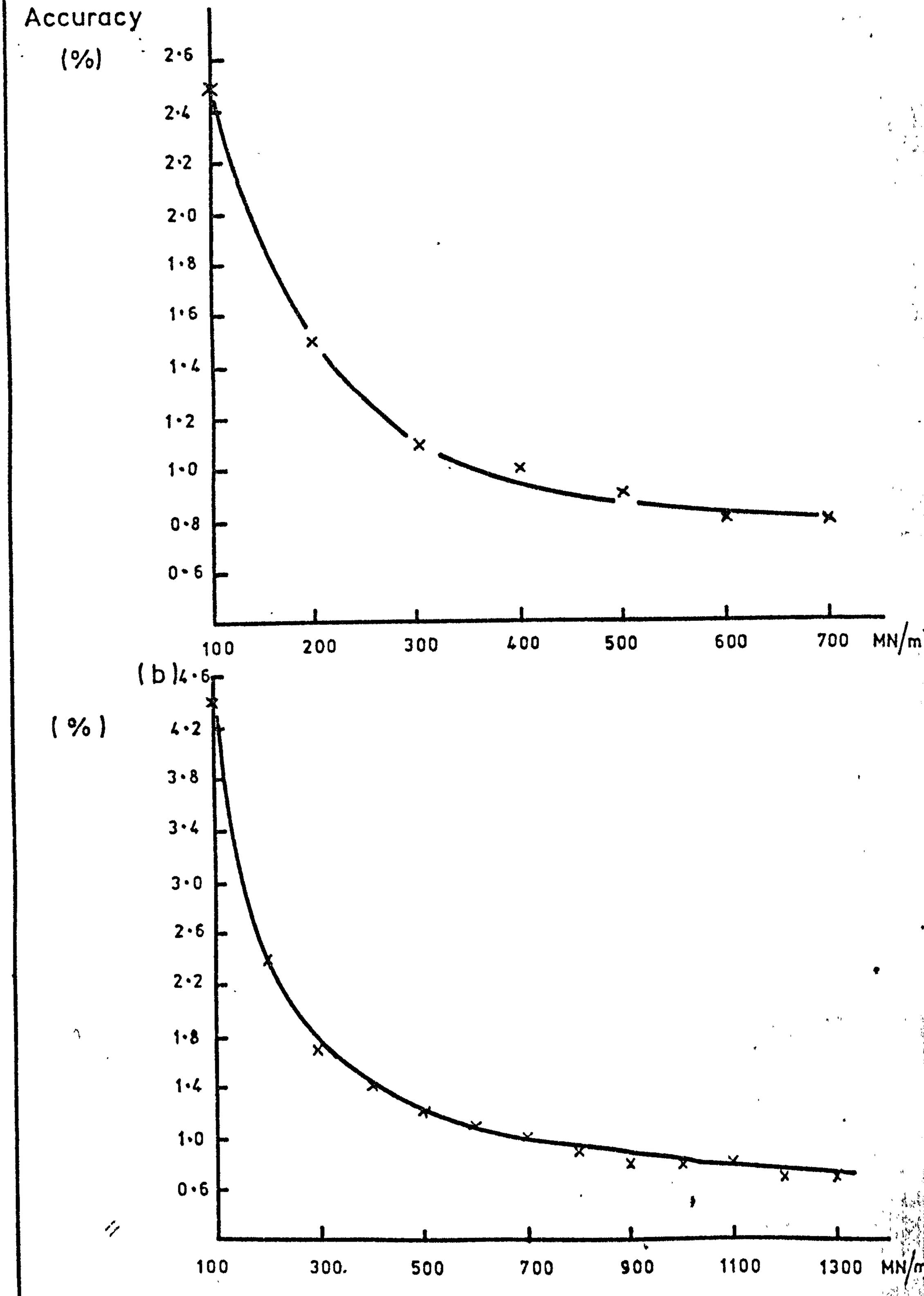

FIG 6·1 (a, b)

Histogram of fibre tensile strengths

Glass B N = 763 K, G = 798 K, t = 3·0 hours

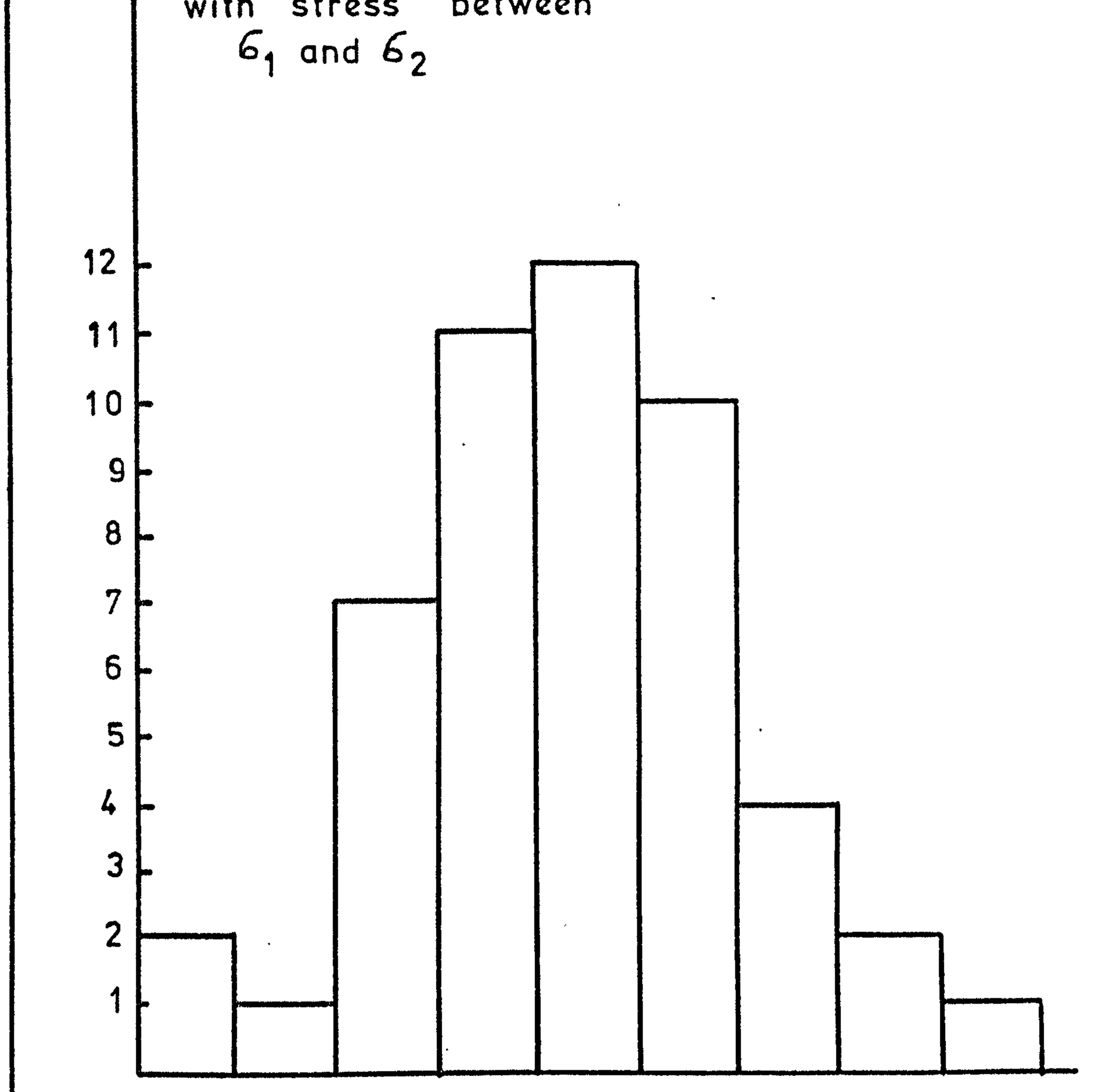

FIG 6·2

CHART WELL Graph Data Ref. 5571

80 Equal Divisions x Probability

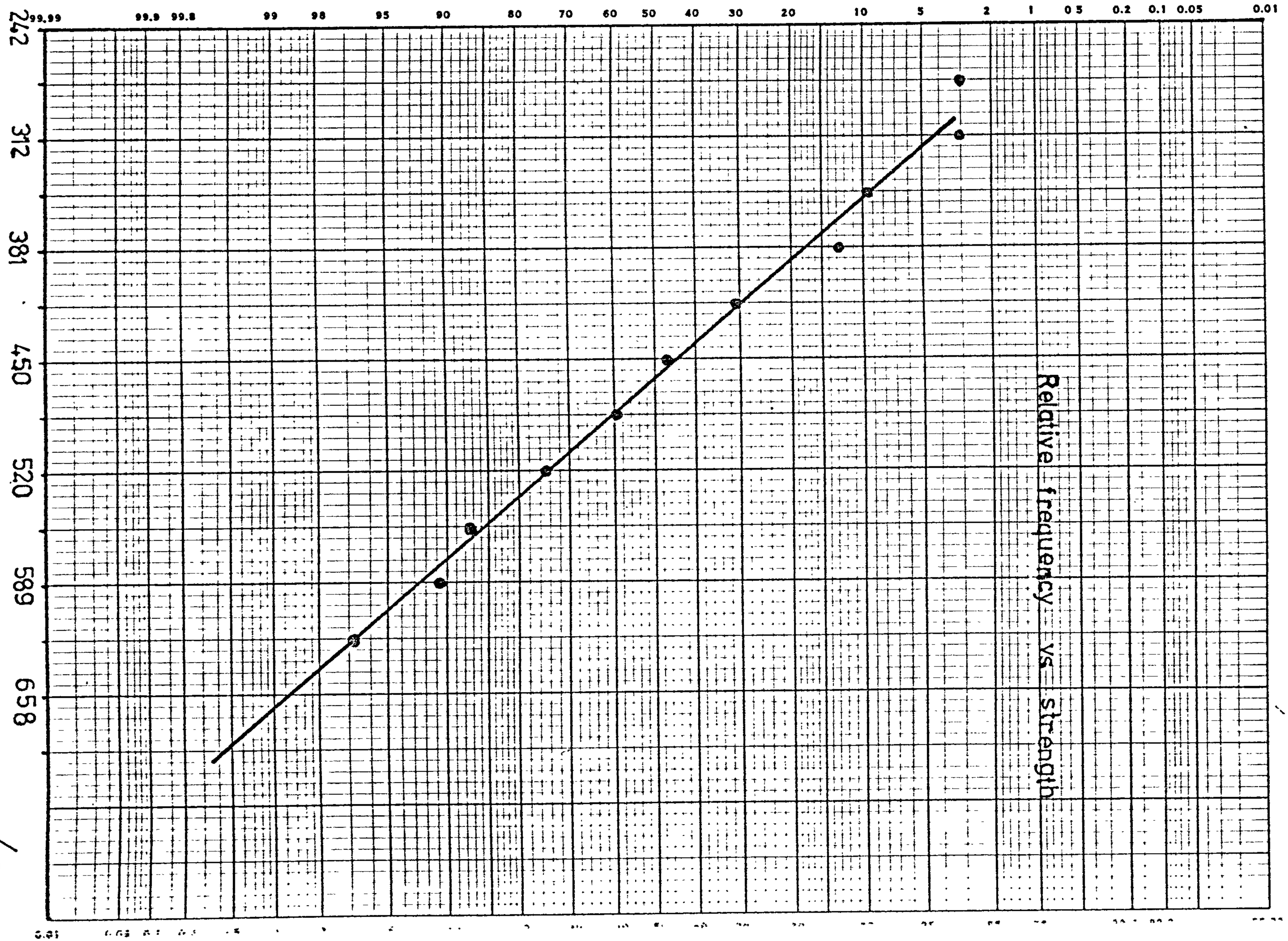

FIG 6.3

samples belonged to a Weibull population with only a slight degree of skewness. A test for skewness was performed on several samples and the values indicated various degrees of skewness all of which were slight. The test used the second and third moments of the distributions to calculate the ratio

$$\beta = \frac{U_3^2}{U_2^3}$$

where U_3 = the third moment of the distribution and U_2 the second moment. For a symmetrical distribution $\beta = 0$. The values calculated here were in the range 0.2 to 0.4. Now if a Weibull distribution is the correct form for strength values then median strengths should be representative of particular heat treatments rather than the arithmetic mean but if the distribution is only slightly skewed these values will be similar. In the discussion, attempts are made to show relationships between strength and heat treatment conditions and throughout use is made of such tests as significance, correlation and regression. These tests have been well established for the normal distribution but the equivalent tests are not readily applicable to the Weibull distribution. For this reason it was decided that tests should be carried out as if the data were normally distributed and that the accuracy of such an approach would be acceptable in order to show the trends discussed in chapter 7.

The mean strengths of glass A fibres are plotted against crystallization times for various nucleation and crystallization temperatures in figures 6.4 to 6.7. Two attempts were made to establish a relationship between strength and crystallization time. The first was a linear regression curve fit carried out on a P.D.P.8 computer. The programme uses curvilinear regression to find the best fit of the data to the equation:

$$y = A\, x^b \qquad (6.3)$$

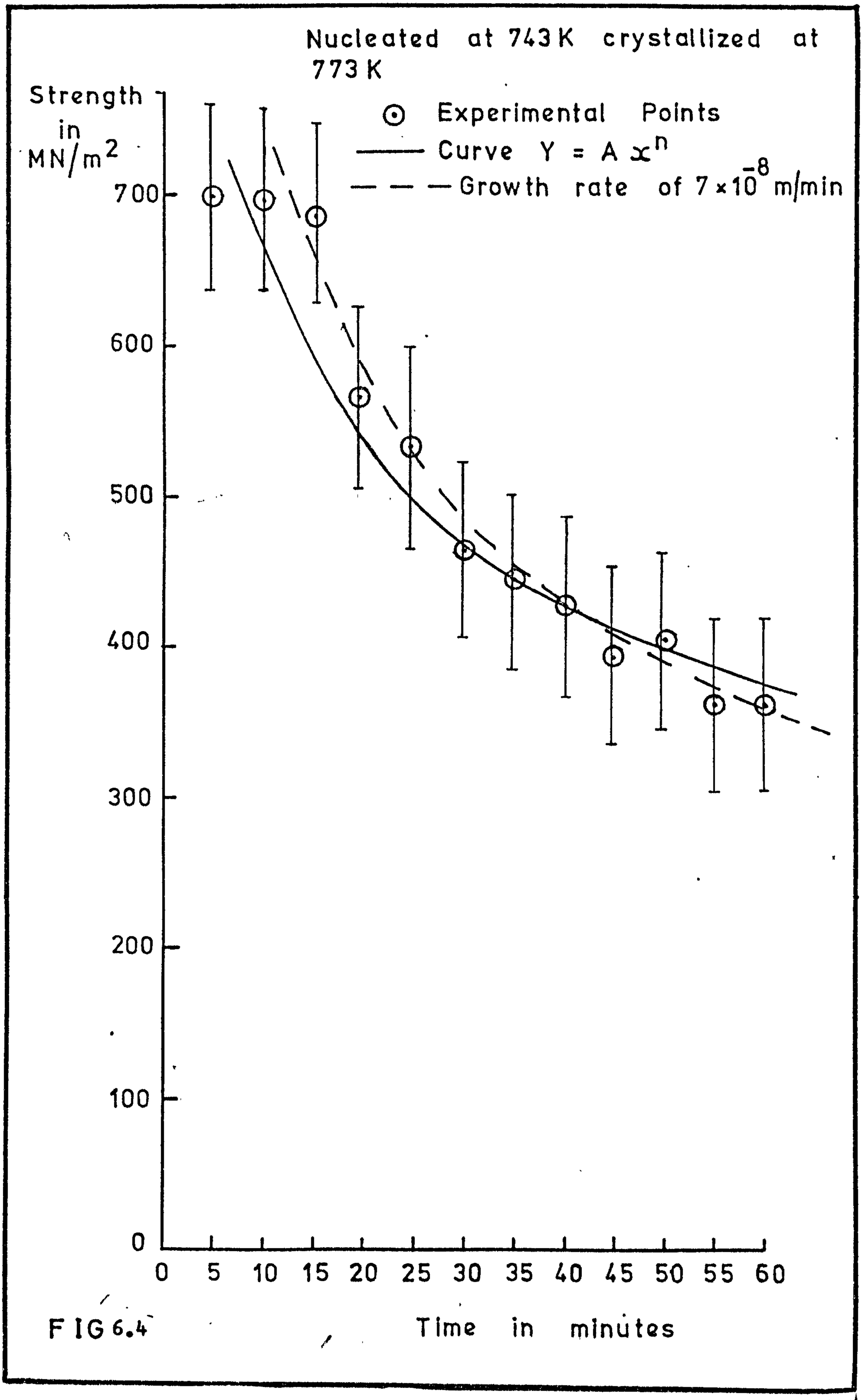
Nucleated at 743 K crystallized at 773 K
Strength in MN/m2
700
600
500
400
300
200
100
0
Experimental Points
Curve Y = A x^n
Growth rate of 7 x 10^-8 m/min
0 5 10 15 20 25 30 35 40 45 50 55 60
Time in minutes

FIG 6.4

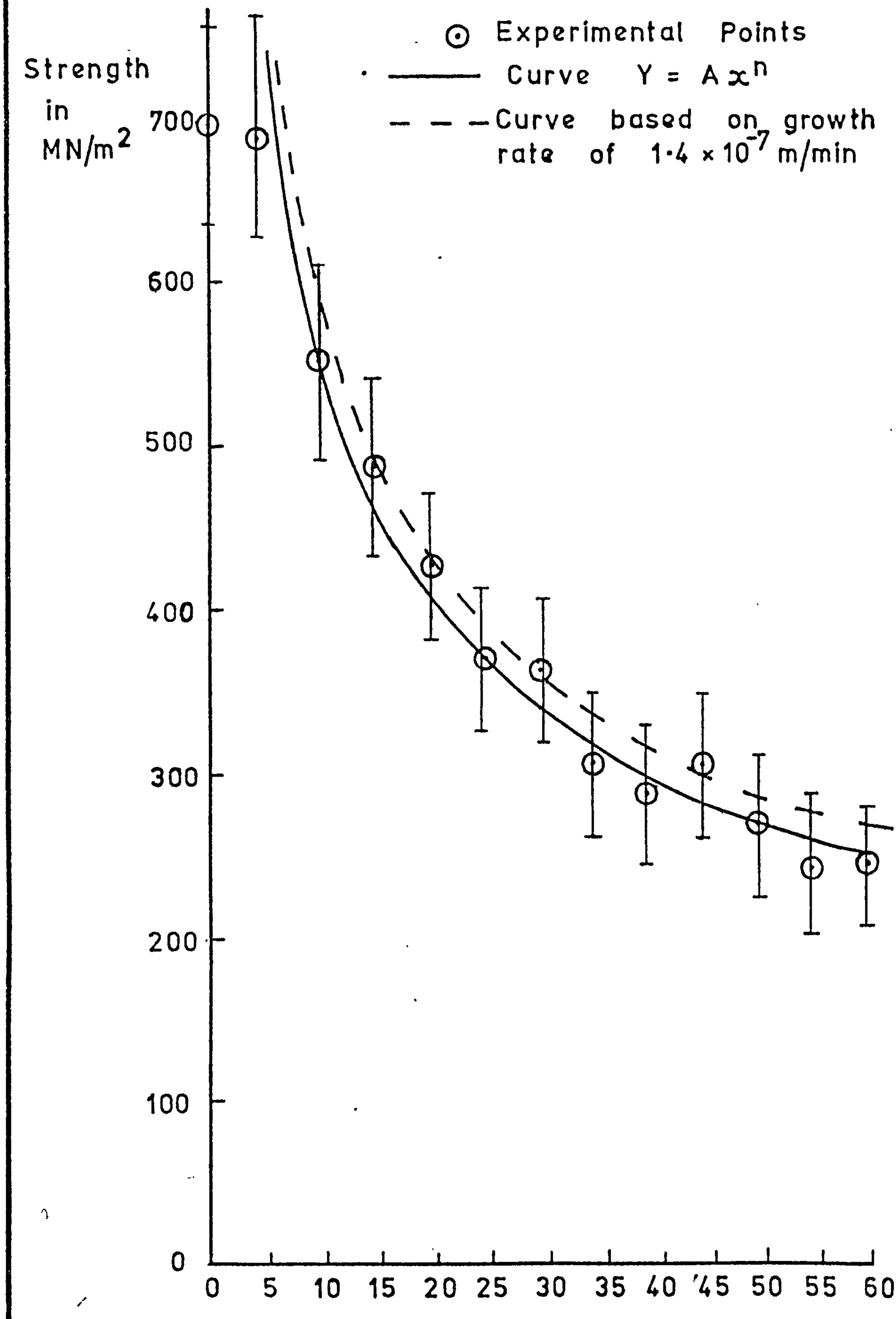
Nucleated at 743 K crystallized at 798 K.
⊙ Experimental Points
——— Curve Y = A x^n
— — — Curve based on growth rate of 1·4 × 10^-7 m/min
Strength in MN/m^2
700
600
500
400
300
200
100
0
0 5 10 15 20 25 30 35 40 45 50 55 60
Time in minutes

FIG 6.5

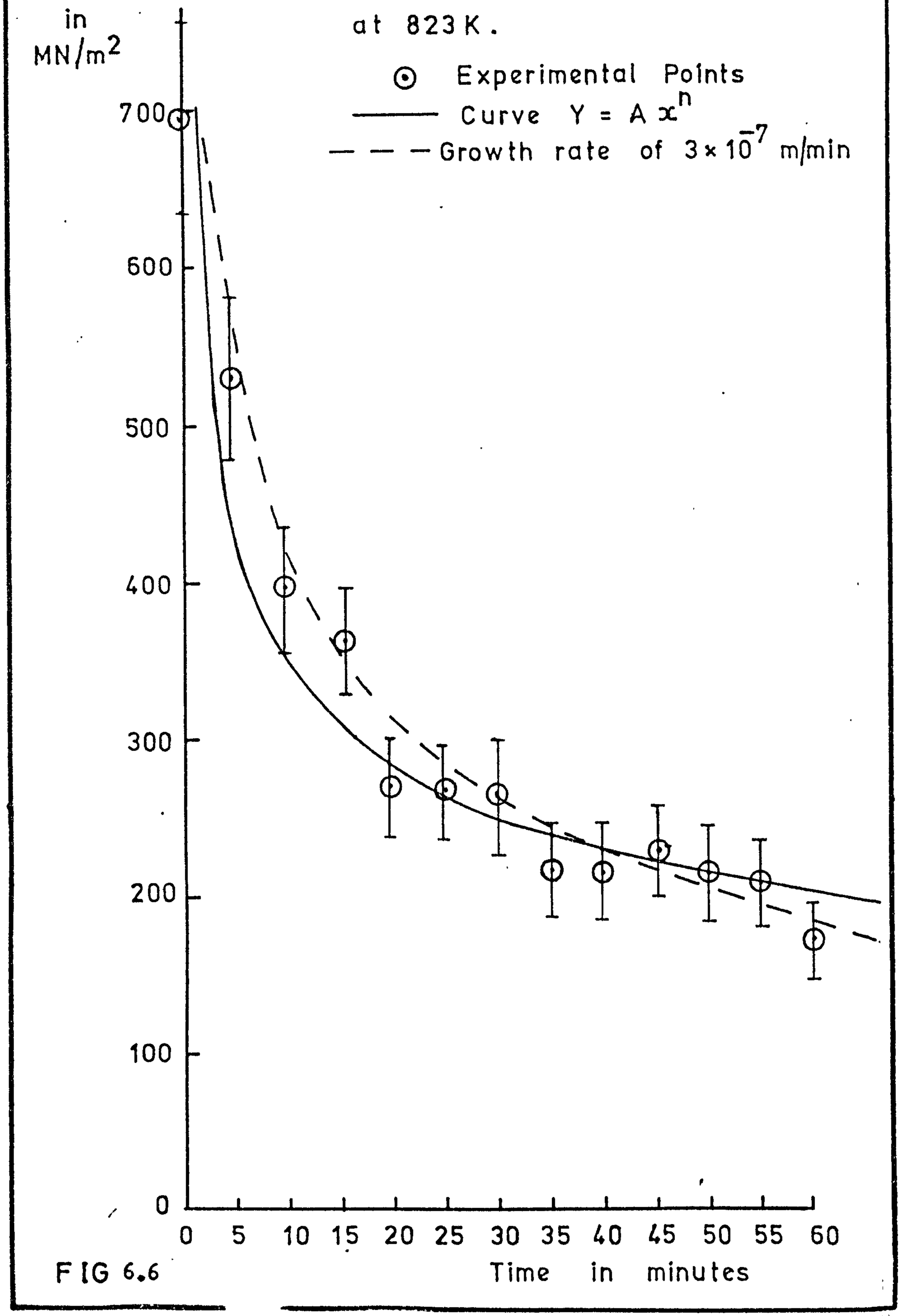
Strength in MN/m2
700
600
500
400
300
200
100
0
0 5 10 15 20 25 30 35 40 45 50 55 60
Time in minutes
Nucleated at 743K crystallized at 823K.
⊙ Experimental Points
——— Curve Y = A x^n
— — — Growth rate of 3 × 10^-7 m/min

FIG 6.6

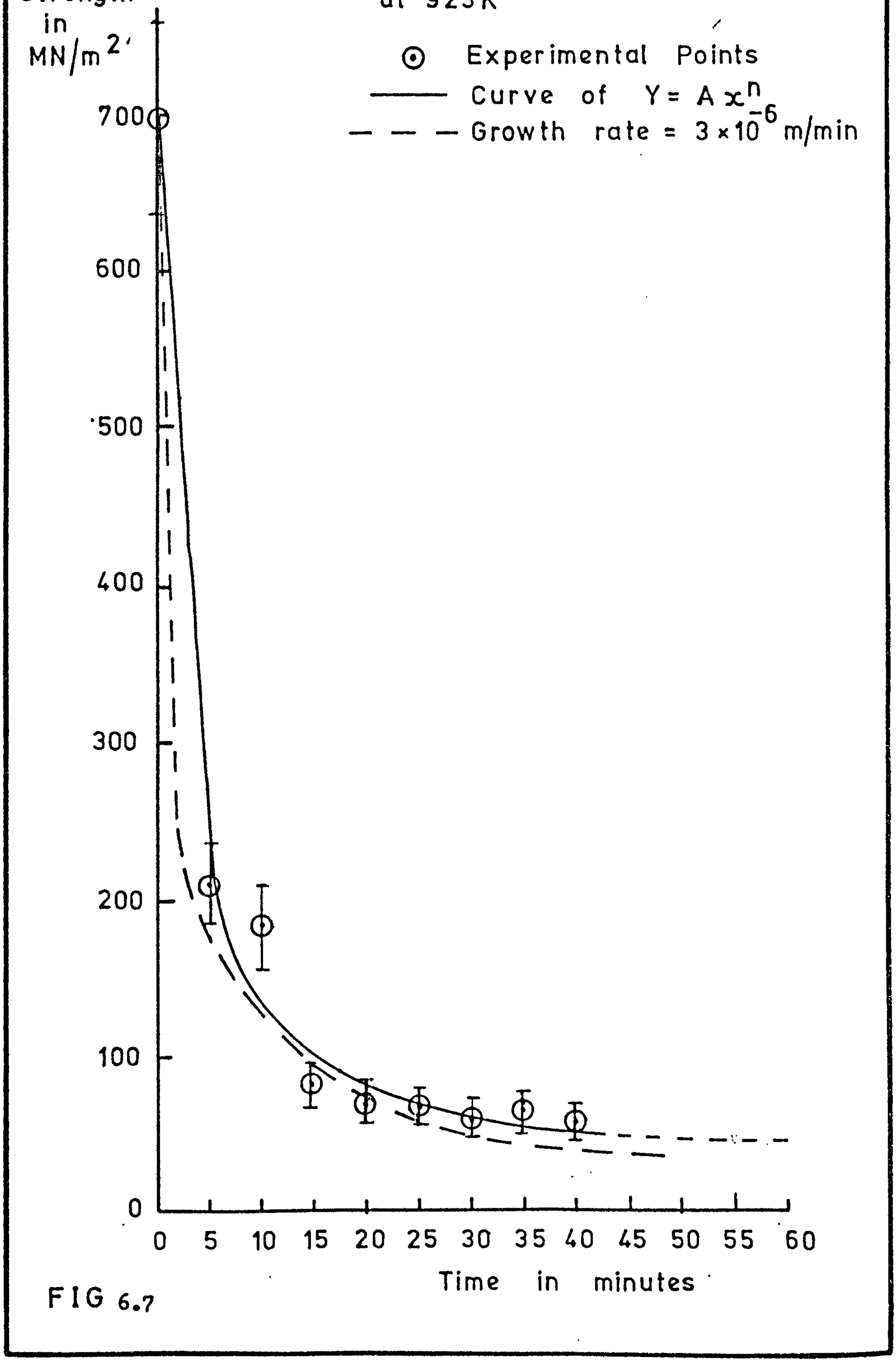
Nucleated at 743K crystallized at 923K
⊙ Experimental Points
——— Curve of $Y = A x^n$
— — — Growth rate = 3×10^{-6} m/min
Strength in MN/m^2
700
600
500
400
300
200
100
0
0 5 10 15 20 25 30 35 40 45 50 55 60
Time in minutes

FIG 6.7

Visual inspection shows that a reasonable fit exists for each heat treatment and in the figure 6.4 to 6.7 the 95% confidence limits are included for each value. The regression was tested to establish the significance of the fit. The values of crystallization time were taken as the controlled variable since its variance could be considered the same for all times chosen. The regression was that of y on x or strength on time. Now the total variance of the y values is made up of the variance due to the regression and the residual variation about the regression. Both quantities were calculable from the differences between actual and calculated y values. A significance test could now be carried out. The null-hypothesis was that A = 0 or that the regression appeared by chance fluctuations in the sample. The statistic used to test this hypothesis was

$$F = \frac{\text{variance due to regression}}{\text{variance about regression/number of degrees of freedom}}$$

F distribution tables were used to determine the appropriate value for which there is only a 1% chance of F being exceeded by the calculated value. In all cases the F values obtained from the regression exceeded the value 7.13 for 1% significance level by almost an order of magnitude showing strong evidence that a regression exists between the data and the curve. In the table below some indication is given of the acceptability of the relationship $y = A\ x^b$ by listing the percentage fit for three heat treatment conditions. The percentage fit is defined as :

$$\frac{\text{the sum of the squares due to regression x 100}}{\text{the total sum of the squares}}$$

Nucleation/Crystallization	F Calculated	Percentage Fit
763/798	516	97%
743/798	317	97%
743/923	708	99%

Analysis of variance in regression curve fitting requires a knowledge of the mean and variance of the error between the measured and calculated variate but in this case there is a further variance of each strength value which unfortunately could not be included in the analysis described above. There are systems available in the form of computer sub-routines capable of including this additional variance, but this facility was not available to the author. Some inferences can be made, however, based on the evidence available. The mean strength values are significantly representative of the population mean as shown by the confidence limits. Instead of performing the regression on the mean values if a random sample of strengths were taken from within the confidence limits and substituted for the means in the regression analysis the percentage fit after regression would be expected still to show a significant relationship between the data and equation $y = A\,x^{b}$. This test was performed and the percentage fit was always found to be greater than 80%.

The mean strength vs. crystallization time data for glass B fibres did not appear to follow a simple functional relationship. Strengths decreased initially, increased slightly then decreased again. A regression curve fitting procedure was not available for this functional form thus an estimated curve was drawn by eye. The data are tabulated in Appendix I and presented graphically in figures 6.8 and 6.9. The particular heat treatment (N = 753, G = 798) is taken to illustrate the goodness of fit to the drawn curve. Confidence limits (95%) are presented for each strength value. As can be seen range of strengths in the 95% confidence limits lie outside of each other when considering the three regimes on the graph. For instance the strength clearly decreases from 0 to 0.5 hours. Likewise the limits on the strength after 3 hours are outside of the range of the minimum value after 1 h showing a general increase in strength. The same reasoning can be applied to the last regime of the graph showing a strength

Tensile Strength of Glass B vs Crystallization Time

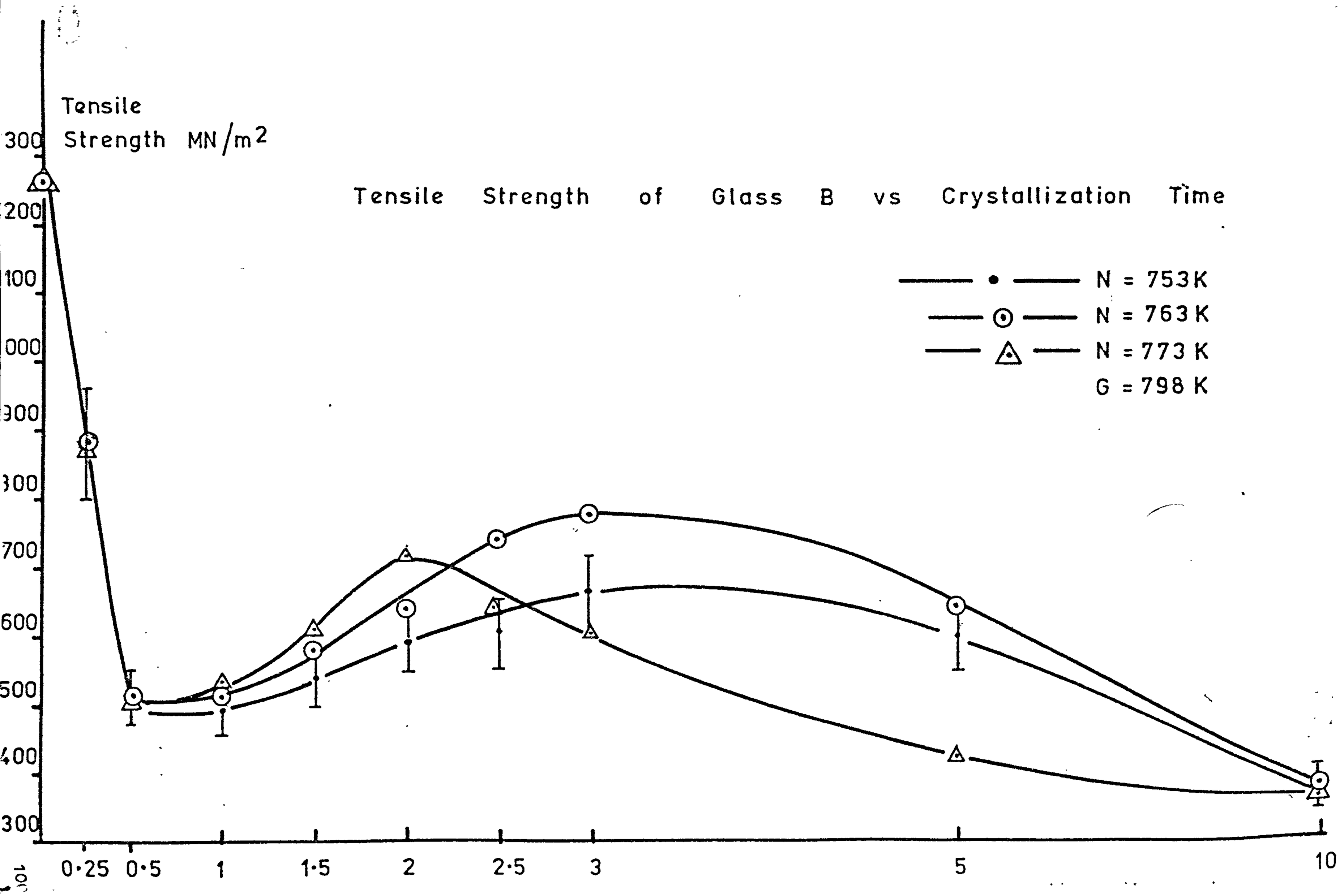

Tensile Strength of Glass B vs Crystallization Time

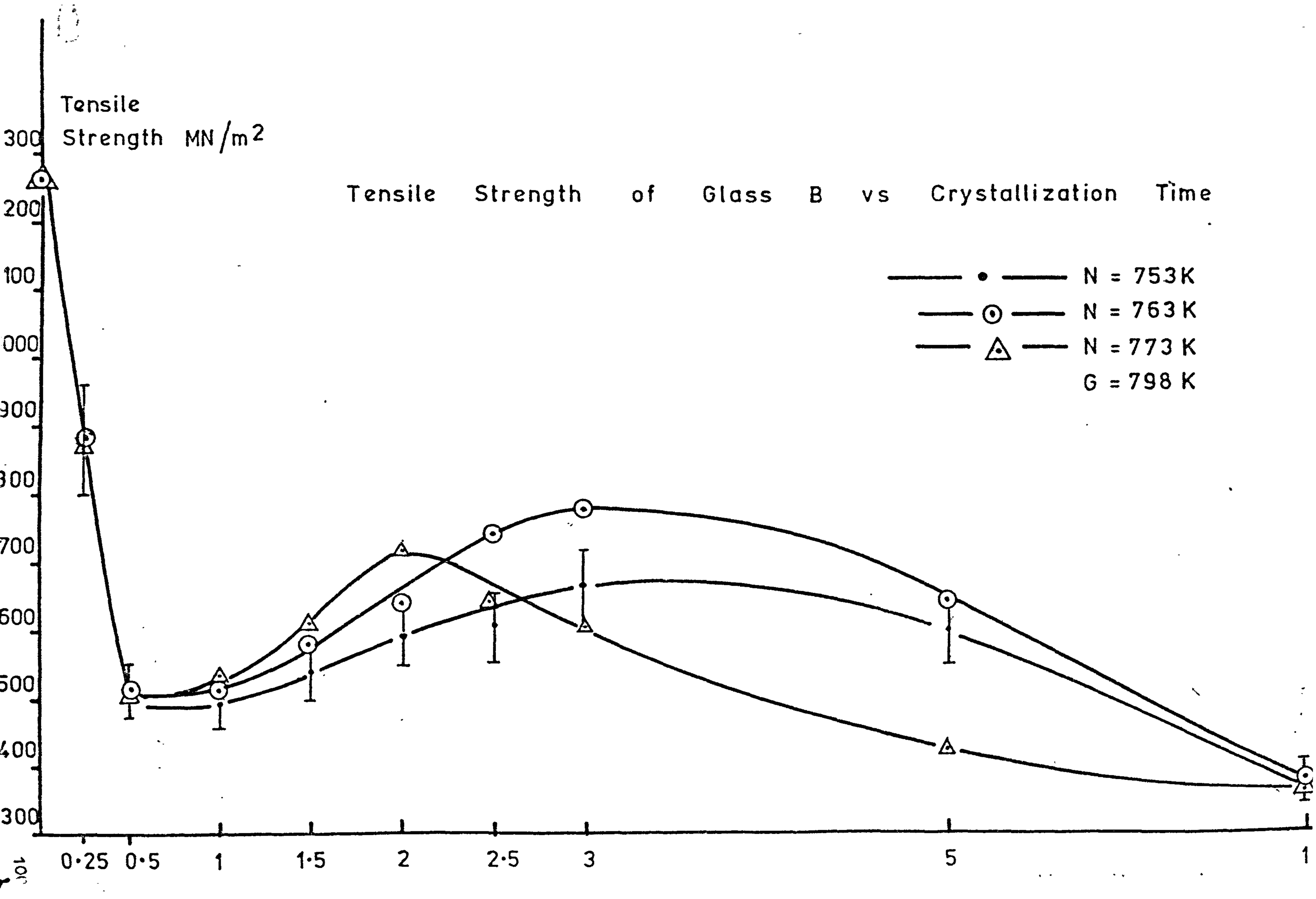

decrease after long crystallization times. Confidence limits have not been included on the other curves since this specific example exhibits the least difference between strength values for particular crystallization times and thus if some degree of fit can be established for these data, it is a reasonable assumption that it is equally applicable to the other data.

Fitting Data to A Weibull Distribution

The data for any single heat treatment were fitted to a two-parameter Weibull distribution. The procedure for doing this was as follows:

1. Breaking stresses were ranked in decreasing order.
2. Using a sample size of n = 50 the survival probabilities were calculated using the formula $P_i = 1 - (\frac{i - 0.3}{50.4})$.
3. Each stress value was normalized by dividing it by the arithmetic mean stress.
4. Survival probabilities were plotted against stress ratios on 2-parameter Weibull paper and the gradient m (the Weibull modulus) determined from the graph.

The Weibull modulus or moduli are tabulated in Appendix I. Some data appeared to fall into two groups when plotted this way. This will be discussed in detail in chapter 7 where an explanation will be given in terms of a bimodal distribution.

Three examples of two-parameter Weibull plots are shown in figures 6.10 to 6.12. A standard error can be calculated for the Weibull modulus in terms of the sample size thus

$$m \pm \frac{m}{\sqrt{2n}}$$

and for a sample size of n = 50 the Weibull modulii are quoted to an accuracy of $\pm$ 10%.

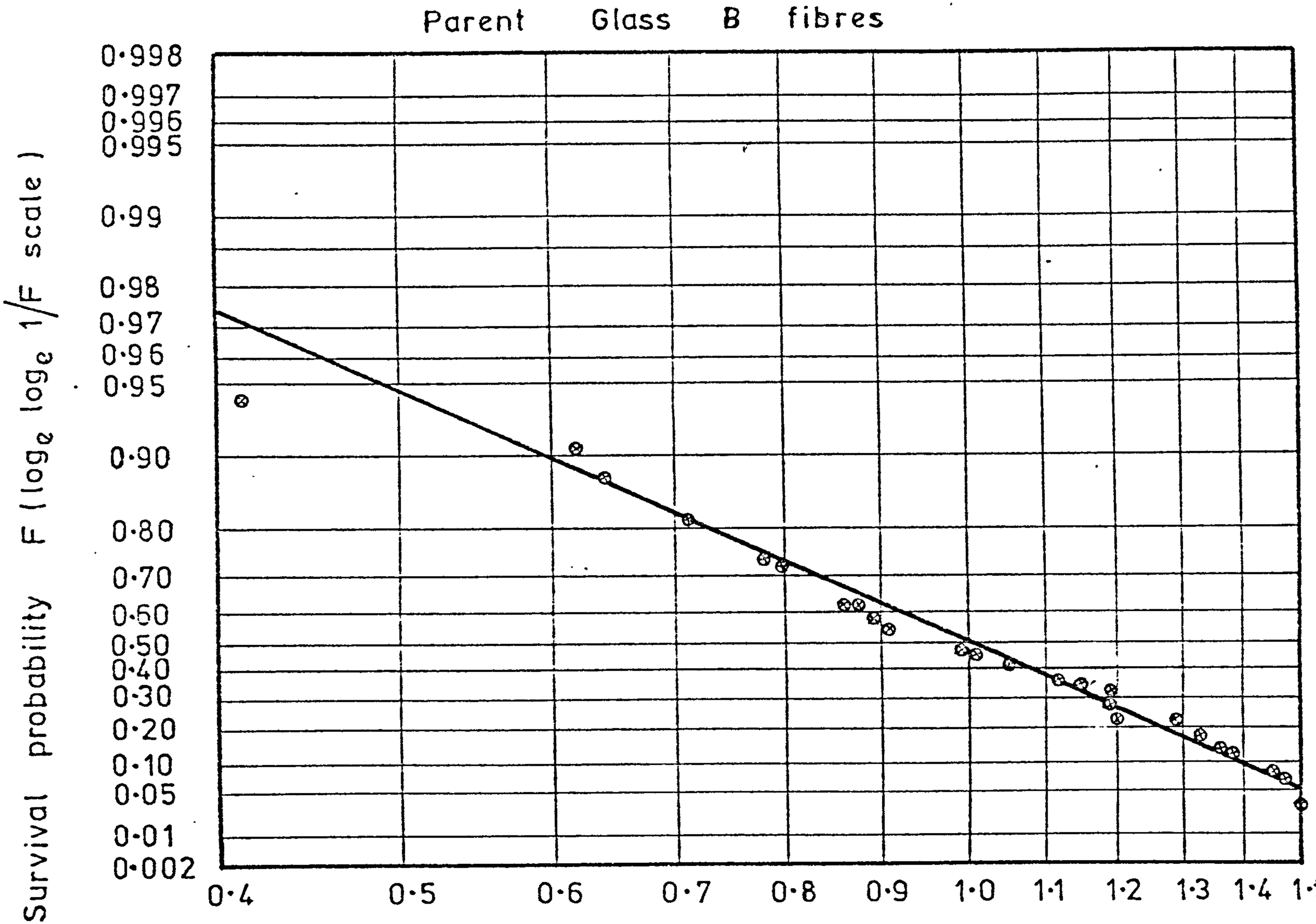

FIG 6.10 (only half the points are shown on each graph)

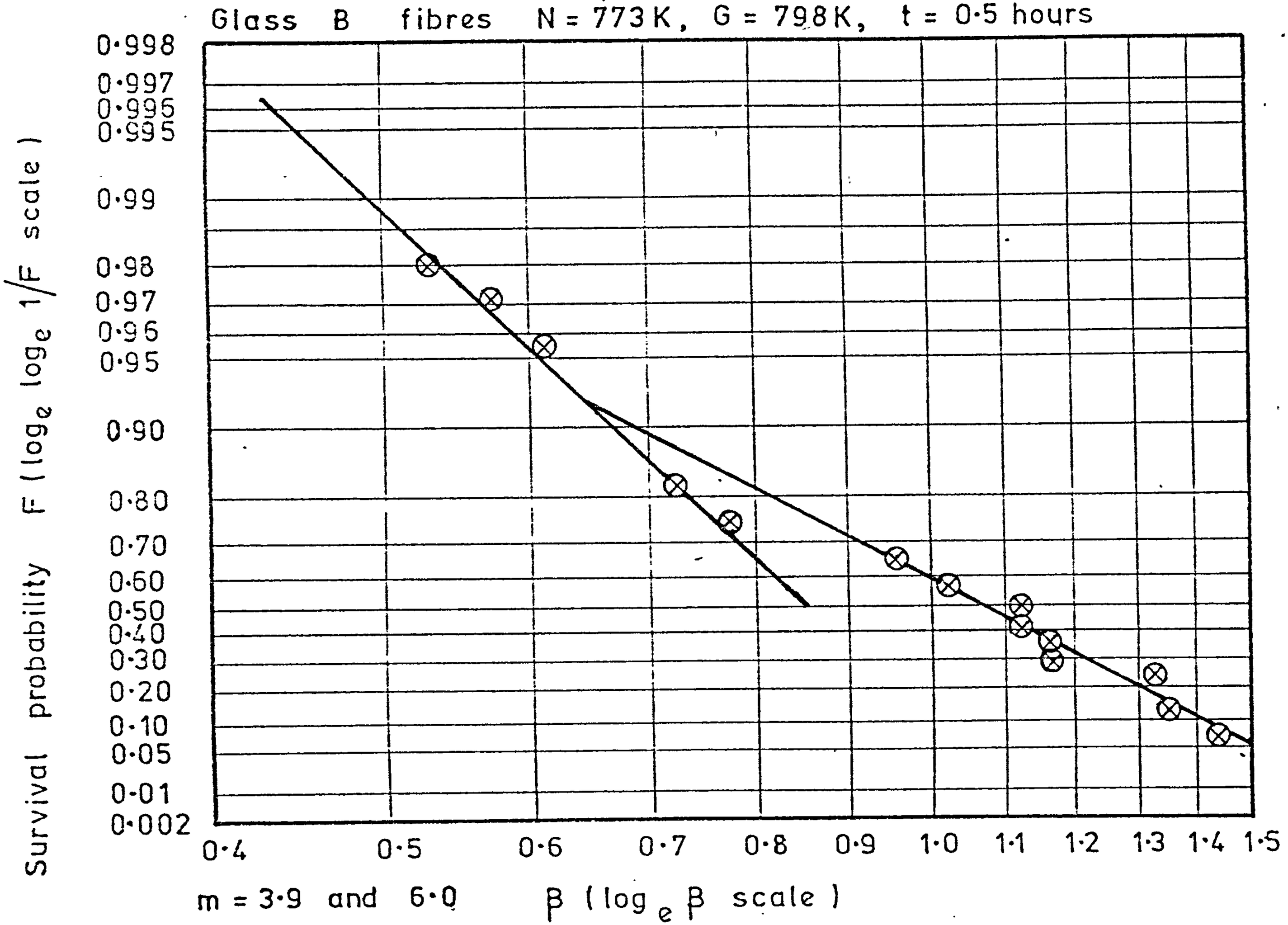
Glass B fibres N = 773 K, G = 798 K, t = 0·5 hours
Survival probability F (log_e 1/F scale)
0·998
0·997
0·996
0·995
0·99
0·98
0·97
0·96
0·95
0·90
0·80
0·70
0·60
0·50
0·40
0·30
0·20
0·10
0·05
0·01
0·002
0·4
0·5
0·6
0·7
0·8
0·9
1·0
1·1
1·2
1·3
1·4
1·5
m = 3·9 and 6·0
β (log_e β scale)

FIG 6.11

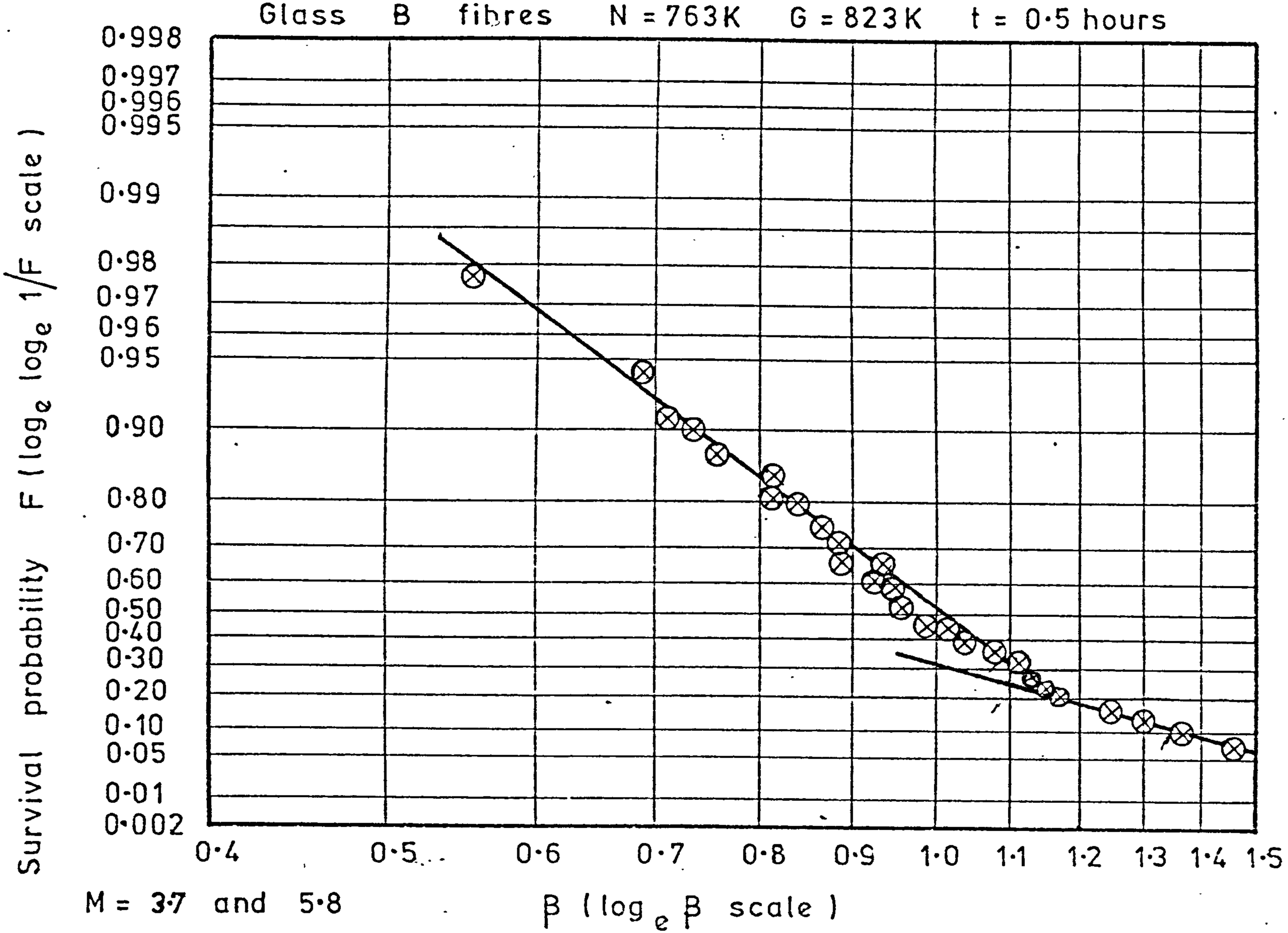
Glass B fibres N = 763K G = 823K t = 0·5 hours
Survival probability F (log_e 1/F scale)
0·998
0·997
0·996
0·995
0·99
0·98
0·97
0·96
0·95
0·90
0·80
0·70
0·60
0·50
0·40
0·30
0·20
0·10
0·05
0·01
0·002
0·4
0·5
0·6
0·7
0·8
0·9
1·0
1·1
1·2
1·3
1·4
1·5
β (log_e β scale)
M = 3·7 and 5·8

FIG 6.12

6.4 Modulus of Elasticity

The dynamic method used here to determine the elastic modulus of the fibres employed the equation

$$E = \frac{Wn \quad wl^4}{\beta_n{}^2 l^2 \, Ig} \tag{6.4}$$

The terms in this expression have been described in chapter 5. The absolute accuracy for each parameter was determined experimentally and thus the relative accuracy of modulus values can be expressed in terms of the accuracy of each parameter:

$$\frac{\Delta E}{E} = \frac{\Delta Wn}{Wn} + \frac{\Delta W}{W} + 4\,\frac{\Delta l}{l} + 4\,\frac{\Delta D}{D} = 2\% + 4\,\% + 0.05\% + 2\%$$

$$\frac{\Delta E}{E} = 8\%$$

The elastic modulus for each heat treatment is presented in Appendix II.

Reproducibility

The reproducibility of the measurements was tested using a paired observation procedure. The modulus was determined for two samples of ten fibres. Let the mean of each batch be $\overline{E}_A$ and $\overline{E}_B$. If the two sets of results belong to the same population $\overline{E}_B - \overline{E}_A = \overline{E} = 0$. The null hypothesis that $\overline{E} = 0$ was tested using the statistic $\frac{\overline{E} - 0}{S/\sqrt{n}}$ which has a t distribution with 9 degrees of freedom. The value of t found from tables for a 1% significance level was 3.25 but the t values calculated using the above statistic were 0.02 for glass A fibres and 0.03 for glass B. Thus there is no significant difference between the pairs of observations in each case. The results are shown in table 6.3.

Table 6.3 Reproducibility of Modulus Results

(a) GLASS A N = 743 K G = 798 K t = 40 mins

Sample (1)	Modulus (GN/m^2)	Sample (2)	Modulus (GN/m^2)
1	96.5	1	97.3
2	93.9	2	95.1
3	95.1	3	96.7
4	97.3	4	93.9
5	94.2	5	95.4
6	95.5	6	95.5
7	97.3	7	95.3
8	96.8	8	97.1
9	95.9	9	96.6
10	97.1	10	96.8

Mean (1) = 96.0 Mean (2) = 96.0
Standard Deviation = 1.2 Standard Deviation = 1.0
Students t = 0.02

(b) GLASS B N = 763 K, G = 798 K t = 1.5 hours

Sample (1)	Modulus (GN/m^2)	Sample (2)	Modulus (GN/m^2)
1	74.5	1	75.9
2	77.1	2	77.9
3	75.3	3	77.1
4	72.3	4	74.6
5	73.5	5	72.4
6	74.9	6	71.2
7	72.6	7	73.8
8	73.6	8	74.7
9	76.1	9	72.7
10	75.8	10	75.2

Mean (1) = 74.6 Mean (2) = 74.6
Standard Deviation = 1.5 Standard Deviation = 2
Students t = 0.03

6.5 Microscopy

6.5.1 Crystal Growth Rates and Size

Crystal growth rates were determined by measuring crystal sizes from micrographs corresponding to a series of crystallization times. Preparation of good micrographs was difficult to achieve but most of the results presented were thought to be sufficiently accurate for the purposes of this investigation. The most accurate and precise measurements were the crystal sizes obtained for surface crystallinity in glass A rods. Table 6.4 lists the mean crystal diameters. The 95% confidence limits were calculated and found to be negligibly small and for this reason they are not included in the table. Some observations are also made about the morphology of the internal crystals. The relative accuracy stated was determined by calibrating the stereoscan microscope and the inaccuracy is almost an order of magnitude greater than the 95% confidence limits on the actual measurements thus the total accuracy is limited by the measurements themselves and not their variance. The relative accuracy of the measurements made from micrographs is represented graphically in figure 6.13. A similar series of measurements were carried out on micrographs of glass B fibres. Micrographs were obtained using both scanning and transmission microscopy and the results are presented in tables 6.5 and 6.6. Because of the variance of crystal diameters in these fibres the precision was poor compared to the accuracy of the individual measurements thus, mean crystal diameters are quoted together with the 95% confidence limits. The crystal morphology of glass B fibres changed during growth adding further complication to the presentation of crystal size thus it was considered better to make a conservative estimate of growth rate by accepting only the order of magnitude and not the actual value of growth rate; this applies particularly to the ion exchanged fibres since the micrographs obtained from fibre debris give results which are somewhat suspect. It must be emphasized that although undesirable, such indirect

Table 6.4 Crystal Growth Rates and Morphology for Glass A

Recrystallization Conditions			Fibre diameter ($mx10^4$)	Mean crystal size (Surface) ($m \times 10^6$)	Relative accuracy of crystal size (%)	Crystal growth rate ($m \times 10^8$/min)	Relative accuracy of growth rate (%)	Morphology of internal crystals
N = (K)	G = (K)	t = (mins)						
753	773	180	3.8	12.3	3.2	6.8	4.0	S
753	773	300	5.8	20.0	1.7	6.7	2.2	S + E
743	798	120	2.7	18.7	1.7	15	2.1	S + E
743	798	180	2.9	28.2	1.1	16	1.6	S + E
743	823	60	3.2	24.6	1.7	41	2.9	S + E
743	823	120	2.2	36.0	1.2	30	3.7	S + E
	773	180	3.6	9.3	4.2	5.2	4.2	S
753		5	3.6	13.0	3.2	~~260~~	4.0	S

S = Spherulite E = Small equiaxed crystal

Relative Accuracy vs Measured Length

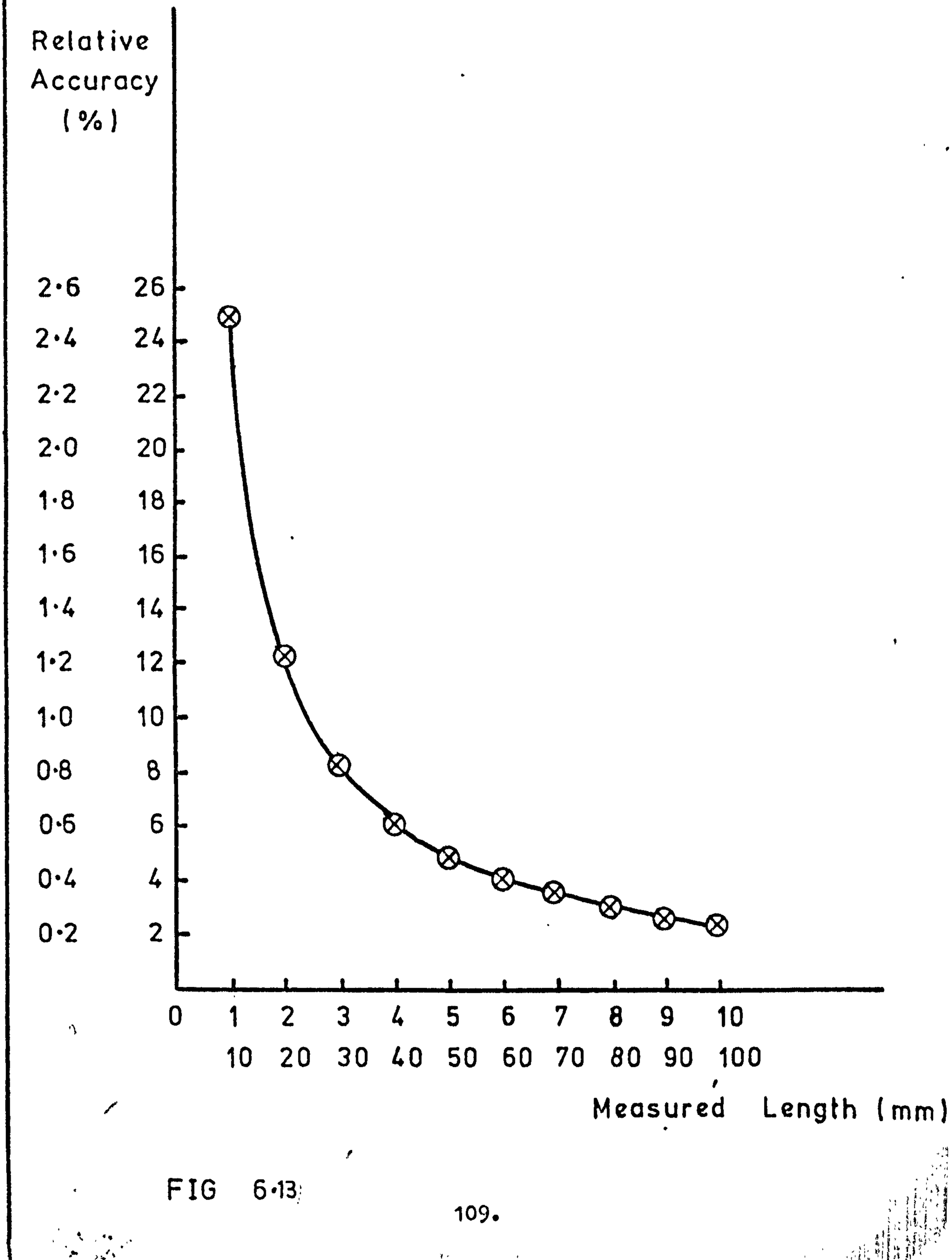

FIG 6·13

Table 6.5 Crystal Growth Rates and Morphology of Internal Crystals in Glass B Fibres.

Crystallization		Fibre diameter ($m \times 10^6$)	Crystal morphology	Mean crystal diameter ± 95% confidence limits. ($m \times 10^7$)	Crystal growth rate ($m \times 10^9$)
Temp. (K)	Time (hours)				
773	1.5	24.1	E	2.0 ± 1.5	2.2
773	3	24.1	E	3.4 ± 2	1.9
798	0.25	24.5	E	1.1 ± 1	7.3
798	3	24.5	L	12.0 ± 5.5	6.7
798	10	640	L + E(D)	L= 63 ± 20 E= 43 ± 22	L= 10.5 E= 7.2
823	0.25	24.5	L	20 ± 12	133
823	10	373	L + E(D)	L= 100 ± 26 E= 90 ± 15	L= 16.7 E= 15.0

L = Elongated crystals

E = Equiaxed or slightly oblate crystals

I [illegible]crographs of fibre debris.

Table 6.6 Interpretation of Transmission Electron Micrographs

Magnification. $\times 10^{-3}$	Crystallization time at 798K (h)	Range of crystal diameters. (m $\times 10^{8}$)	Mean crystal diameter. (m $\times 10^{8}$) $\pm$ 95% confidence limits	Mean crystal growth rate. (m $\times 10^{9}$/min)
48	0.25	3 - 6	4 $\pm$ 1.2	2.8
180	0.25	1.6 - 6.0	4.2 $\pm$ 1.5	
100	0.5	5 - 15	10 $\pm$ 3	3.0
80	0.5	4 - 10	8 $\pm$ 2	
18	3.0	10 - 50	30 $\pm$ 5	1.7

Glass B fibres after ion exchange in KCl/argon vapour (400 l/hour) for 30 mins after which the fibres were nucleated at 763K for 1 hour and crystallized at 798K.

techniques had to be employed because of manipulative problems encountered in preparing fibres for microscopy.

6.5.2 Volume Fraction of Crystallinity

The percentage by volume of crystallinity was determined by two methods

(i) Analysis of electron micrographs

(ii) X-ray diffraction technique.

Merits and disadvantages can be given for each technique and the most appropriate method depends very much on the microstructure of the ceramic. For instance electron microscopy will rarely enable volume fractions of individual phases to be estimated in a multi-phase system if each phase has similar morphology.

Because of surface crystallization, electron microscopy was considered to be unsuitable for glass A fibres hence the results presented in table 6.7 quote values for glass B only. An estimated accuracy for these measurements is $\pm$ 10%.

X-ray diffraction intensity measurements were made here to determine the volume fraction of lithium disilicate specifically and not the total crystallinity. The mixtures used to verify intensity/volume fraction relationship was made up from lithium disilicate and crystobalite and it would have perhaps been more appropriate to have used trydimite since there was some evidence of its presence in the crystallized fibres. The results are shown graphically in fig. 7.3 Accuracy was very difficult to establish for these measurements.

6.5.3 Phase Identification

Two diffraction methods were employed to determine the nature of the phases appearing on crystallization of the fibres

(i) Selected area electron diffraction

(ii) X-ray diffraction.

Table 6.7 Volume Fraction of Crystallinity Determined from Scanning Electron Micrographs

Glass B			
N = (K)	G = (K)	t = (hours)	V_f = (%)
763	773	1.5	5
		3.0	15
763	798	0.25	10
		3.0	30
		10.0	95
763	823	0.25	10
		10.0	95
Glass B after ion exchange			
763	798	3.0	95

Electron diffraction was performed on glass B fibres since these were the only fibres sectioned for transmission electron microscopy, and the "d" spacings calculated from microdensitometer traces made on micrographs. These results are presented in table 6.8. Unfortunately, conclusive phase identification of alkali silicates by X-ray diffraction is difficult since many of the intense lines are found at low angle and are often lost in the halo caused by the presence of the amorphous phase. It was possible, however, to make some reasonable conclusions about the phases present. The lines chosen for identification are shown in table 6.9 and the results of the identification presented in table 6.10.

Throughout this study trydimite was thought to be the crystalline form of silica present.

6.6 Ion Exchange Experiments

An attempt was made to establish a correlation between vapour phase ion exchange process variables and the mean fibre strength. The two process variables considered were:

(i) Vapour flow rate

(ii) Time of exposure to the vapour for a constant flow rate.

The results of the first experiment are presented as a "scatter" diagram in fig. 6.14 and for the second in a similar scatter diagram in figure 6.15. In each case a correlation was sought between strength and process variable. Strength showed only a weak correlation to flow rate with a correlation coefficient of $r = 0.28$ whereas the strength/exposure time correlation was stronger, $r = 0.70$. This second correlation was tested to see if it was significant. The null hypothesis was that the correlation coefficient of the population was zero in which case there would be no correlation between strength and exposure time to the vapour. The test statistic t was

$$t = \frac{r}{\sqrt{1 - r^2}} \sqrt{n - 2} \qquad (6.5)$$

Table 6.8 Selected Area Diffraction of Glass B Fibres

Diameter of diffraction rings. (mm)	"d" Spacing ($m \times 10^{10}$)	Index of the nearest line for $Li_2O.2SiO_2$ $\{h\ k\ l\}$	"d" Spacing from the powder diffraction file. ($m \times 10^{10}$)
44	2.941	200	2.917
55	2.353	002/221	2.395/2.359
65	1.991	170	1.969
74	1.749	152/330	1.804
89	1.454	0,10,0	1.464
106	1.221	?	?

Camera constant $\lambda L = 6.47 \times 10^{-10}$

Table 6.9 Selected Lines for Intensity Measurement and Phase Identification

h k l	"d" (m x 10^{10})	Relative Intensity I/I_1
Lithium Disilicate		
132/241	2.059	8
170	1.969	20
152/330	1.804	8
Lithium metasilicate		
120/200	2.71	90
131/002	2.34	17
132/202	1.773	8
Trydimite		
2020	2.955	60
—	2.286	40
—	1.928	40
Cristobalite		
102	2.841	14
200	2.485	20
211	2.118	6

Table 6.10. Identification of Phases in Crystallized Fibres

Crystallization Temperature (K)	Crystallization Time	Phases present
Glass A N = 753 K		
773	30 mins	LD + A
	60 mins	LD + A
798	30 mins	LD + A
	60 mins	LD + A
823	30 mins	LD + A
	60 mins	LD + T + A
	360 mins	LD + T + A
Glass B N = 763 K		
798	0.25 hours	Identification difficult
	0.5 "	LD + A
	1.5 "	LD + T + A
	3.0 "	LD + T + A
	10.0 "	LD + T + (A)?
Glass B after ion exchange with K^+ N = 763 K		
798	0.25 hours	Identification difficult + LB
	0.5 "	LD/LM + A
	3.0 "	LD + T + A
	10.0 "	LD + T + (A)?

LD = Lithium Disilicate LM = Lithium Metasilicate

T = Trydimite C = Cristobalite

A = Amorphous glass phase

LB = Line broadening

Table 6..10 continued ...

Glass C		
Crystallization Temperature (K)	Crystallization Time (hours)	Phases present
773	1	NDP*
	5	"
798	1	"
	5	"
823	1	"
	5	"
873	1	"
	5	"

*NDP = no detectable crystalline phase present

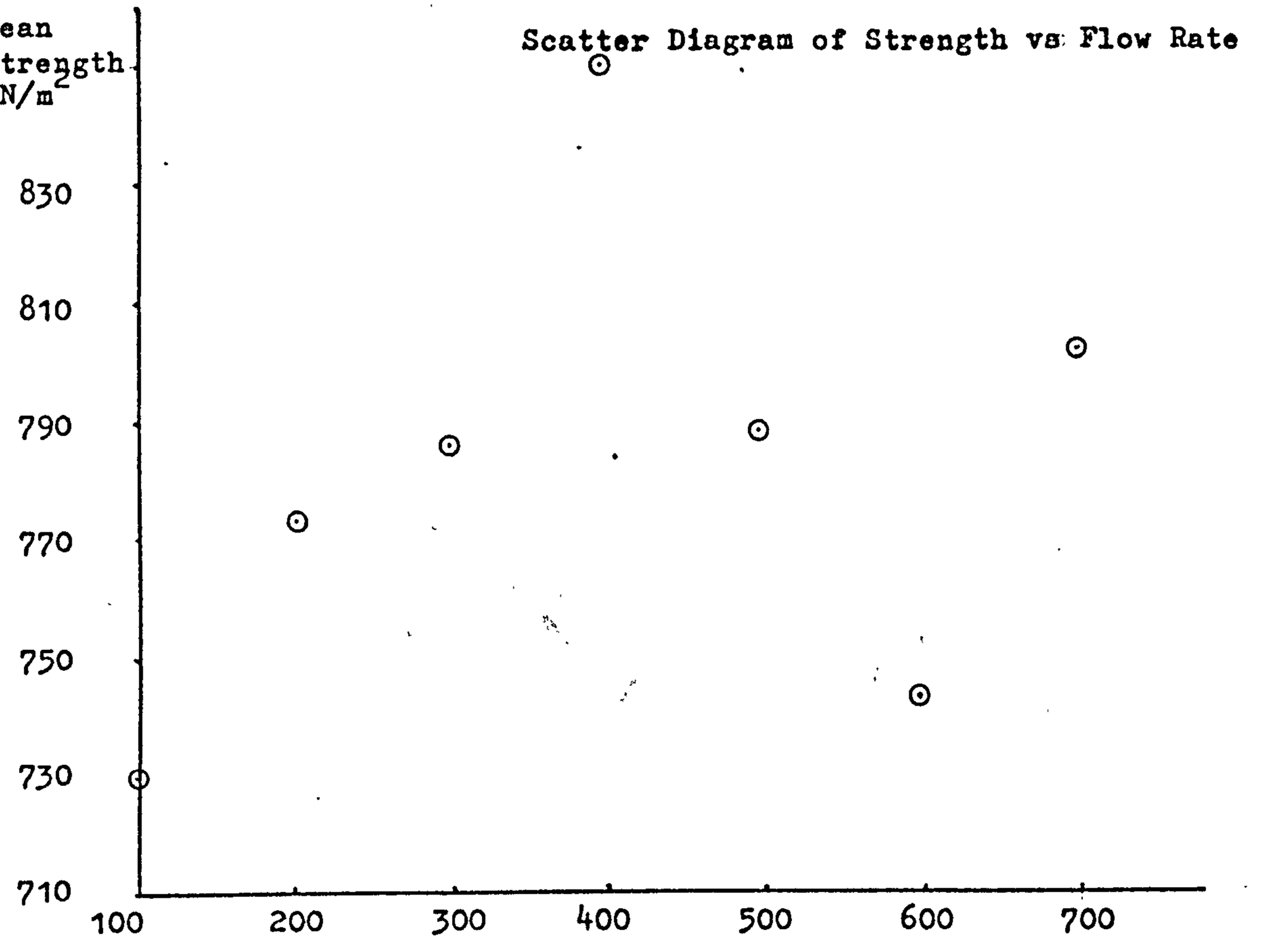

FIG. 6.14

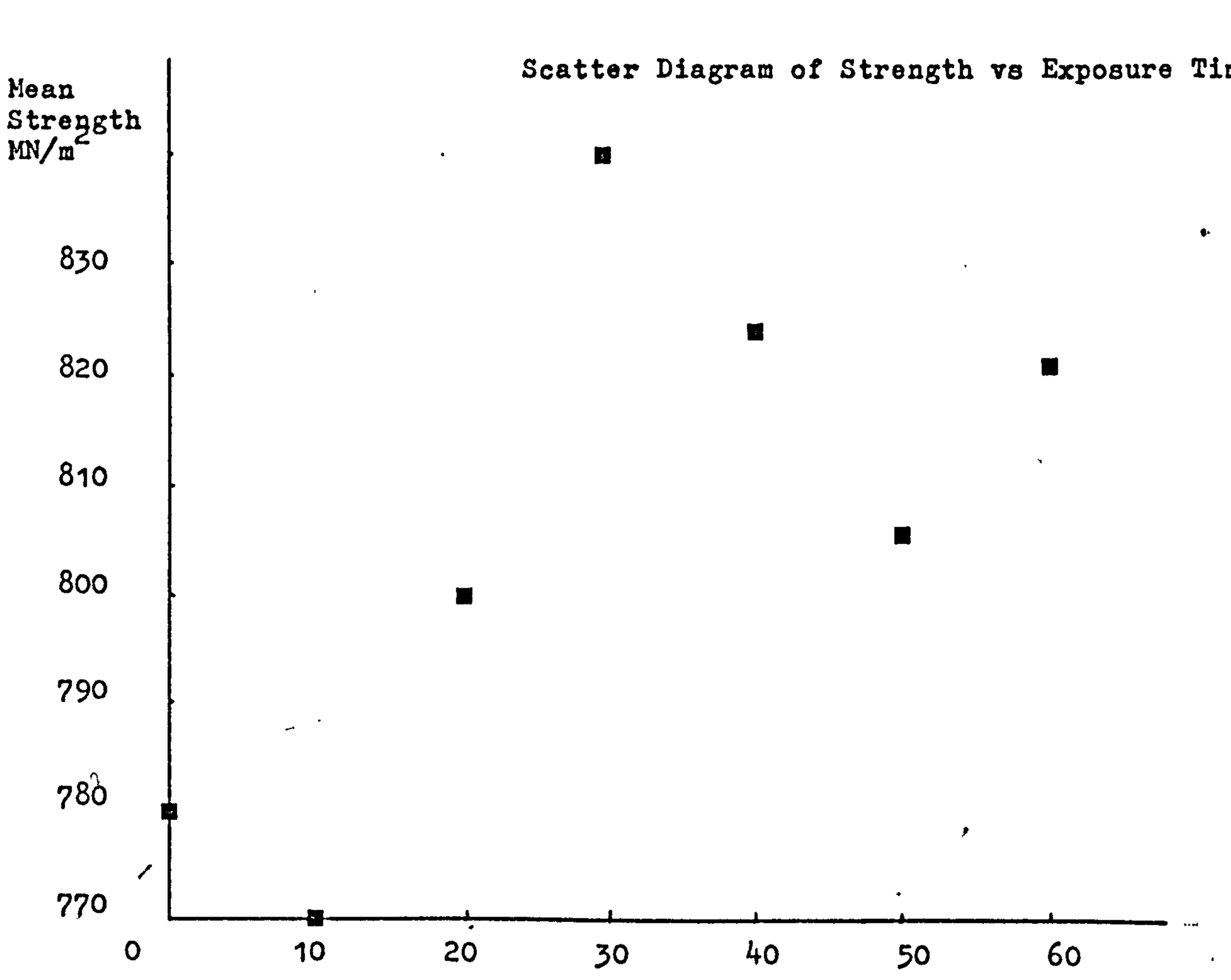

FIG 6.15

This has a t distribution with n - 2 degrees of freedom. The 10% significance level was chosen and the range of values of r, for which the hypothesis was acceptable, found from tables. The calculated statistic was just significant at this level i.e. $|r| = 0.70$ and the value from tables was $|r| = 0.66$ thus a correlation can be said to exist at the 10% level but not at the 5% level.

6.7 Determination of K^+ Concentration Profiles in Fibres

6.7.1 Electron Microprobe Analysis

No useful results were obtained using this technique.

6.7.2 Radioactive Tracer Analysis

Preliminary experiments showed the fibres to dissolve at a linear rate in 4% hydrofluoric acid.

The measured rate = $2.22 \pm 0.17 \times 10^{-6}$ m/min

The experiment was repeated several times and the result appeared to be consistent.

Aliquots of dilute hydrofluoric acid containing dissolved K^+ ions from the fibre were analysed in a γ-ray spectrometer in which six γ-ray peaks were monitored. The results obtained by plotting log I/I_o against time showed two gradients detectable on the graphs suggesting the presence of two isotopes suspected to be ^{42}K and ^{59}Fe. Apart from the problems presented by the over-lapping of γ-ray peaks the plots of activity against dissolution time showed scatter and overlap making it difficult to make any quantitative predictions of ^{42}K concentration profiles.

6.7.3 Flame Photometry

In this work the fibres were again dissolved in dilute hydrofluoric acid (1%). Lack of time did not allow a complete investigation to be made by this technique but it was possible to determine approximate values of

the K^+/Li^+ ion ratio at various depths in the fibre. For the following ion exchange conditions a set of results are included.

Argon flow rate	400 l/hour
Salt	K Cl
Salt temperature	1065 K

Distance from fibre surface (m x 10^6)	$Li^+:K^+$ ratio
0.1	1:1
0.8	2:1
1.6	5:1
3.0	10:1
5.0	10:1

It was again very difficult to establish an order of accuracy for these results.

7. Discussion

7.1 The Strength, Modulus and Microstructure of Glass-Ceramic A Fibres

7.1.1 Dependence of Strength on Surface Crystallization

The majority of data derived from the tensile tests relate mean fibre strength to crystallization time and temperature. It is the intention of this discussion to explain these strength variations in terms of the microstructure of the fibres. Information about these microstructural features was obtained from direct investigations using electron microscopy and the indirect technique of X-ray diffraction.

The graphs presented in figures 6.4 to 6.7 illustrate that in all cases the mean strength of glass A fibres decreased during crystallization and the rate at which this occurred appeared to be related to the crystallization temperature. To explain such behaviour the assumption is made here that the fibres, whether uncrystallized, partly or highly crystallized, could be considered to be truly brittle solids. Thus it is assumed that the effective surface energy for fracture is close to the thermodynamic surface energy of the solid. There is evidence that this is not the case [37] particularly in a glass where it is possible that a small plastic zone may be associated with the crack tip during fracture of the material. This would make the effective surface energy higher than the thermodynamic energy and there is experimental evidence to suggest this is the case [38]. However, the effect is small enough to allow the Irwin-Orowan relationship

$$\sigma = \sqrt{\frac{2EY}{\pi C}} \qquad (7.1)$$

to be used with reasonable accuracy and it is this relationship that will be employed to explain the microstructural dependence of fibre strength.

There are two prominent features displayed by the strength vs

crystallization time curves figs. 6.4 to 6.7. Firstly when the fibres were crystallized at the lowest temperature of 773K the strength appeared to be almost unaffected by crystallization time for the first 15 minutes after which it decayed rapidly. This region did not appear to be present in fibres crystallized at 823K but was just detectable in fibres crystallized at 798K. The second feature of the curves is that the strength/time relationship in the region where strength decreases, is not linear and may thus have exponential or power law dependence. It was known from microscopy that glass A experienced surface as well as internal crystallization. This surface crystalline layer could present a possible source of strength controlling flaw. For instance during surface crystallization if there is a volume change interfacial stresses between the crystal and residual glass phase would be established. Should the residual glass become silica rich by the migration of ions to the growth interface then it is possible that the glass phase cannot relieve these stresses at the crystallization temperature. This may then lead to inter-facial cracks of the same magnitude as the surface crystal length. Another possibility is that the difference in thermal expansion coefficients between lithium disilicate crystals and the residual glass phase could also give rise to stresses during cooling. If the glass phase at the crystal boundaries is depleted in Li^+ ions, and therefore silica rich, it is likely to have a lower expansion coefficient than lithium disilicate. This would give rise to tensile stresses in the surface layer which could cause interfacial cracks between the crystals. There is little documented information about the expansion coefficients of lithium disilicate so it was not possible to perform a calculation to determine the possible thermal stresses, however, McMillan, Hodgson and Booth[40] measured the expansion coefficient of a sample of fully crystallised lithia silica glass with 70 mole % silica and found that it was higher than the parent glass i.e.

$$\alpha_{ceramic} = 96 \times 10^{-7}$$

$$\alpha_{glass} = 86 \times 10^{-7}$$

This would indicate that tensile thermal stresses could arise in the surface layer on cooling. Such cracks would be oriented normally to the long axis of the fibre and therefore normal to the stress field making them the most effective flaws for fracture initiation. If this is the case it should be possible to establish a relationship between the mean thickness of the surface crystal layer and the fibre strength. In the early stages of crystallization the surface crystals will be small. If their size is less than the inherent flaw size in the glass fibre then strength would be unaffected until the depth of the surface exceeded this inherent flaw size. After this stage the strength should then decrease in proportion to the thickness of the surface layer. In a model system this strength/time functional relationship can be derived from equation 7.1. If the depth of the surface layer is linearly related to crystallization time then

$$c \propto t$$

thus from (7.1)

$$\sigma \propto \frac{1}{\sqrt{t}} \qquad (7.2)$$

to verify this model the experimental data must enable the following points to be verified

i) That the strength/time data can be described by a relationship of the type $= At^{-\frac{1}{2}}$

ii) That the dominant flaw size is of the same magnitude as the depth of the surface crystal layer.

iii) That the growth rate of this layer can be shown to the linear.

The experimental data in this thesis are incomplete in parts and thus each point cannot be proven conclusively, however, the general indication from this work is that the hypothesis is correct. Each point will now be dealt with separately.

Two techniques were used to establish the functional form of the strength/time curves. As mentioned previously a regression method was used to fit the data to the form $y = Ax^b$. In chapter 6 it was shown that this regression was significant. The important feature arising from the regression is the value of the exponent b. In table 7.1 the regression equation is listed for each heat treatment. As can be seen the exponent varies but in several cases it is close to -0.5. The exponents appear to be classified into two groups one giving an inverse square and the other an inverse cubic relationship between σ and t. On this evidence alone it was not possible to accept or reject the hypothesis that $\sigma \propto \frac{1}{\sqrt{t}}$ since the data values used were mean values each having its own variance. Thus slightly different values equally likely from each distribution may have given an exponent closer to -0.5. Another procedure was now used. It was assumed that the relationship $\sigma \propto \frac{1}{\sqrt{t}}$ was correct in which case appropriate values of E and γ could be used to solve equation (7.1) and so develop a theoretical prediction for the strength/time relationship. This required a value for crystal growth rate, elastic modulus and surface energy for each crystallization temperature. Crystal growth rates will be discussed in some detail later in this chapter. However, this aspect of the work was somewhat incomplete and approximate rates were only available for a limited number of temperatures.

Extensive measurements of elastic modulus had been made for a wide range of heat treatments thus enabling the appropriate elastic modulus to be chosen for a particular degree of crystallinity. Finally a value of 2.8 J/m^2 was used for the surface energy. This value had been measured previously by Clucas[67] using four point bend in vacuum. The reason for choosing this particular value was that these investigations were carried out on specimens of glass ceramic with an identical composition to A. These specimens had also been subjected to similar heat treatment conditions as the fibres.

TABLE 7.1

Nucleation Temperature K	Crystallization Temperature K	Curve Fitting Equation $Y = Ax^b$
743	773	$y = 1364\ x^{-.31}$
753	773	$y = 1397\ x^{-.32}$
763	773	$y = 1870\ x^{-.45}$
743	798	$y = 1406\ x^{-.42}$
753	798	$y = 1509\ x^{-.45}$
763	798	$y = 1405\ x^{-.42}$
743	823	$y = 687\ x^{-.31}$
753	823	$y = 693\ x^{-.31}$
763	823	$y = 701\ x^{-.37}$
	773	$y = 1347\ x^{-.32}$
743	923	$y = 684\ x^{-.7}$

Where approximate growth rates were available the Irwin-Orowan relationship was solved thus generating a set of strength values for the corresponding crystallization times. The calculated strengths were compared with the measured mean strengths for three heat treatments. The data are shown in table 7.2. A paired observation test was performed to see if the differences between calculated and observed stress were significant or due merely to random fluctuations in the values. Using a t distribution it was found that there was no significant difference between values at the 5% significance level. Since the error in crystal growth rate was the probable cause of the discrepancies between calculated and observed strengths it was decided to make use of the assumption that $\sigma \propto \frac{1}{\sqrt{t}}$ and so find the best regression fit of experimental data to this equation and thereby determine the crystal growth rate which gave the maximum correlation in each case. These curves are also shown in figures 6.4 to 6.7 and the optimized growth rates listed. Finally a comparison was made between the calculated and measured growth rates, the values of which are listed in table 7.3. Again a paired observation test was performed to establish if the pairs of observations were significantly different but at the 5% level this was found not to be the case. It was concluded that there is some evidence to suggest that the fibre strength is controlled by the depth of the surface crystalline layer during crystallization. However, it can also be argued that such statistical tests and regression analyses do not provide conclusive evidence alone of this relationship and that more information is required to validate the physical basis of the model. It was mentioned previously that some discussion would be given to the two assumptions made concerning this physical basis, and these points are now amplified in turn.

Microscopy was used to identify the important microstructural features in the fibres. Plates 7.1 to 7.6 are scanning electron micrographs

TABLE 7.2

Heat Treatment (K)	Crystallization time (minutes)	Calculated strength (MN/m^2)	Observed mean strength (MN/m^2)
N = 753	0	-	696
G = 773	10	785	680
	20	578	565
	30	482	485
	40	421	412
	50	381	347
	60	355	325
N = 743	0	-	696
G = 798	10	539	586
	20	405	380
	30	338	333
	40	300	290
	50	269	291
	60	248	225
N = 743	0	-	696
G = 823	10	364	398
	20	279	270
	30	231	266
	40	203	216
	50	181	219
	60	165	171

Table 7.3 Measured vs Predicted Growth Rate

Nucleation Temperature (K)	Crystallization Temperature (K)	Measured Growth Rate (m x 10^8/min)	Predicted Growth Rate (m x 10^8/min)
753	773	6.8	7.0
743	798	16	14
743	823	36	30
—	773	52	70
753	923	260	310

Correlation coefficient = 0.99

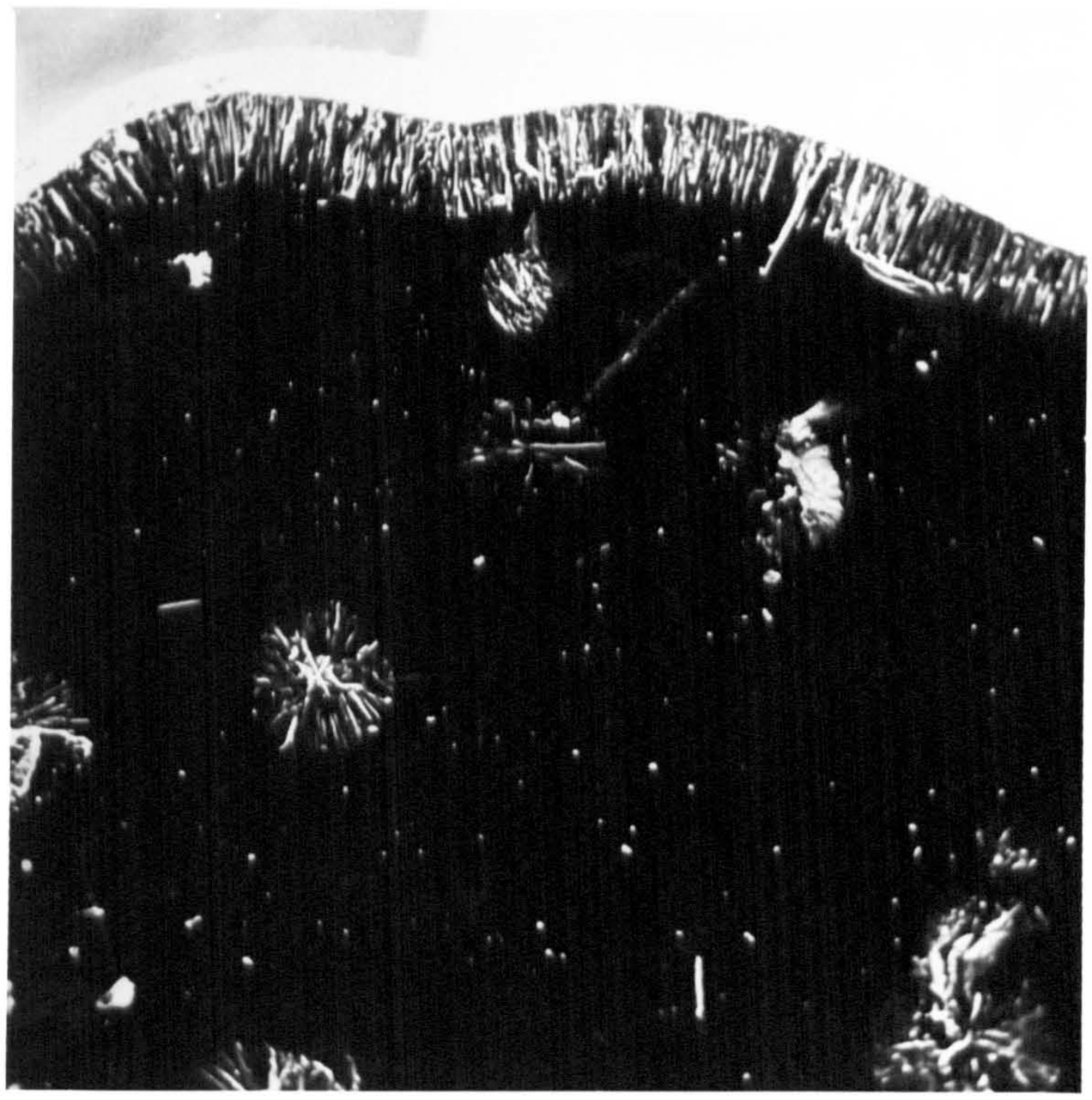

Plate 7.1 Glass A (N = 753K, G = 773K) Crystallized for 3 hours.
Diameter = 3.8×10^{-4} m Mag. = X 650.

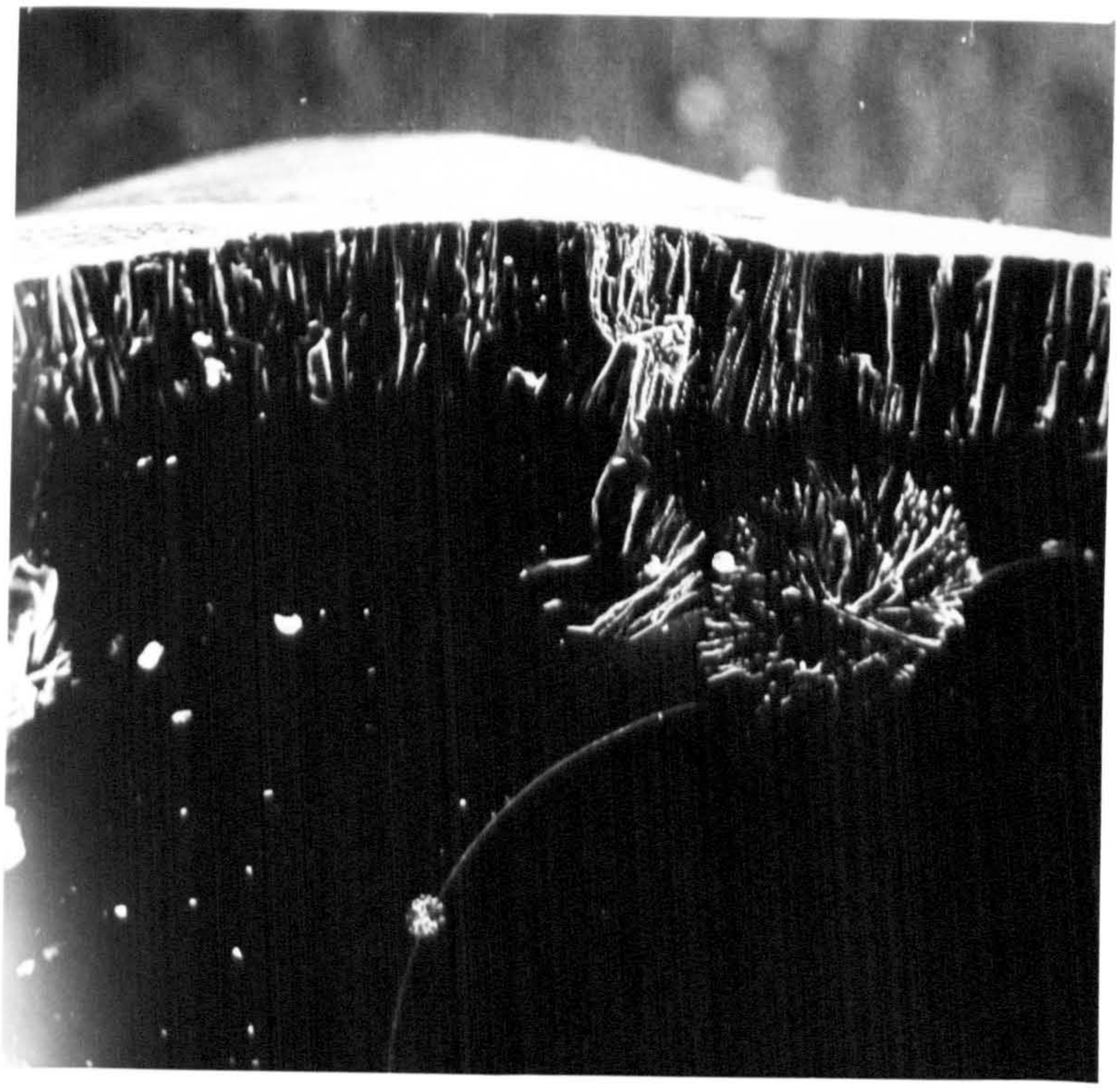

Plate 7.2 Glaqs A (N = 753K, G = 773K) Crystallized for 5 hours.
Diameter = 5.8×10^{-4} m. Mag. X 750.

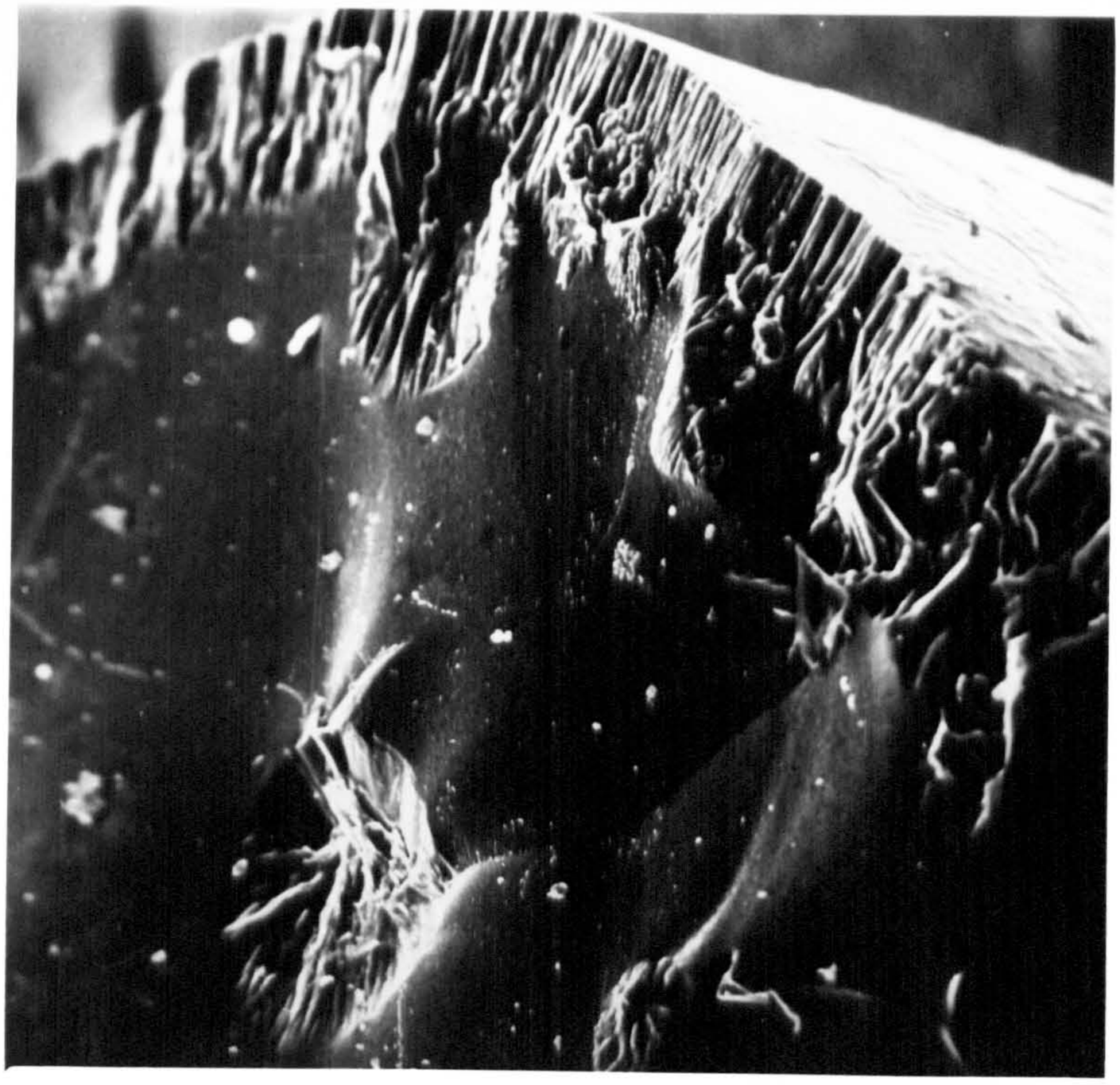

Plate 7.3 Glass A (N = 743K, G = 798K) Crystallized for 2 hours.
Diameter = 2.7×10^{-4} m Mag. = X 800.

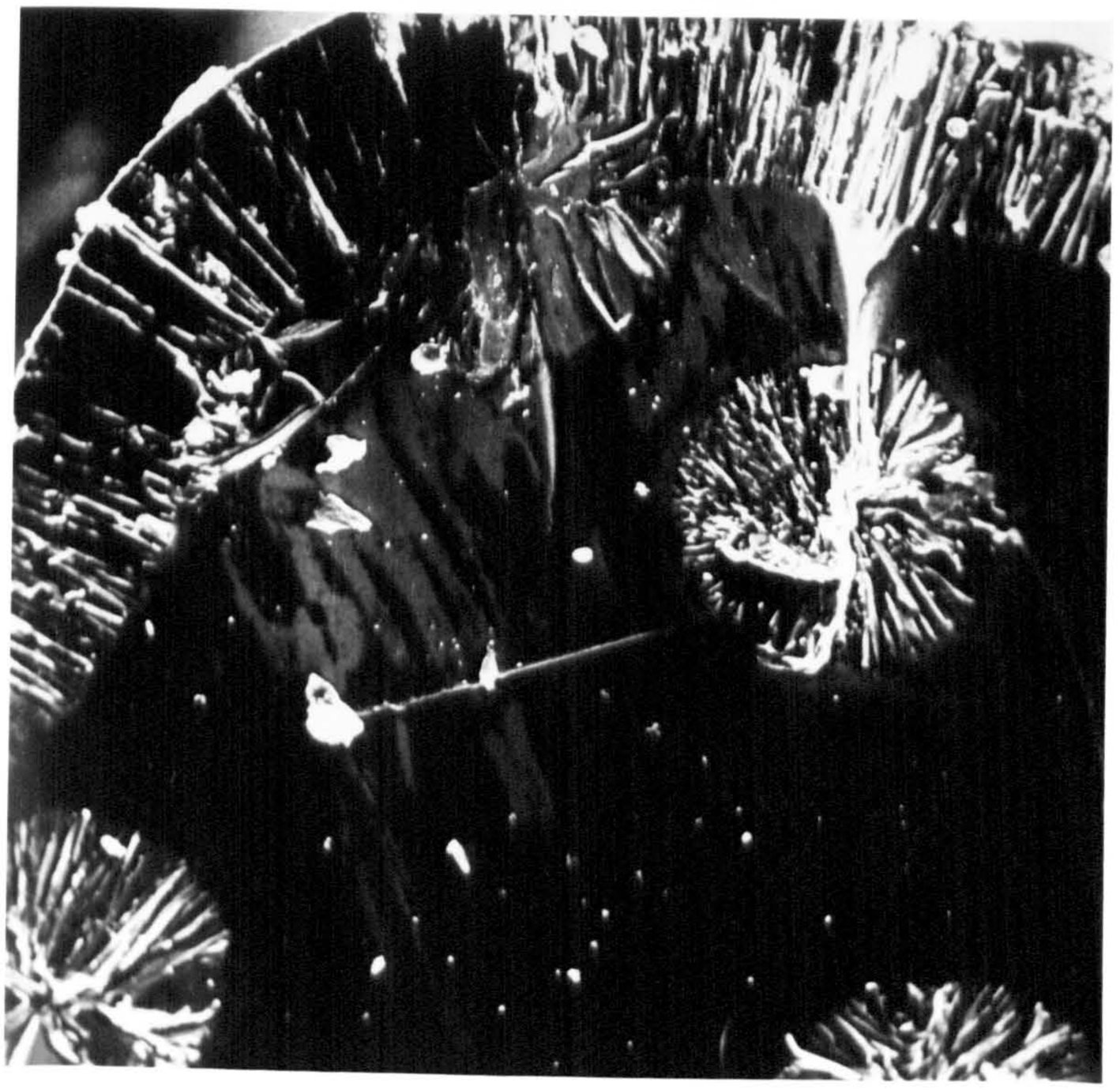

Plate 7.4 Glass A (N = 743K, G = 823K) Crytallized for 2 hours.
Diameter = 2.2×10^{-4} m Mag. = X 550

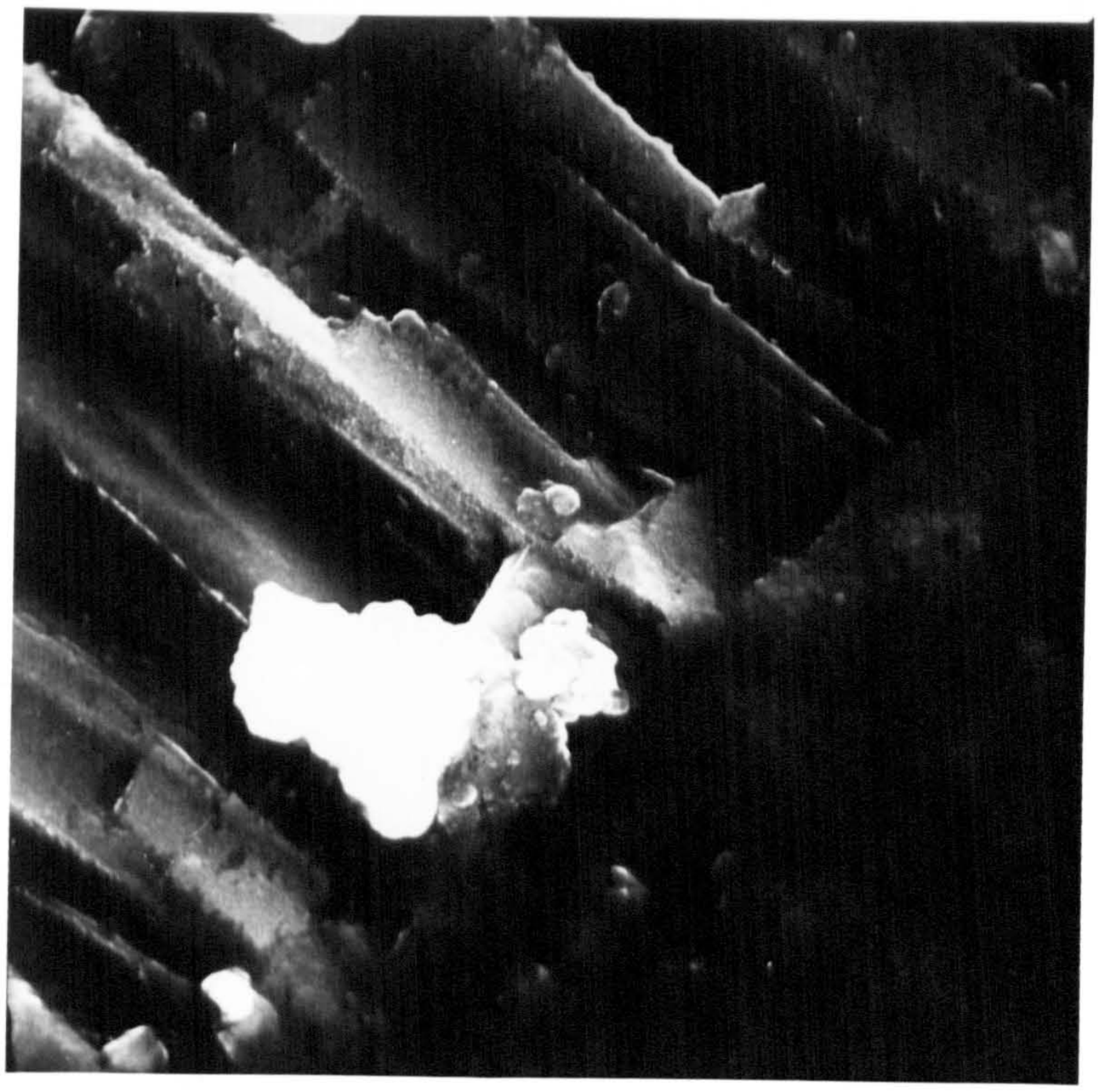

Plate 7.5 Glass A (N = 743K, G = 823K) Crystallized for 2 hours. Growth interface X 11,000.

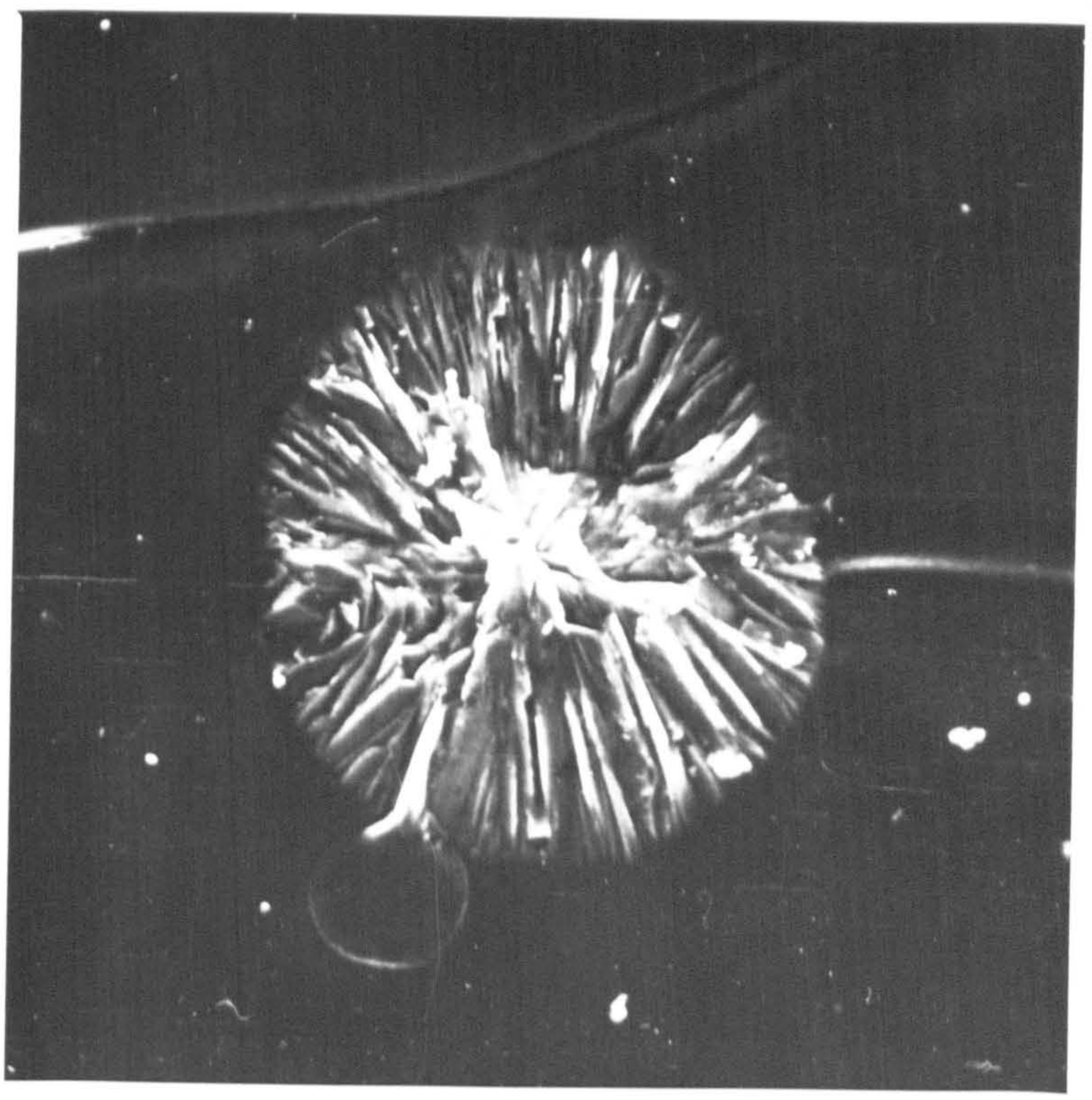

Plate 7.6 Glass A (N = 743K, G = 823K) Crystallized for 2 hours. Internal spherulitic crystals X 1,100.

displaying both surface crystallinity and some isolated spherulitic crystals within the body of the fibre. The micrographs were infact produced using thin rods which were approximately one order of magnitude larger than the fibres. The surface crystal layer was quite uniform but at high magnification (plate 7.5) there is evidence of cleavage between the grain boundaries of the surface crystals. This effect can arise readily if a volume change takes place during crystal growth. In many polycrystalline ceramics it is well accepted that flaw size distribution can be related to the grain size distribution and it would therefore be reasonable to make a similar assumption for glass-ceramic fibres. The difference here is that the aspect ratio of the crystals is such that the flaw size is likely to be determined by the long axis of the crystal which is the depth of the surface crystal layer. Since this surface layer is uniform, after prolonged crystallization, the crystal and therefore flaw size distribution will have a small variance. The stress function $(\frac{\sigma}{\sigma_o})^m$ in the two parameter Weibull equation is equivalent to a flaw density distribution and the Weibull modulus is a measure of the variance of this distribution. During the early stages of crystallization the strength data gave a Weibull modulus of approximately 3 when fitted to a Weibull distribution. After prolonged crystallization, however, there was evidence of the data exhibiting a bimodal distribution each with its associated Weibull modulus. The existance of bimodal strength distributions is not uncommon and in particular the effect is reported when testing long optical glass fibres [47, 48, 49]. The expla nation for this effect in glass fibres is that random surface abrasion is responsible for the low strength, high variance flaw population whilst the inherent flaws in the fibres give rise to the high strength low variance population. Glass A fibres showed evidence of two quite different distributions with approximate values of 3 and 2. This effect occurred only after

crystallization and not in the parent glass fibres. It was thought that the relatively short fibres tested would not exhibit a bimodal distribution since there was insufficient stressed material to sample the flaw distributions sufficiently in order to differentiate between the flaw populations. This is because the distribution of flaws caused by abrasion tends to mask the inherent flaw distribution. However, after crystallization the flaws introduced by surface crystallization would probably have a high enough density to compete with the flaw population present. Thus the bimodal distribution appears as a marked feature after certain crystallization times. A proposed explanation for this behaviour is that the flaw size population in the fibres during the early stages of crystallization is controlled by the depth of penetration of the surface crystal layer. Since this layer is relatively uniform the variance of the population will be small and thus the Weibull modulus will take on a high value. As crystallization proceeds internal spherulitic crystals appear in the fibre (plates 7.1 to 7.6). It is possible that the inter-spherulite spacing now controls the flaw size distribution. This spacing will have a greater variance than the surface crystal size thus a lower Weibull modulus. Observing the crystallization time after which the bimodal distribution appears there seemsto be no real correlation and thus little can be said about this except that no evidence of a bimodal distribution was found for fibres crystallized at the highest temperature of 923K. In this case the higher crystallization temperature may cause a reduction in effective internal nuclei before crystals have chance to grow from these sites. The surface crystals, however, appear to be well established and therefore the surface crystal layer dominates strength throughout.

The significance of the difference between the pairs of Weibull moduli in the bimodal distribution was tested using the standard error

$$m \pm \frac{m}{\sqrt{2n}}$$

In all cases the error was $\pm$ 10% of the Weibull modulus which indicates that the moduli are significantly different. The appearance of a bimodal distribution discussed above can sometimes occur if the data has been fitted to the wrong distribution. Some data will appear to be grouped when fitted to a two-parameter Weibull distribution indicating that the data belongs to a bimodal distribution, yet the same data may exhibit unimodal behaviour when fitted to a three-parameter distribution. However, if the data are fitted to the wrong Weibull distribution the modulus, or moduli in the bimodal case, will give a value that is not physically sensible. In this case there is strong evidence that the two-parameter distribution is more appropriate since the Weibull moduli derived from the graphs give values that would be expected for a material exhibiting a large variance in strength. Another factor favouring the adoption of the two-parameter distribution is the significance of the threshold stress σ_u. This term was originally introduced by Weibull as an empirical factor enabling the equation to fit test data. It is often referred to as the threshold stress below which there is an infinite survival probability. In recent years attempts have been made to interpret this parameter in terms of the flaw size distribution in the material. Thus it is assumed that there is a limit to the flaw size which can exist in the material. In general this parameter is considered to be independent of the volume of the material. This appears to be a sensible assumption since in most instances the flaws responsible for fracture are many orders of magnitude smaller than the dimensions of the body. However, the dimension of fibre diameter can be of the same order as the flaws causing fracture. In this case the concept of a threshold stress is not sensible and thus $\sigma_u \rightarrow 0$ indicating that the two parameter distribution is the more appropriate.

The second assumption in this model was that the surface crystal

growth kinetics exhibit a linear relationship to crystallization time. The arguments in favour of this are that the measured crystal growth rates generate strength values, from the Irwin-Orowan equation, which show a good agreement with the observable values and secondly the crystal morphology suggests that its needlelike morphology would be compatible with a linear growth rate. The growth rates were, however, determined from micrographs of thin rods whose diameters were at least an order of magnitude greater than the average fibre diameters. Crystal growth kinetics usually assume that a crystal grows in a semi infinite medium thus if ions diffuse to the growth interface they are continually replenished in the zone ahead of the growing crystal. A fibre, however, is a finite source of ions and it is possible that compositional changes will take place during crystal growth which may change the growth rate during crystallization. Unfortunately in this work no experimental evidence was available to verify a linear growth rate over the total range of crystallization in the fibres and so the assumption is made only on circumstantial evidence but it does appear to fit the experimentally observed strength/time data.

Since crystal growth data was available for a range of crystallization temperatures a simple Arrhenius equation was used to calculate an activation energy for growth of the surface crystals. The data gave a reasonable fit to a linear relationship when the logarthim of the growth rate was plotted gainst the reciprocal of temperature as shown in figure 7.1. The activation energy derived from the graph was 1.5×10^8 J/kg mole which is low compared to the values reported by Ito[1] and Tomozawa[11]. These were 4.62×10^8 J/kg mole for the temperature range 703-753K and 3.8×10^8 J/kg mole. These values were, however, obtained for $Li_2O \cdot 2SiO_2$ glass without the addition of P_2O_5.

Finally the critical stress intensity factor was estimated for the

Graph of $\ln u$ vs $\frac{1}{T}$

Activation energy $Q = 1{\cdot}5 \times 10^8$ J/kg

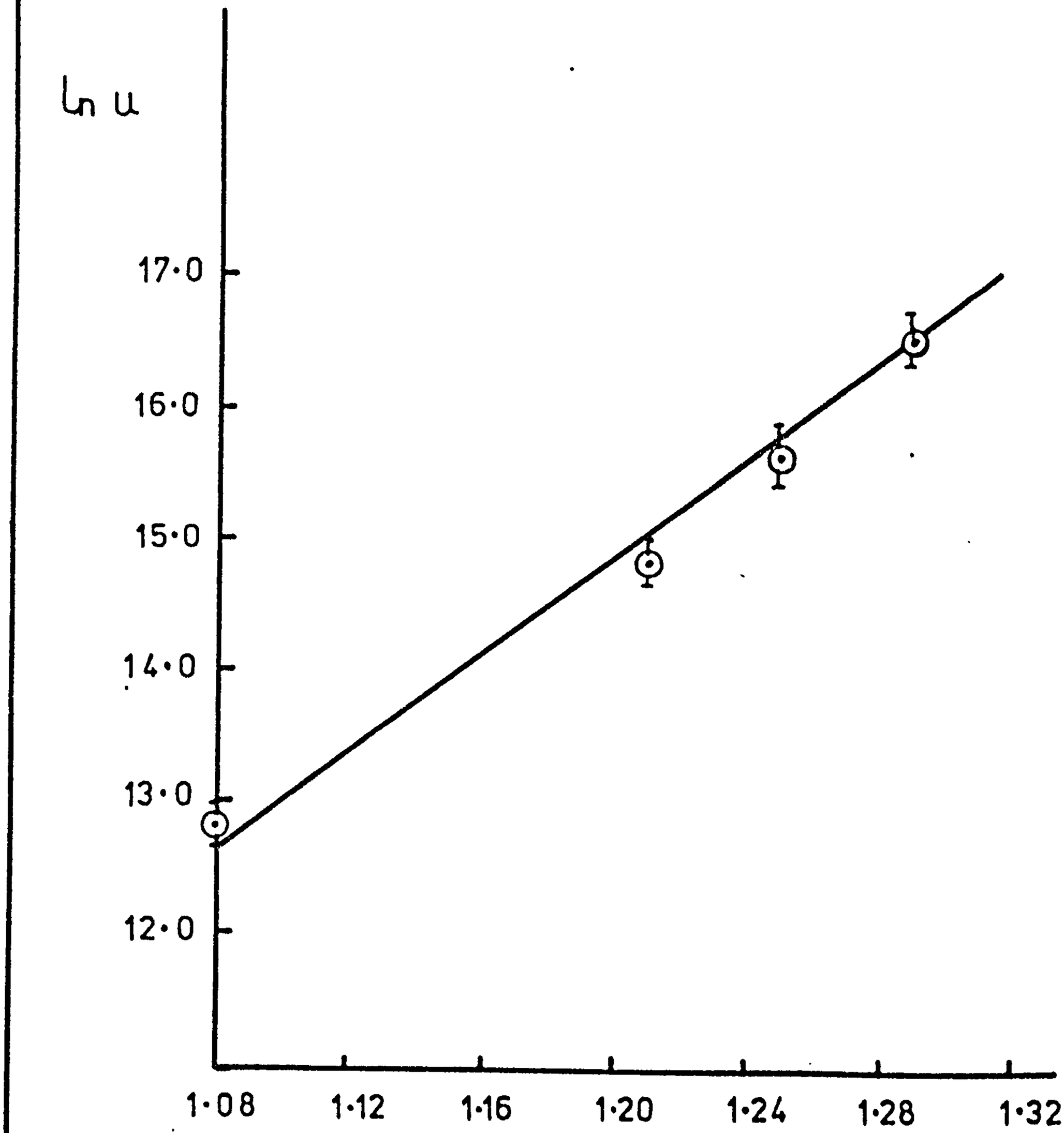

FIG 7·1

fibres using the depth of the surface crystal layer as the critical flaw size. The initial values after 5 minutes crystallization ranged between 0.7 and 1 $MNm^{-\frac{3}{2}}$ but eventually the steady value of 1.2 $MNm^{-\frac{3}{2}}$ was attained in most cases. For glass-ceramics generally this value seems reasonable.

7.1.2 Dependence of Modulus on Volume Fraction of Crystallinity

In a two phase system where one phase is discrete and distributed homogeneously throughout the continuous phase properties such as elastic modulus obey the "law of mixtures" thus the sum of the moduli of each phase multiplied by its volume fraction should give a close approximation to the experimentally measured modulus of a two phase material. Micrographic examination of glass A fibres, however, revealed a far from homogeneous distribution of crystals since the dominant morphology of lithium disilicate was as a surface layer. Since lithium disilicate has a higher elastic modulus than the parent glass or crystalline silica it will be the distribution of this phase which effects the modulus of the fibres. If the fibre is modelled as a composite beam of circular cross-section then lithium disilicate will be the outer annulus and the parent glass the inner core as shown schematically in figure 7.2. Now the product EI (where E = elastic modulus and I = 2nd moment of area) for the beam is a measure of its "bending stiffness". Thus if this model is corrent the measured bending stiffness for the fibres should be equivalent to that calculated as follows:

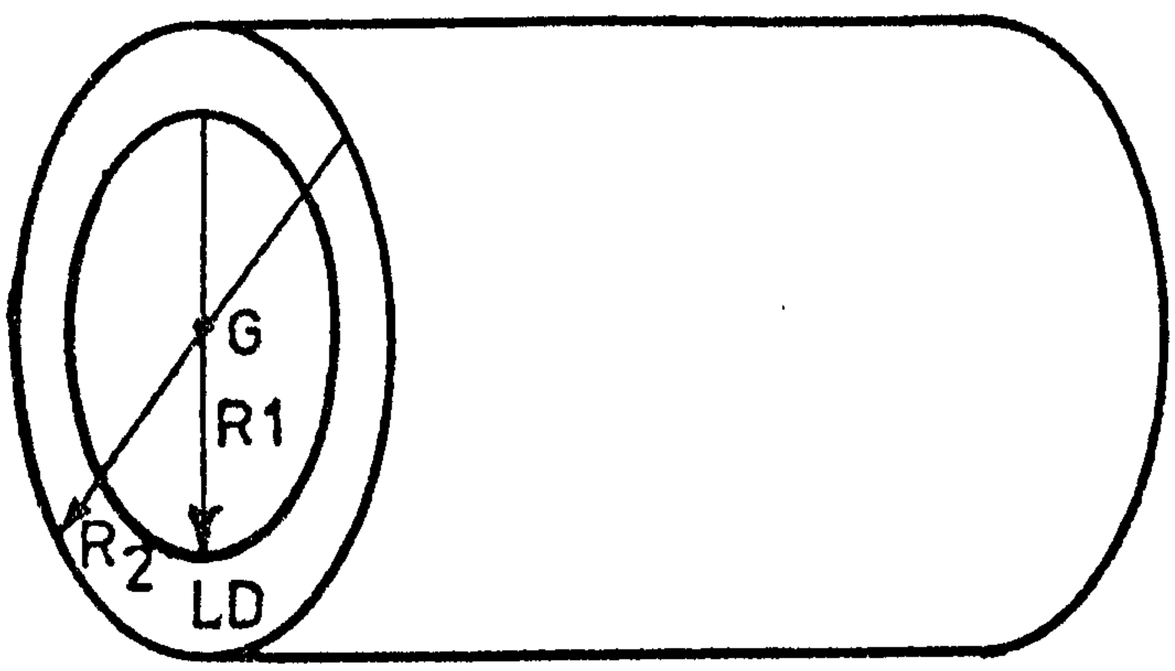

$$I_{LD} = \pi \frac{(R_2^4 - R_1^4)}{4}$$

$$I_G = \pi \frac{R_1^4}{4}$$

LD = Surface crystal layer

G = Parent glass core

FIG 7·2.

$$E_f I_f = E_{LD} I_{LD} + E_G I_G \qquad (7.3)$$

E_f = Measured fibre modulus

E_{LD} = Modulus of lithium disilicate

E_G = Modulus of parent glass

I_F = Second moment of area of fibre as measured

I_{LD} = Second moment of area of surface crystal annulus

I_G = Second moment of area of inner glass core

$$E_f \times \frac{(R_2^4)}{4} = E_{LD} \frac{(R_2^4 - R_1^4)}{4} + E_G \frac{R_1^4}{4} \qquad (7.4)$$

Equation 7.4 can be written in terms of E_f alone as

$$E_f = \frac{E_{LD} (R_2^4 - R_1^4)}{R_2^4} + E_G \frac{R_1^4}{R_2^4}$$

$$= E_{LD} - E_{LD} \frac{R_1^4}{R_2^4} + E_G \frac{R_1^4}{R_2^4} \qquad (7.5)$$

Values of E_{LD} = 109 GN/m^2 and E_G = 70.4 GN/m^2 were used to solve equation 7.5 for various crystallization times. The thidness of the surface layer was calculated using the measured crystal growth rates.

The results obtained are compared with the measured values from Appendix II in table 7.4 Also shown in this table are the values calculated on the assumption that the modulus is dependent only on the volume fraction of lithium disilicate present and not its distribution in which case

$$E_f = E_{LD} - E_{LD} \frac{R_1^2}{R_2^2} + E_G \frac{R_1^2}{R_2^2} \qquad (7.6)$$

The correlation coefficient was calculated for the observed and calculated moduli. The calculated moduli gave a good correlation in each case. A paired observation test, however, showed that the results from equation 7.5

Table 7.4 Comparison of Calculated and Observed Elastic Moduli

All fibres nucleated at 743 K

G = (K)	t = (mins)	Observed E_f (GN/m^2)	Calculated E_f from (7.3)	Calculated E_f from (7.4)
773	20	79.2	79.07	75.2
773	40	83.7	86.6	79.7
773	60	89.9	92.7	83.9
798	20	87.7	88.9	80.8
798	40	96.5	99.4	89.7
823	20	97.6	101.3	91.9

were not significantly different from the observed values at the 1% level whereas the results from equation 7.6 were significantly different even at the 0.1% level. This suggests that the "composite cylinder" model is the more appropriate for glass A fibres.

7.2 Strength Modulus and Microstructure of Glass-Ceramic B Fibres

7.2.1 Dependence of Strength on Microstructure

The glass composition 29 Li_2O, 68 SiO_2, 1 P_2O_5, 1 K_2O, 1 ZnO has been investigated by Hing and McMillan[41]. They found a relationship between the strength of the glass-ceramic and the intercrystal spacing. This particular composition can be crystallized so as to produce a homogeneous distribution of small crystals throughout the body. This is an ideal system for the investigation of strength/microstructure relationships since the intercrystal spacing can be varied by the appropriate heat treatment.

Tensile tests were performed on samples of fibres crystallized at various temperatures for a range of crystallization times. In all cases when the mean strength was plotted against time the strength decreased. In specific cases there was also evidence that after the initial decrease, the strength began to increase then finally to decrease again. These graphical results are presented in figures 6.8 and 6.9 with the 95% confidence limits on the mean strengths. As mentioned in chapter 6 statistical tests were performed which showed the strength increase to be significant. The curve drawn to the results gives some indication of the strength maximum, but it must be emphasized again that this curve is only an estimate and not a regression fit. As with glass A fibres a model is now proposed in order to explain the strength/time variation and an attempt is then made to justify this model using the experimental data derived from this investigation.

The mean intercrystal spacing in a body is not an easy parameter to measure but it can be expressed in terms of two quantities which are more readily obtainable.

Thus $$\lambda = \bar{L}\left(\frac{1-V_f}{V_f}\right) \qquad (7.7)$$

where λ = mean intercrystal spacing

$\bar{L}$ = mean crystal diameter

V_f = the volume fraction of crystallinity.

If the glass-ceramic is not highly crystalline then λ will be greater than $\bar{L}$. Also if cracks are present in the residual glass phase between crystals the strength controlling flaw distribution will be a function of λ. The initiation of flaws in the glassy phase can arise from volume change during crystal growth or thermal stresses if the expansion coefficients of the crystal and glass phase is different. Even if such flaws are not present after crystallization they may arise at low stress levels due to incompatibility strains if the elastic moduli of the crystalline and vitreous phases are different. If crystal growth is allowed to proceed in the glass-ceramic eventually the mean crystal diameter exceeds the intercrystal spacing. For equiaxed crystals uniformly distributed throughout the body then $\lambda = \bar{L}$ when the volume fraction reaches 50% thus there should be a maximum strength owing to a minimum flaw size when this occurs. Thus if fibre strength is similarly controlled by intercrystal spacing the strength maximum observed for certain heat treatments in figs. 6.8 and 6.9 should correspond to the time required to attain volume fraction of crystallinity equal to 50%. The explanation for the initial strength decrease is similar to that given for A fibres in that the uncrystallized fibres have a distribution of very small surface flaws whose size is exceeded by either the appearance of cracks at the crystal/glass interface or intercrystalline flaws. To test the hypothesis about the strength

maximum, the volume fraction determinations made by X-ray diffraction were used in conjunction with microscopical data for crystal size. Figure 7.3 is a graph showing the experimentally determined volume fraction of lithium disilicate as a function of crystallization time. The X-ray determinations were used in preference to the microscopical volume fraction determinations since micrographs were difficult to interpret at high volume fractions and this would have led to a larger error. From the graphs in 7.3 it was found that a 50% volume fraction should be attained after 3.4 hours at 798K and 2 hour at 823K. If these values are compared with the time to reach maximum strength at each crystallization temperature (3.0 hours at 798K and 1.75 hours at 823K) there appears to be some correspondence. Fibres crystallized at 873K did not appear to go through a strength maximum but behaved in a similar way to glass A fibres. Examination of the micrograph in plate 7.9 indicates that a surface crystal layer appears after prolonged crystallization of glass B. At the highest temperature 873K surface crystallization may now control the flaw distribution in the fibres which would give a strength/time relationship similar to the curves for glass A. This surface layer does not appear only at high temperatures but also seems to be present after long crystallization times. This would indicate that the strength of the fibre will be controlled by two flaw distributions; one due to the intercrystal spacing and the other to the depth of the surface crystal layer. It is difficult to test this proposition directly but indirect evidence indicated this to be the case. For instance the bimodal distribution appeared in Weibull plots after certain crystallization times. Such a distribution has already been proposed as being indicative of two strength controlling flaw regimes. It is interesting to note that the Weibull distribution returns to its unimodal form after prolonged crystallization at 798K, 823K and 873K but not at 773K, and the Weibull modulus generally appears to increase after returning to a single value. An explanation for this is that the surface crystal layer

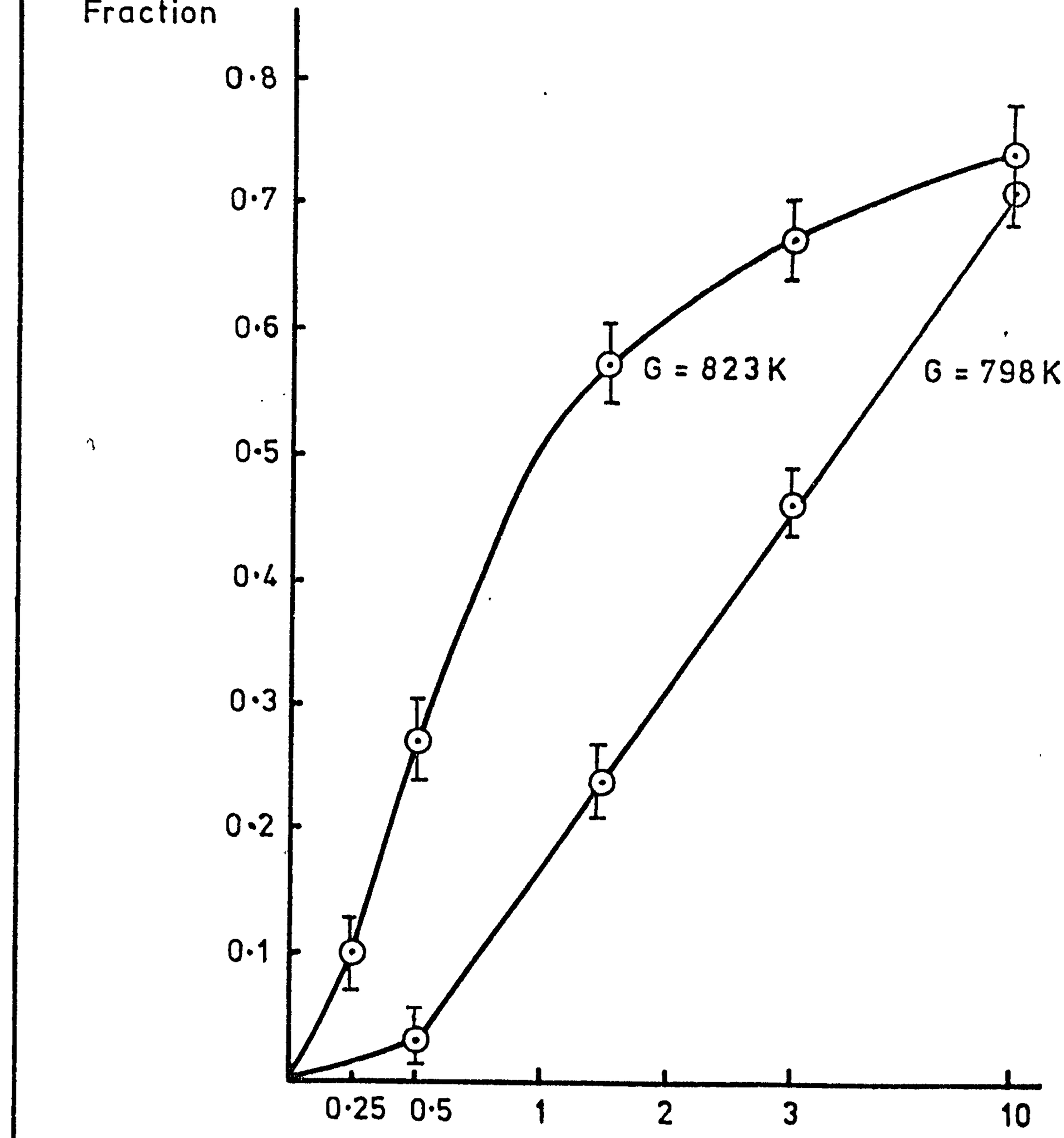
Volume
Fraction
0·8
0·7
0·6
0·5
0·4
0·3
0·2
0·1
G = 823 K
G = 798 K
0·25
0·5
1
2
3
10
Crystallization time
(hours)

FIG 7·13

eventually grows sufficiently to dominate the flaw size distribution. The crystal growth rate at 773K is such that this situation is not reached even after 10 hours crystallization. These arguments are probably over-simplifications of the strength controlling factors since one assumption made was that the crystals were equiaxed. Plate 7.7 verifies this is the case after a short crystallization time but plate 7.8 shows the crystals developing needle-like morphology after prolonged crystallization. It is likely that both morphologies are present and some evidence to support this can be seen in plate 7.10 which is a micrograph of fibre debris.

The strength/crystallization time behaviour has been discussed but reference to fig. 6. 9 shows that the nucleation temperature also appears to influence the strength. Fibres nucleated at 753 and 763K reach their strength maxima after longer crystallization time than fibres nucleated at 773K. It is possible that some crystal growth also takes place at 773K which would account for this behaviour. Error bars are only included on one curve for the sake of clarity.

From the measured growth rates at 773 and 798K an activation energy for crystal growth was calculated to be 2.5×10^8 J/kg mole which is in agreement with reported values for this composition. Again a single activation energy is an oversimplification of the growth kinetics since the growth rate will depend on the composition, and this is unlikely to remain constant during crystallization. Also the change in crystal morphology will affect the growth rate as crystallization proceeds and this will be associated with a change in activation energy. The value calculated here is merely an average energy for the whole process.

Determination of Surface Energy

The Irwin-Orowan equation was used to determine the fracture energy of the fibres. Taking λ to be the inherent flaw size the breaking stresses σ

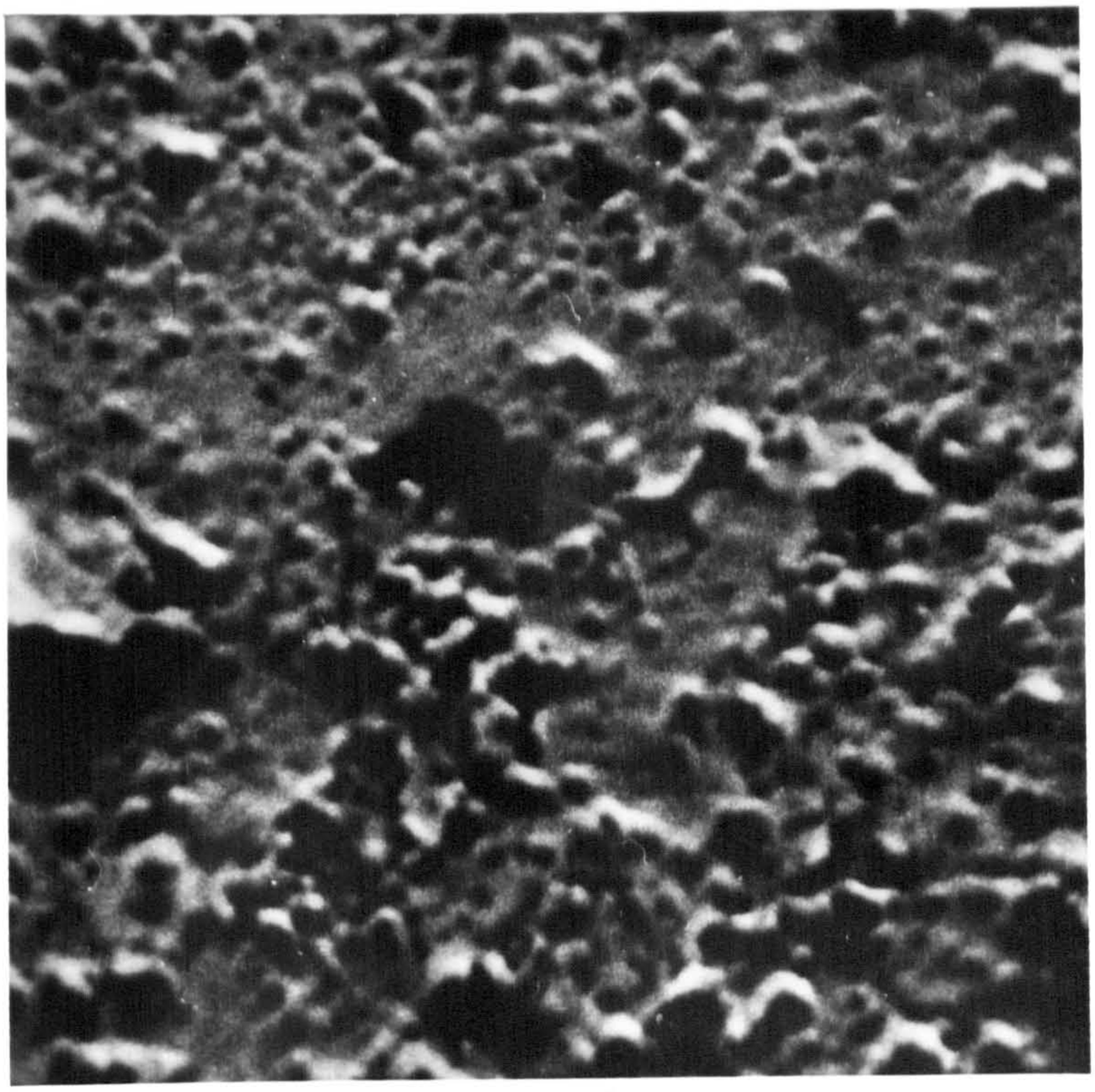

Plate 7.7 Glass B (N = 763K, G = 798K) Crytallized for 0.25 h.
Diameter = 24.5×10^{-6} m Mag. X 55,000.

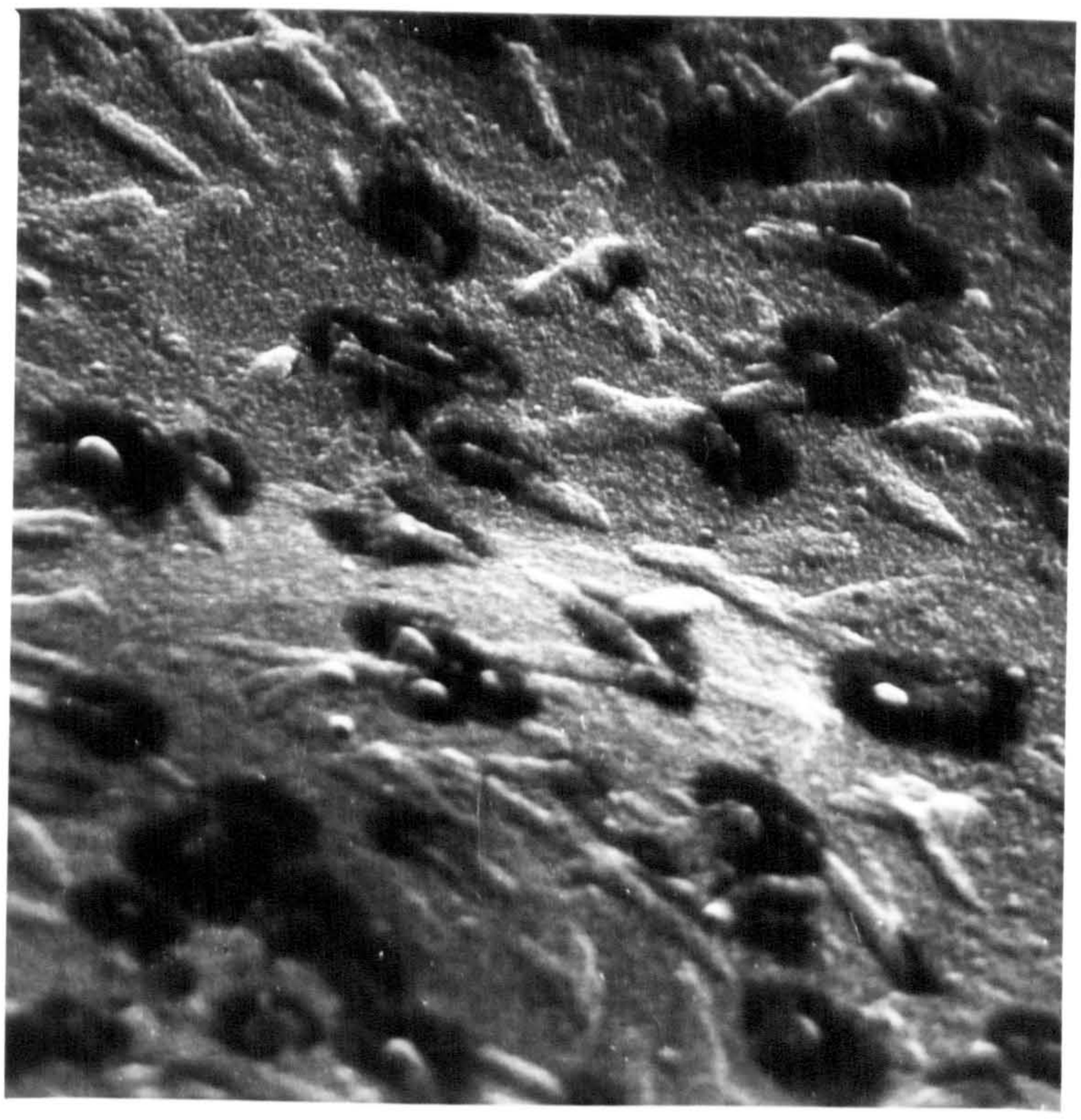

Plate 7.8 Glass B (N = 763K, G = 798K) Crystallized for 3 h.
Diameter = 24.5×10^{-6} m Mag. X 12,500.

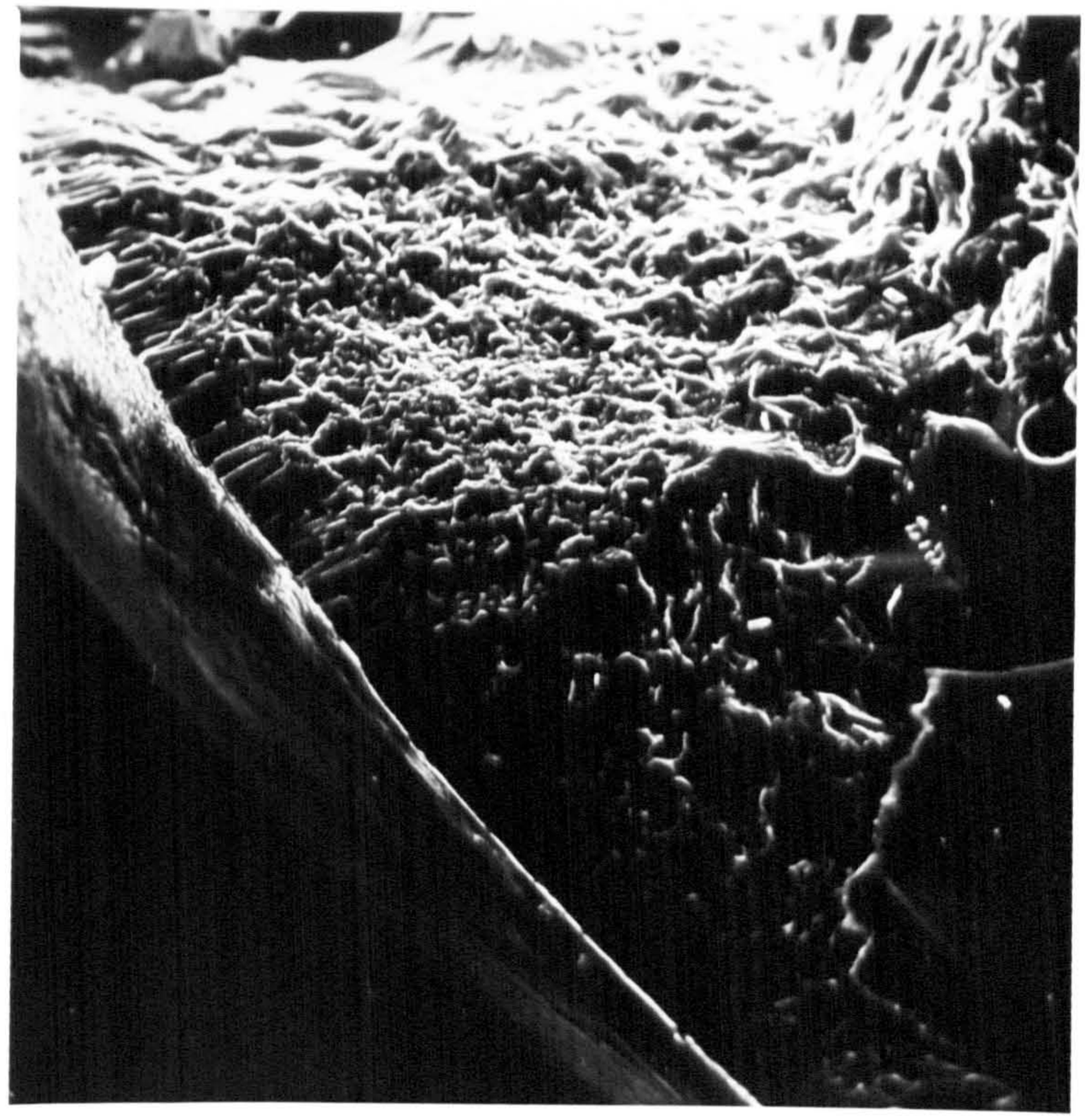

Plate 7.9 Glass B (N = 763K, G = 798K) Crystallized for 10 h.
Diameter = 6.4×10^{-4} m Mag. = 1,100.

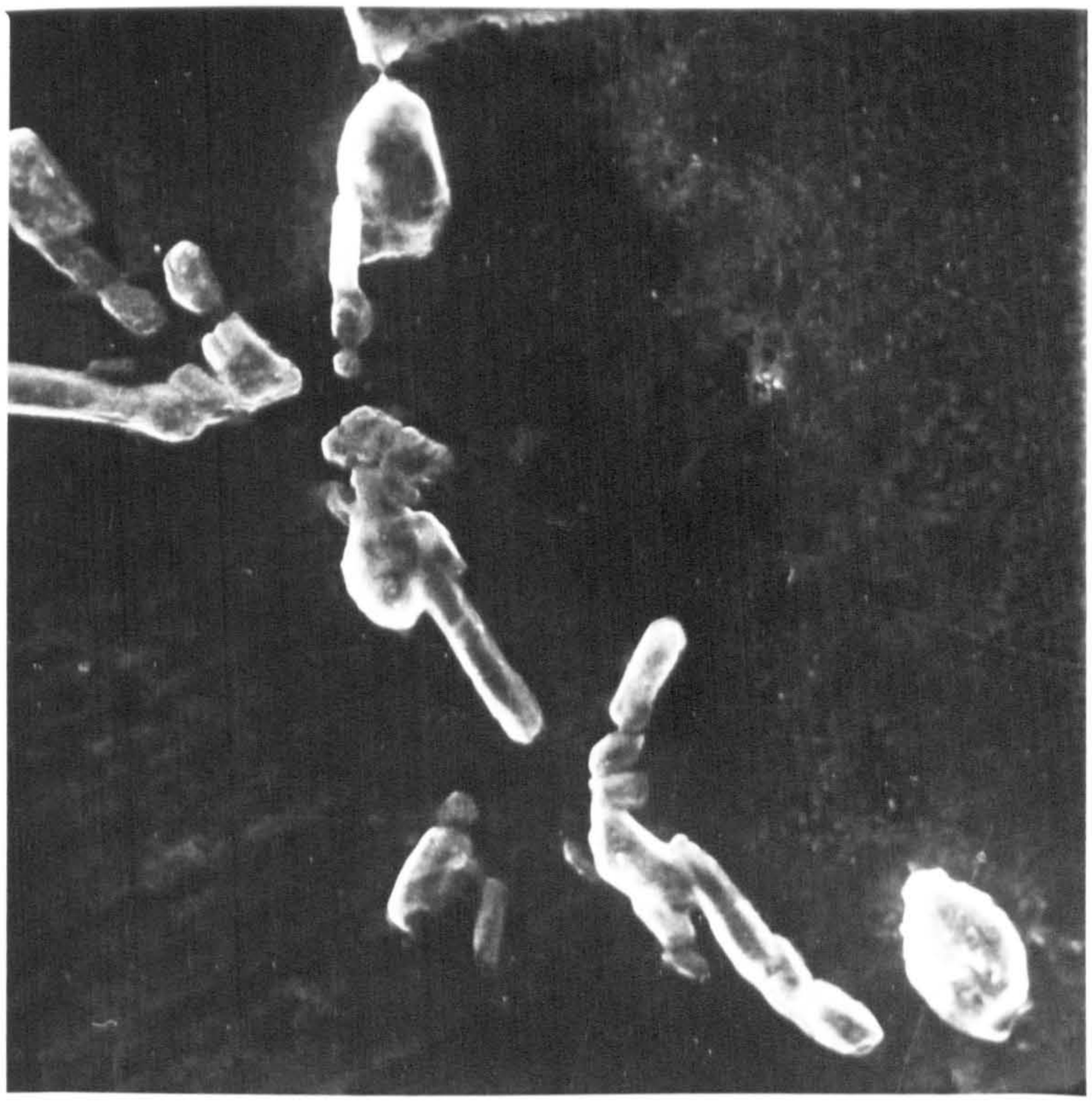

Plate 7.10 Glass B fibre debris as for plate 7.9 showing longitudinal and equiaxed crystals. Mag X 3,900.

were plotted against $1/\lambda^{\frac{1}{2}}$. This graph should give a straight line but the results in this investigation did not obey such a linear relationship. There are several possible reasons for this discrepancy. Firstly the Irwin-Orowan equation would assume that the elastic modulus was a constant whereas the results in this work show that the modulus increases with degree of crystallinity. To test the effect of changing the modulus the equation was solved for each crystallization time using the appropriate elastic modulus. The results are shown in table 7.5 and 7.6 but again there is little consistency. Secondly, the estimation of λ is suspect, being prone to a large error. Finally at high volume fractions the more appropriate parameter for the determination of surface energy may be $\bar{L}$ and not λ . Had the critical flaw size been reliably determined it would have been possible to calculate K_{IC} for the material but this exercise was not performed.

7.2.2 Variation of Elastic Modulus with Degree of Crystallinity

When a glass-ceramic crystallizes with a dominant phase dispersed discretely throughout a glassy matrix it can be treated in the same way as a composite material. The discrete phase, having a higher modulus than the continuous phase, behaves as a reinforcement. The factors which have to be considered are the geometry of the discrete phase and its distribution. The model proposed here considers the phase to be statistically homogeneous in its distribution but expresses the modulus in terms of the volume fraction only and not the geometrical shape of the phase because in a complex body it is difficult to define the suspension geometry precisely and it would be advantageous if the elastic properties could be expressed in terms of merely the phase volume fractions.

It is not possible to derive an exact expression but bounds can be calculated for the observed elastic moduli in terms of this simple data. A set of bounds for the elastic modulus of a two-phase material of irregular

Table 7.5 SURFACE ENERGIES CALCULATED AT VARIOUS CRYSTALLIZATION TEMPERATURES AND TIMES FOR GLASS B FIBRES

G = (K)	t = (hours)	λ = (m x 10^6)	E = (GN/m^2)	σ = (MN/m^2)	γ = (J/m^2)
773	1.5	3.8	64.9	612	10.9
	3	1.9	72.6	654	5.5
798	0.25	1.0	64.3	883	6.4
	3	1.4	87.0	780	4.9
	10	6.3	92.2	374	4.8
823	0.25	18	68.6	676	59.9
	10	10	97.6	332	5.6

A value of γ was calculated for the parent glass B fibres assuming an inherent flaw size similar to glass A fibres.

$$\gamma = 10.5 \text{ J/m}^2$$

Table 7.6 SURFACE ENERGIES CALCULATED FOR GLASS B FIBRES DURING CRYSTALLIZATION AT 798 K.

t = (hours)	E = (GN/m^2)	σ = (MN/m^2)	λ = (m x 10^6)	γ = (J/m^2)
0.5	64.4	510	6.7	13.5
1.0	70.0	512	2.5	4.7
1.5	74.5	577	2.0	4.5
2.0	79.2	633	1.5	3.8
2.5	83.6	730	1.4	4.5
3.0	87.0	780	1.5	5.2

geometry were derived by Paul[68] and are as follows

$$\frac{1}{\frac{V_1}{K_1} + \frac{V_2}{K_2}} \leqslant K^* \leqslant K_1 V_1 + K_2 V_2 \qquad (7.8)$$

where K^* = the effective bulk modulus

K_1 & K_2 = the bulk modulus of phases 1 and 2 respectively

V_1 & V_2 = the volume fractions of phases 1 and 2 respectively

The elastic modulus can be written in terms of bulk modulus K^* and shear modulus G^* thus:

$$E^* = \frac{9K^* G^*}{3K^* + G^*} \qquad (7.9)$$

The same bounding equations apply to the shear modulus thus K^* is replaced by G^* in equation 7.8 Using these three equations an expression can then be written for the bounds on the elastic moduli. Often, however, the tensile elastic modulus is expressed in a less complicated form as for equation 7.8 i.e.

$$\frac{1}{\frac{V_1}{E_1} + \frac{V_2}{E_2}} \leqslant E^* \leqslant E_1 V_1 + E_2 V_2 \qquad (7.10)$$

By expressing E^* in this way a good first order approximation to the bounds on E^* is obtained and thus the expression 7.10 is more commonly used. In fact the right hand side of the equation is often called the law of mixtures. The equation, however, only provides good bounds when the difference between phase moduli is small. Hence the above expression is not an accurate representation of the upper and lower bounds although it is frequently used to calculate the modulus of composite materials where the phase moduli differ by an order of magnitude. A better expression derived by Haskin and Shtrikman[69,70] requires accurate determination of the elastic

constants of each phase. Since the bulk and shear moduli of lithium disilicate and the parent glass had not been determined in this work it was not possible to use their expression and therefore the more approximate equation (7.10) was used. Volume fraction data were taken from the X-ray diffraction investigations and the measured elastic moduli E_{LD} = 110 GN/m^2 and E_G = 63.6 GN/m^2 used to calculate the upper and lower bounds for crystallization at 798 and 823K. The moduli are plotted as a function of log time in figure 7.4 and the appropriate error bars included except for 10 hours crystallization which have been omitted for the sake of clarity. In both cases there is evidence to suggest that the data approximate better to the upper bound curve but because of the magnitude of the relative error little else can be said about the experimentally determined moduli.

7.3 Ion Exchange of Glass B Fibres

Insufficient time was available to complete this part of the investigation and hypothesis made about the experimental data obtained cannot be substantiated.

7.3.1 Correlation between Strength and Process Variables

Attempts were made to correlate strength to both vapour flow rate and exposure time to vapour as discussed in chapter 6. There appeared to be a significant relationship between strength and exposure time to the vapour but none to the vapour flow rate. Many more trials would have to be performed in order to establish relationships conclusively. However, there is some indirect evidence to show that the ion exchange process did affect surface crystallization. Examining the strengths after long crystallization times the ion exchanged fibres had significantly higher strengths after 5 and 10 hours than untreated fibres nucleated and crystallized at the same temperatures (N = 763K, G = 798K).

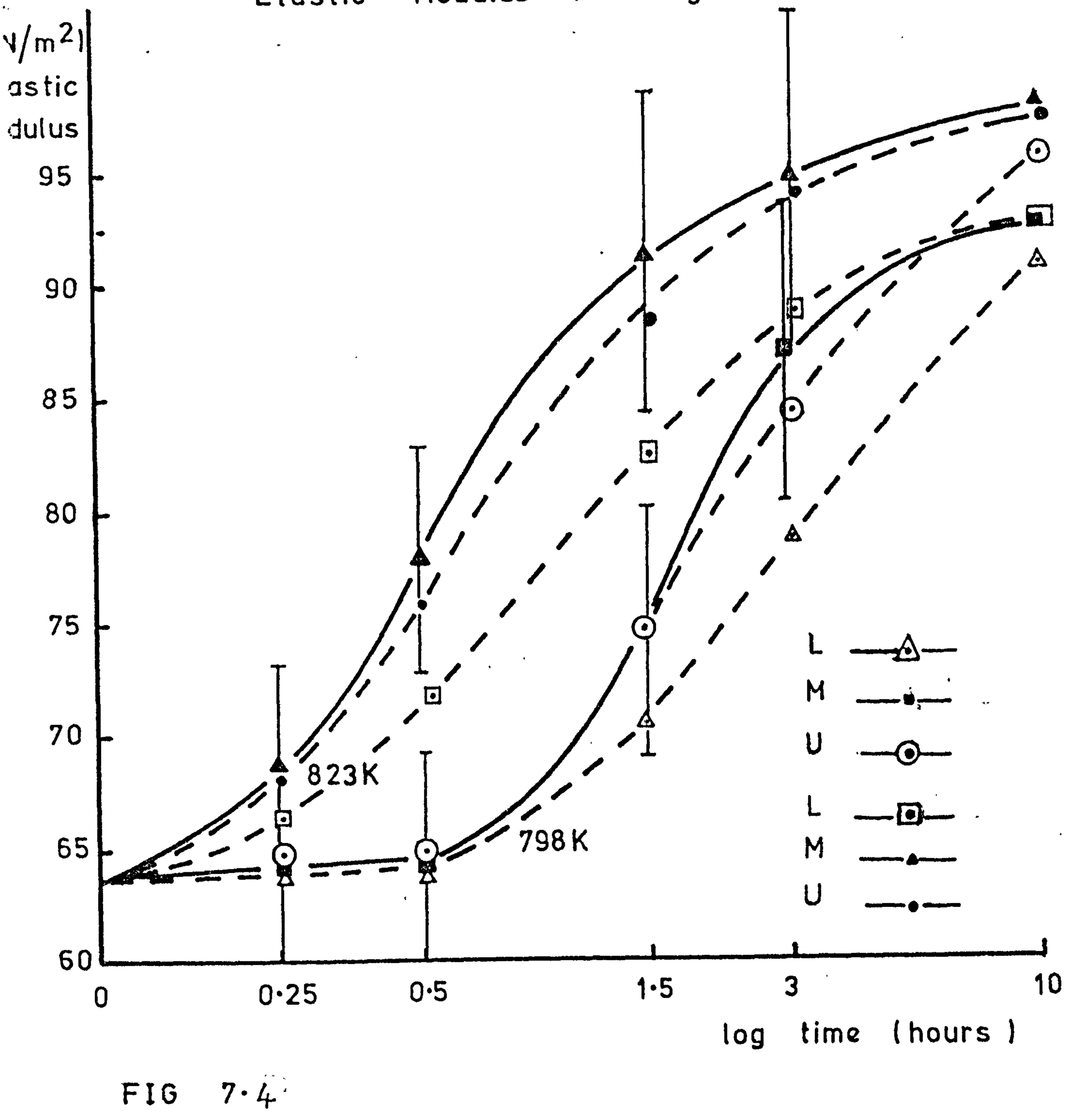

FIG 7·4

L = LOWER BOUND

M = MEASURED

U = UPPER BOUND

ERROR BARS = 8%

When the strength data were plotted on two-parameter Weibull paper there was no evidence of the data forming a bimodal distribution upto 10 hours crystallization.

Plates 7.11 show evidence of a surface layer on an ion exchanged rod which does not appear to be crystalline. Plate 7.12 is a poor micrograph of a sectioned ion exchanged fibre. This was etched heavily and there does not appear to be any evidence of surface crystallization present.

Within the limits of the errors in elastic moduli it was not possible to detect any significant difference between treated and untreated fibres.

7.3.2 Development of a Model for Ion Exchange and Diffusion

An attempt was made to develop a model which explains ion exchange and diffusion kinetics of K^+ ions into the fibres. Whilst this work was incomplete it did indicate that the continuation of such work would generate worthwhile results. For this reason it was considered important to outline the form of the investigations made in order to aid future investigations in this area.

The work was divided into two distinct aspects which were

(i) A model which develops a diffusion equation capable of predicting diffusion profiles in the fibres.

(ii) Experimental determination of K^+ concentration profiles within the fibre.

Details of the analytical and mathematical procedures adopted for the model can be found in Appendix III but briefly the approach taken was to consider the fibre as a finite cylinder and assume that during the diffusion process the interdiffusion coefficient between Li^+ and K^+ would be

Plate 7.11 Glass B. Ion exchanged specimen treated in KNO_3 and crystallized at 798K for 5h. Mag. X 60.

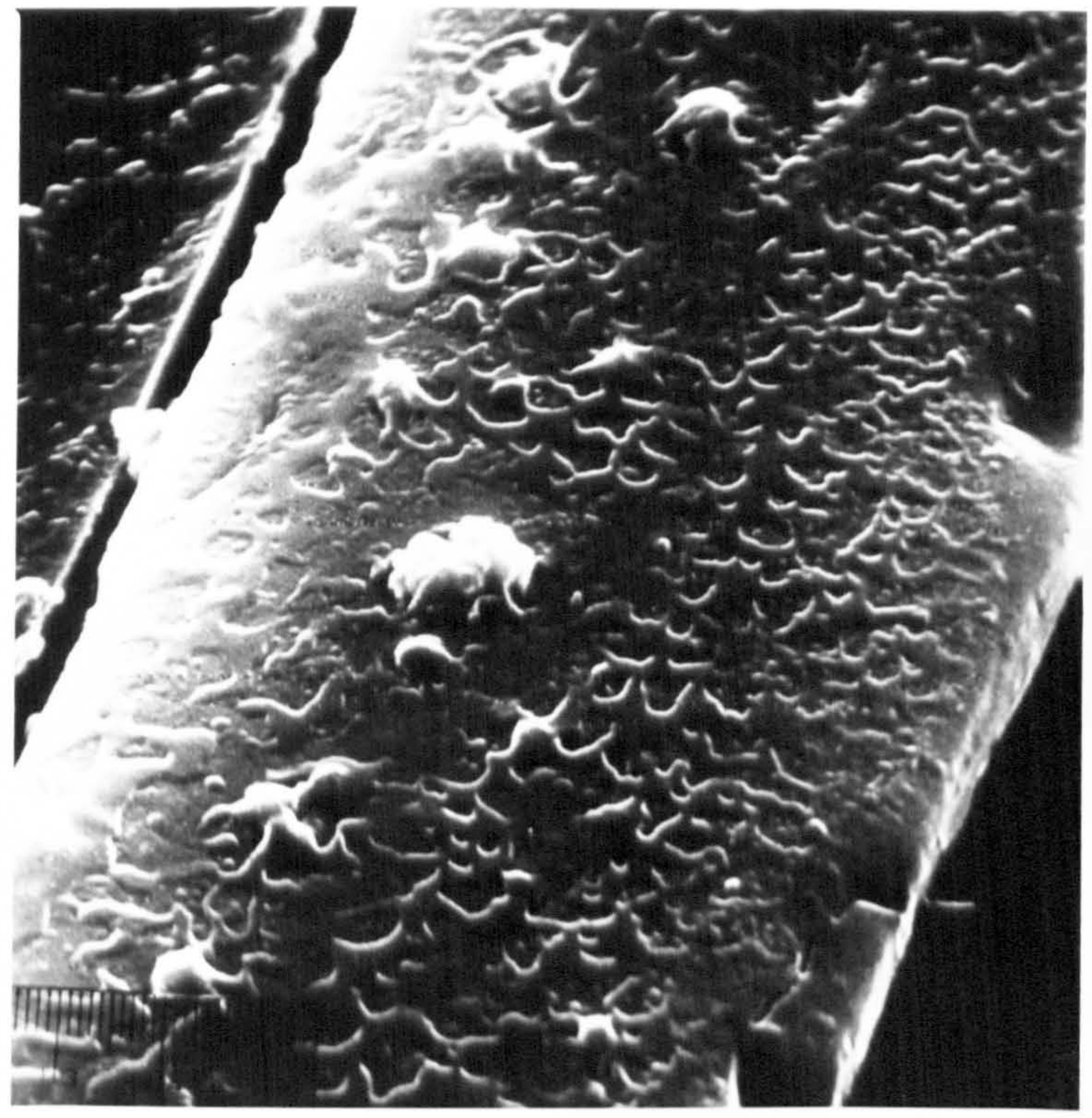

Plate 7.12 Glass B fibre after ion exchange. Diameter = 24.6 x 10^{-4} (N = 763K, G = 798K) crystallized for 3 h. Mag. X 3,200.

concentration dependent. No analytical solutions were available for this model hence a finite difference numerical method was employed. The functional form assumed for D, the interdiffusion coefficient, was that it passed through a maximum at a particular Li^+/K^+ value in which case the function could have had quadratic or higher power dependence of D on C (concentration). Conductivity data of Lengyel and Boksay [71, 72] were corrected to the appropriate temperature[73] and used to establish a graph of interdiffusion coefficient vs. $\frac{Li^+}{Li^+ + K^+}$. A curve was obtained which had a similar form to the Na^+/Rb^+[74] system. It was difficult to establish the precise functional relationships between D and C since too little data was available. The quadratic form was therefore assumed and tried in the numerical analysis but no sensible solutions were obtained. It was thought that this was caused by D having a maximum value in which case $\frac{dD}{dC}$ is underfined here and could cause instability in the numerical method.

The experimental investigations carried out to determine the K^+ concentration profile were discussed in chapters 5 and 6. However, it would appear that flame photometry was a potentially useful technique and these results could be supported with a modern energy dispersive analyser in conjunction with an electron microscope.

Conclusions

1. The viscosity/temperature characteristics of glasses A and B were such that they could be drawn into continuous fibre using a single tip platinum bushing.

2. Fibres crystallized from glass A always exhibited a strength decrease as crystallization proceeded. A functional relationship was sought between strength σ and crystallization time t and within the limitations of the statistical analysis applied it was infered that:

$$\sigma \alpha \frac{1}{\sqrt{t}}$$

Based on this relatioship a model was proposed which related the critical flaw size distribution to the depth of the surface crystal layer and indirect statistical evidence was used to reinforce this hypothesis. Assuming that the surface crystal layer grew linearly with time crystal growth rates were calculated using the above model and these were in reasonable agreement with the experimentally determined values. Hence it was concluded that the proposed model gave a plausible explanation for the relationship between strength and fibre microstructure.

3. After certain periods of crystallization the bimodal two-parameter Weibull distribution was appropriate for certain strength data and indicated that two strength controlling flaw regimes were present. These were thought to be related to surface and internal crystallinity.

4. The experimentally determined elastic modulus of glass A fibres appeared to increase with degree of crystallinity. This was explained by the fact that the modulus of lithium disilicate was

higher than for the parent glass. Two possibilities were proposed for the relationship between the elastic modulus and the volume fraction of lithium disilicate in the fibre. The model proposing that the fibre behaved as a composite cylinder of lithium disilicate and glass, gave reasonable agreement between calculated and measured modulus. This agreement was better than the calculated modulus obtained by assuming that lithium disilicate is homogeneously dispersed throughout the fibre.

5. The strength of glass B fibres was shown initially to decrease with crystallization time but then to increase slightly before decreasing again after a prolonged period of crystallization. The initial decrease was explained by the appearance of crystals within the fibre creating a flaw size distribution larger than the inherent flaw distribution in the parent glass fibres. The strength increase was explained by assuming that the flaw size distribution, at low volume fractions, was controlled by the mean intercrystal spacing. This meant that the strength should reach a maximum when the volume fraction equalled 50%. Evidence to support these ideas was obtained by comparing the time taken to reach maximum strength with the time to reach 50% lithium disilicate as determined by X-ray diffraction. For two crystallization temperatures these times showed reasonable agreement. After prolonged crystallization the two-parameter Weibull plots returned to a bimodal distribution as had been the case for glass A. It was concluded that surface crystallization was now beginning to influence flaw size distribution in the fibres.

6. The initiation of the flaws in the surface crystal layer could be caused either by a volume contraction during crystallization or by thermal expansion mismatch between the crystal and the phase surrounding

it. This intercrystalline phase should tend towards a silica rich composition if alkali ions incorporated in the growing crystal are not replenished; as would be the case for a fibre with small volume in comparison to the size of the crystal.

Similar volume or thermal stress effects could create cracks in the amorphous phase in between crystals.

7. The elastic modulus of glass B fibres appeared to obey the law of mixtures which is an upper bound relationship for the modulus of a two phase material.

8. Preliminary ion exchange experiments indicated that surface crystallization could be supressed. A process was developed to enable ion exchange to take place at the fibre surface using a vapour containing the exchange ion K^+. The fibres crystallized after ion exchange treatment appeared to be stronger after prolonged crystallization. The flow rate of argon containing K^+ did not appear to influence the fibre strength but the exposure time to the vapour did have an effect.

9. The K^+ ion profile in the fibres could be estimated approximately using flame photometry but it was thought that modern energy dispersive analysers may provide a more powerful means of determining the K^+ concentration. The attempt made to model the ion exchange and diffusion process did not prove entirely successful but this was due to the lack of work carried out in this area. Thus it should be possible to predict the effect of the ion exchange process variables if in future investigations accurate K^+ concentration profiles are determined and the numerical analysis of the diffusion problem is adopted successfully for the experimental data.

BIBLIOGRAPHY

1. M. ITO, T. SAKAINO, and T. MORIYA, Bulletin of the Tokyo Institute of Technology. No.88 (1968) 127.

2. L.L. HENCH, S.W. FRIEMAN and D.L. KINSER, Phys. Chem. Glasses. 12 2 (1971) 58.

3. K. MATUSITA and M. TASHIRO, J. Non-Crystal. Solids. 11 (1973) 471.

4. K. MATUSITA and M. TASHIRO, J. Phys. Chem. of Glasses. 14 (1973) 77.

5. K. MATUSITA, S. SAKKA, T. MAKI and M. TASHIRO, J. Mat. Sci. 10 (1975) 94.

6. K.K. EVSTROP'EV, The Structure of Glass Vol. 2. Consultants Bureau. New York. (1960) 237.

7. G.E. RINDONE, J. Am. Ceram. Soc. 45 (1962) 7.

8. S.D. STOOKEY and R.D. MAURER, Progress in Ceramics. J.E. BURKE (Ed) Pergamon. New York. (1962) 77.

9. R.D. MAURER, J. Appl. Phys. 29 (1958) 1.

10. S.D. STOOKEY, U.S. Patent. 2,515,275 (1950).

11. M. TOMOZAWA, Phys. Chem. Glasses. 13 (1972) 161.

12. R.H. DOREMUS and A.M. TURKALO, Phys. Chem. Glasses. 13 (1972) 14.

13. E. PLUMAT, Silicates Industrials. Ann. Meeting of Am. Ceram. Soc. (April 1971) 97.

14. H. HARPER, P.F. JAMES and P.W. McMILLAN, Disc. of Faraday Soc. 50 (1970) 206.

15. H. HARPER and P.W. McMILLAN, Phys. Chem. Glasses. 13 (1972) 97.

16. R.H. DOREMUS, Glass Science. John Wiley. New York. (1973).

BIBLIOGRAPHY

1. M. ITO, T. SAKAINO, and T. MORIYA, Bulletin of the Tokyo Institute of Technology. No.88 (1968) 127.

2. L.L. HENCH, S.W. FRIEMAN and D.L. KINSER, Phys. Chem. Glasses. 12 2 (1971) 58.

3. K. MATUSITA and M. TASHIRO, J. Non-Crystal. Solids. 11 (1973) 471

4. K. MATUSITA and M. TASHIRO, J. Phys. Chem. of Glasses. 14 (1973) 77.

5. K. MATUSITA, S. SAKKA, T. MAKI and M. TASHIRO, J. Mat. Sci. 10 (1975) 94.

6. K.K. EVSTROP'EV, The Structure of Glass Vol. 2. Consultants Bureau. New York. (1960) 237.

7. G.E. RINDONE, J. Am. Ceram. Soc. 45 (1962) 7.

8. S.D. STOOKEY and R.D. MAURER, Progress in Ceramics. J.E. BURKE (Ed) Pergamon. New York. (1962) 77.

9. R.D. MAURER, J. Appl. Phys. 29 (1958) 1.

10. S.D. STOOKEY, U.S. Patent. 2,515,275 (1950).

11. M. TOMOZAWA, Phys. Chem. Glasses. 13 (1972) 161.

12. R.H. DOREMUS and A.M. TURKALO, Phys. Chem. Glasses. 13 (1972) 1

13. E. PLUMAT, Silicates Industrials. Ann. Meeting of Am. Ceram. Soc. (April 1971) 97.

14. H. HARPER, P.F. JAMES and P.W. McMILLAN, Disc. of Faraday Soc. 50 (1970) 206.

15. H. HARPER and P.W. McMILLAN, Phys. Chem. Glasses. 13 (1972) 97.

16. R.H. DOREMUS, Glass Science. John Wiley. New York. (1973).

17. V.N. FILIPOVICH and A.M.KALINA, Inorg. Mats. Consultants Bureau. 6 (1970) 303.

18. G.W. SCHERER and D.R. UHLMANN, J. Non-Crystal. Solids. 21 (1976) 199.

19. P. HAUTOJÄRVI and I. LEMUSOKSA, J. Non-Crystal. Solids. 18 (1975) 395.

20. P.F. JAMES, A. PAUL, R.M. SINGARU, C. DAUWE, L. DORIKENS-VANPRAET and M. DORIKENS. J. Phys. C. 8 (1975) 393.

21. P.F. JAMES and S.R. KEOWN, Phil. Mag. 30 (1974) 789.

22. A.A. GRIFFITH, Phil. Trans. Roy. Soc. (Lond.) A221 (1920) 163.

23. C.E. INGLIS, Trans. Inst. Naval. Archit. 55 (1913) 219.

24. J.W. OBREIMOFF, Proc. Roy. Soc. (LOND.) A127 (1930) 290.

25. G.R. IRWIN, Handbuch der Physik. 6 (1958) 551.

26. P.L. GUTSHALL and G.E. GROSS, Eng. Frac. Mech. 1 (1969) 463.

27. A.G. EVANS and R.W. DAVIDGE, J. Nuclear Mat. 33 (1969) 249.

28. L.A. SIMPSON, J. Am. Ceram. Soc. 56 (1973) 610.

29. R.W. DAVIDGE and G. TAPPIN, Proc. Br. Ceram. Soc. 15 (1970) 47.

30. E.M. PASSMORE, R.M. SPRIGGS and T. VASILOS, J. Am. Ceram. Soc. 48 (1965) 1.

31. D.J. GREEN, P.S. NICHOLSON and D.J. EMBERY, Fracture Mechanics of Ceramics. (1974) 541. Plenum. New York.

32. R.H. DOREMUS and W.A. JOHNSON, J. Mat. Sci. 13 (1978) 855.

33. F.F. LANGE, Phil. Mag. 22 (1970) 983.

34. A.G. EVANS, Phil. Mag. 26 (1972) 1327.

35. R.W. DAVIDGE and T.J. GREEN, J. Mat. Sci. 3 (1968) 629.

36. M. TASHIRO, The Glass Industry. Part 2. (1966) 428.

37. D.M. MARSH, Proc. Roy. Soc. 279 (1964) Ibid 282 (1964).

38. K.R. LINGER and D.G. HOLLOWAY, Phil. Mag. 18 (1968) 1269.

39. P.W. McMILLAN, S.V. PHILLIPS and G. PARTRIDGE, J. Mat. Sci. 1 (1966) 269.

40. P.W. McMILLAN, B.P. HODGSON and R.E. BOOTH, J. Mat. Sci. 4 (1969) 1029.

41. P. HING and P.W. McMILLAN, J. Mat. Sci. 8 (1973) 1041.

42. S.W. FREIMAN and L.L. HENCH, J. Am. Ceram. Soc. 55 (1972) 86.

43. G.K. BANSAL and W.H. DUCKWORTH, J. Am. Ceram. Soc. 60 (1977) 304.

44. W. WEIBULL, Ing. Vetenskaps. Akad. Handl. 155 (1939) 1.

45. D.R. THOMAN, L.J. BAIN and C.E. ANTLE, Technometrics. 11 (1969) 445.

46. D.G.S. DAVIES, Proc. Brit. Ceram. Soc. (1973) 429.

47 W.E. SNOWDEN. Fracture Mechanics of Ceramics. Vol 3. (1977) 143.

48. W.D. SCOTT and A. GADDIPATI, Fracture Mechanics of Ceramics. Vol 3. (1977) 125.

49. R. OLSHANSKY and R.D. MAURER, J. Appl. Phys. 47 (1976) 4497.

50. A.G. EVANS and T.G. LANGDON, Structural Ceramics. Progress in Materials Science. (1976) 325.

51. R.M. HAKIM and D.R. UHLMANN, Phys. Chem. Glasses. 8 (1967) 174.

52. A.K. [illegible]RSHNEYA, J. Am. Ceram. Soc. 57 (1974) 37.

53. J.S. OLCOTT and S.D. STOOKEY, Sixth International Congress on Glass. Washington D.C. (July 1962) 400.

54. S.S. KISTLER, J. Am. Ceram. Soc. 45 (1962) 59.

55. P. ACLOQUE and J. TOCHON, Colloquim on Mechanical Strength of Glass. Florence, Italy. (September 1961) 25.

56. D.A.DUKE, J.F. MACDOWELL and B.R. KARSTETTER, J. Am. Ceram. Soc. 50 (1967) 67.

57. J. CRANK, The Mathematics of Diffusion. Oxford University Press. 1956.

58. G.H. FRISCHAT, Phys. Chem. Glasses. 11 (1970).

59. L.W. BARR, J.N. MUNDY and A.H. ROWE, Amorphous Materials. Wiley Interscience. (Lond.) (1970) 235.

60. G.H. FRISCHAT, Amorphous Materials. Wiley Interscience. (Lond.) (1970) 235.

61. S.E. SVANSON and R. JOHANSSON, Acta. Chem. Scanda. 24 (1970) 755.

62. F. HELFERICH and M.S. PLESSET, J. Chem. Phys. 28 (1958) 418.

63. F. HELFFERICH, J. Phys. Chem. 66 (1962) 39.

64. R.H. DOREMUS, Glass Science, Wiley Interscience. (1973) 165.

65. G. McVAY and D.E. DAY, J. Am. Ceram. Soc. 53 (1970) 508.

66. R. TERAI, J. Non-Crystal. Solids. 6 (1971) 121.

67. R.H. CLUCAS, Ph.D. Thesis. Sessile Drop Investigations of Metals on Glass-Ceramics. Liverpool Polytechnic. (1976).

68. B. PAUL, Trans. A.I.M.E. 218 (1960).

69. Z. HASHIN and S. SHTRICKMAN, J. Mech. Phys. Solids. 10 (1962) 335.

70. Z. HASHIN and S. SHTRICKMAN, J. Mech. Phys. Solids. 11 (1963) 127.

71. B. LENGYEL and Z. BOKSAY, Z. Phys. Chem. 203 (1954) 93.

72. B. LENGYEL and Z. BOKSAY, Z. Phys. Chem. 204 (1955) 157.

73. H. NAMIKAWA, J. Non-Crystal. Solids. 18 (1974) 173.

74. G.H. FRISCHAT and R. KRICHMEYER, J. Am. Ceram. Soc. 56 (1973) 552.

75. J. DOUGLAS and B.F. JONES, J. Soc. Industrial Appl. Maths. 2 (1963).

APPENDIX I

GLASS A	TEMPERATURE	CONDITION:
NUCLEATION	743 K	
CRYSTALLIZATION	773 K	

TIME (MINUTES)	MEAN TENSILE STRENGTH (MN/m^2)	STANDARD DEVIATION OF STRENGTH	95% CONFIDENCE LIMITS OF THE MEAN $\pm$ MN/m^2	WEIBULL MODULUS
0	696	223	63	3.2
5	698	223	63	
10	697	222	63	3.1
15	682	220	63	
20	565	214	61	3.1
25	532	234	67	
30	465	227	65	2.7
35	443	222	63	
40	427	213	61	2.6
45	391	215	61	
50	402	217	62	2.4 1.6
55	361	202	57	
60	362	203	58	2.5 1.6
120	260	172	49	
180	247	156	44	
240	232	162	46	
300	221	152	43	
360	203	146	42	2.2

GLASS A	TEMPERATURE	CONDITION:
NUCLEATION	753 K	
CRYSTALLIZATION	773 K	

TIME (MINUTES)	MEAN TENSILE STRENGTH (MN/m^2)	STANDARD DEVIATION OF STRENGTH	95% CONFIDENCE LIMITS OF THE MEAN $\pm$ MN/m^2	WEIBULL MODULUS
0	696	223	63	3.2
5	692	221.	63	
10	680	224	64	3.1
15	678	223	63	
20	565	214	61	3.1
25	540	211	60	
30	485	204	68	2.9
35	452	199	57	
40	412	189	54	3.0
45	425	200	57	
50	385	200	57	2.8 1.9
55	347	177	50	
60	325	179	51	2.7 1.9
120	232	139	40	
180	227	138	39	
240	204	126	36	
300	191	132	38	.
360	190	124	35	2.5

GLASS A	TEMPERATURE	CONDITION:
NUCLEATION	763 K	
CRYSTALLIZATION	773 K	

TIME (MINUTES)	MEAN TENSILE STRENGTH (MN/m^2)	STANDARD DEVIATION OF STRENGTH	95% CONFIDENCE LIMITS OF THE MEAN $\pm$ MN/m^2	WEIBULL MODULUS
0	696	223	63	3.2
5	696	221	63	
10	675	230	65	3.0
15	692	228	65	
20	550	214	61	2.9
25	475	199	57	
30	481	197	56	2.9 1.8
35	449	202	57	
40	381	187	53	2.8 1.8
45	376	146	42	
50	298	173	49	2.7 1.9
55	243	151	43	
60	244	157	45	2.6
120	236	156	44	
180	229	160	45	
240	217	156	44	
300	211	146	42	
360	207	147	42	2.3

GLASS A	TEMPERATURE	CONDITION:
NUCLEATION	743 K	
CRYSTALLIZATION	798 K	

TIME (MINUTES)	MEAN TENSILE STRENGTH (MN/m^2)	STANDARD DEVIATION OF STRENGTH	95% CONFIDENCE LIMITS OF THE MEAN $\pm$ MN/m^2	WEIBULL MODULUS
0	696	223	63	3.2
5	688	214	61	
10	586	199	57	2.7
15	443	182	52	
20	380	152	43	3.0
25	344	155	44	
30	333	153	43	2.9 1.9
35	322	158	45	
40	290	151	43	3.0 1.9
45	306	159	45	
50	291	157	45	2.8 1.1
55	264	148	42	
60	225	128	36	2.7
120	217	132	38	
180	198	118	34	
240	189	115	33	
300	181	112	32	
360	176	107	30	2.9

GLASS A	TEMPERATURE	CONDITION:
NUCLEATION	753 K	
CRYSTALLIZATION	798 K	

TIME (MINUTES)	MEAN TENSILE STRENGTH (MN/m^2)	STANDARD DEVIATION OF STRENGTH	95% CONFIDENCE LIMITS OF THE MEAN $\pm$ MN/m^2	WEIBULL MODULUS
0	696	223	63	3.2
5	687	216	44	
10	559	176	58	3.1
15	487	180	51	
20	426	166	47	3.1
25	370	151	43	
30	361	155	44	3.0
35	306	141	40	
40	289	139	40	3.1
45	302	151	43	
50	269	132	38	3.0
55	240	125	36	
60	245	125	36	3.9 1.8
120	199	107	30	
180	182	106	30	
240	171	103	29	
300	165	101	29	
360	161	97	28	2.9 1.9

GLASS A	TEMPERATURE	CONDITION:
NUCLEATION	763 K	
CRYSTALLIZATION	798 K	

TIME (MINUTES)	MEAN TENSILE STRENGTH (MN/m^2)	STANDARD DEVIATION OF STRENGTH	95% CONFIDENCE LIMITS OF THE MEAN $\pm$ MN/m^2	WEIBULL MODULUS
0	696	223	63	3.2
5	695	223	63	
10	556	200	57	3.1
15	450	185	53	
20	425	187	53	3.1
25	380	156	44	
30	324	149	42	3.0
35	302	145	41	
40	307	150	43	2.8 1.9
45	371	138	39	
50	249	127	36	2.7 1.9
55	255	128	36	
60	238	129	37	2.9
120	202	125	36	
180	185	113	32	
240	169	100	28	
300	157	94	27	
360	149	95	27	2.6

GLASS A	TEMPERATURE	CONDITION:
NUCLEATION	K	
CRYSTALLIZATION	773 K	

TIME (MINUTES)	MEAN TENSILE STRENGTH (MN/m^2)	STANDARD DEVIATION OF STRENGTH	95% CONFIDENCE LIMITS OF THE MEAN $\pm$ MN/m^2	WEIBULL MODULUS
0	696	223	63	3.2
5	675	222	63	
10	682	218	62	2.9
15	690	207	59	
20	549	231	66	3.0
25	481	231	66	
30	484	227	65	2.9 1.9
35	405	227	65	
40	435	230	65	2.8 1.9
45	400	228	65	
50	377	226	64	2.6 1.8
55	336	212	60	
60	352	211	60	2.5
120	341	222	63	
180	320	205	58	
240	266	186	58	
300	229	169	48	
360	211	158	45	2.3

GLASS A	TEMPERATURE	CONDITION:
NUCLEATION	743 K	
CRYSTALLIZATION	823 K	

TIME (MINUTES)	MEAN TENSILE STRENGTH (MN/m^2)	STANDARD DEVIATION OF STRENGTH	95% CONFIDENCE LIMITS OF THE MEAN + MN/m^2	WEIBULL MODULUS
0	696	223	63	3.2
5	531	181	51	
10	398	138	39	3.1
15	362	116	39	
20	270	113	33	3.1
25	269	130	32	
30	266	106	37	3.0
35	216	105	30	
40	216	106	30	2.8
45	225	105	30	
50	219	107	30	2.9 1.9
55	208	104	30	
60	171	91	26	2.8 1.9
120	158	85	24	
180	132	73	21	
240	121	70	20	
300	116	68	19	
360	109	68	19	2.7

GLASS A	TEMPERATURE	CONDITION:
NUCLEATION	753 K	
CRYSTALLIZATION	823 K	

TIME (MINUTES)	MEAN TENSILE STRENGTH (MN/m^2)	STANDARD DEVIATION OF STRENGTH	95% CONFIDENCE LIMITS OF THE MEAN + MN/m^2	WEIBULL MODULUS
0	696	223	63	3.2
5	475	171	49	
10	427	166	47	3.0
15	374	153	43	
20	275	129	37	3.0
25	282	135	38	
30	235	115	33	2.9
35	190	99	28	
40	230	110	31	3.0
45	196	100	28	
50	192	102	29	3.0 1.9
55	168	87	25	
60	186	97	28	2.9 1.9
120	171	84	24	
180	163	83	24	
240	149	82	23	
300	132	75	21	
360	124	69	20	2.8

GLASS A	TEMPERATURE	CONDITION:
NUCLEATION	763 K	
CRYSTALLIZATION	823 K	

TIME (MINUTES)	MEAN TENSILE STRENGTH (MN/m^2)	STANDARD DEVIATION OF STRENGTH	95% CONFIDENCE LIMITS OF THE MEAN $\pm$ MN/m^2	WEIBULL MODULUS
0	696	223	63	3.2
5	500	170	48	
10	425	162	46	
15	375	150	43	
20	349	150	43	2.9
25	282	133	38	
30	226	111	32	2.9 1.9
35	250	118	34	
40	210	107	30	2.8 1.9
45	211	106	30	
50	175	96	27	2.7 1.8
55	183	102	29	
60	175	96	27	2.6 1.8
120	158	96	27	
180	141	89	25	
240	126	83	23	
300	101	72	20	
360	93	65	18	2.3

GLASS A	TEMPERATURE	CONDITION:
NUCLEATION	743 K	
CRYSTALLIZATION	923 K	

TIME (MINUTES)	MEAN TENSILE STRENGTH (MN/m^2)	STANDARD DEVIATION OF STRENGTH	95% CONFIDENCE LIMITS OF THE MEAN $\pm$ MN/m^2	WEIBULL MODULUS
0	696	223	63	3.2
5	208	87	24	
10	182	80	23	3.1
15	84	39	11	
20	71	35	10	3.1
25	68	33	9	
30	61	32	9	3.0
35	63	33	9	
40	57	30	9	3.1

GLASS B	TEMPERATURE	CONDITION:
NUCLEATION	763 K	
CRYSTALLIZATION	773 K	

TIME (Hours)	MEAN TENSILE STRENGTH (MN/m^2)	STANDARD DEVIATION OF STRENGTH	95% CONFIDENCE LIMITS OF THE MEAN	WEIBULL MODULUS
0	1264	361	103	3.7
0.25	1200	336	95	
0.5	935	253	72	4.1
1.0	733	183	67	
1.5	612	153	43	4.9
2.0	589	153	43	
2.5	600	162	46	5.2
3.0	654	170	48	
5.0	737	206	58	3.9 5.3
10	474	133	38	3.7 5.4

GLASS B	TEMPERATURE	CONDITION:
NUCLEATION	763 K	
CRYSTALLIZATION	798 K	

TIME (Hours)	MEAN TENSILE STRENGTH (MN/m^2)	STANDARD DEVIATION OF STRENGTH	95% CONFIDENCE LIMITS OF THE MEAN	WEIBULL MODULUS
0	1264	361	103	3.7
0.25	883	238	68	
0.5	510	127	36	3.7 6.0
1.0	512	133	38	
1.5	577	161	46	3.7 5.9
2.0	633	165	47	
2.5	730	197	56	5.3
3.0	780	203	58	
5.0	640	166	47	5.3
10	374	97	27	5.8

GLASS B	TEMPERATURE	CONDITION:
NUCLEATION	763 K	
CRYSTALLIZATION	823 K	

TIME (Hours)	MEAN TENSILE STRENGTH (MN/m^2)	STANDARD DEVIATION OF STRENGTH	95% CONFIDENCE LIMITS OF THE MEAN	WEIBULL MODULUS
0	1264	361	102	3.7
0.25	676	183	52	
0.5	527	132	38	3.7 5.8
1.0	597	161	46	
1.5	690	186	53	3.7 6.0
2.0	718	201	57	
2.5	611	165	47	5.0
3.0	523	146	42	
5.0	391	113	32	4.8
10	332	90	26	4.6

GLASS B	TEMPERATURE	CONDITION:
NUCLEATION	763 K	
CRYSTALLIZATION	873 K	

TIME (Hours)	MEAN TENSILE STRENGTH (MN/m^2)	STANDARD DEVIATION OF STRENGTH	95% CONFIDENCE LIMITS OF THE MEAN	WEIBULL MODULUS
0	1264	361	102	3.7
0.25	733	198	56	
0.5	603	169	48	3.5 4.0
1.0	521	146	42	
1.5	430	112	32	3.7 5.4
2.0	402	109	31	
2.5	393	110	31	3.7 4.6
3.0	380	110	31	
5.0	317	95	27	4.1
10	280	81	23	4.4

GLASS B	TEMPERATURE	CONDITION:
NUCLEATION	753 K	
CRYSTALLIZATION	798 K	

TIME (Hours)	MEAN TENSILE STRENGTH (MN/m^2)	STANDARD DEVIATION OF STRENGTH	95% CONFIDENCE LIMITS OF THE MEAN	WEIBULL MODULUS
0	1264	361	102	3.7
0.25	896	242	69	
0.5	497	139	40	3.7 5.0
1.0	499	140	40	
1.5	531	143	41	3.6 5.2
2.0	593	148	42	
2.5	602	150	43	3.7 5.7
3.0	664	173	49	
5.0	601	156	44	3.9 5.7
10	353	121	34	4.6

GLASS B	TEMPERATURE	CONDITION:
NUCLEATION	773 K	
CRYSTALLIZATION	798 K	

TIME (Hours)	MEAN TENSILE STRENGTH (MN/m^2)	STANDARD DEVIATION OF STRENGTH	95% CONFIDENCE LIMITS OF THE MEAN	WEIBULL MODULUS
0	1264	361	102	3.7
0.25	871	253	72	
0.5	502	141	40	3.9 6.0
1.0	521	146	42	
1.5	606	158	45	3.8 5.8
2.0	713	193	55	
2.5	629	176	50	3.8 5.7
3.0	603	175	50	
5.0	428	120	34	4.6
10	361	105	30	3.8

GLASS B	TEMPERATURE	CONDITION:
NUCLEATION	763 K	Mean fibre diameter = 32.1 μm
CRYSTALLIZATION	798 K	

TIME (Hours)	MEAN TENSILE STRENGTH (MN/m^2)	STANDARD DEVIATION OF STRENGTH	95% CONFIDENCE LIMITS OF THE MEAN	WEIBULL MODULUS
0	1264	361	103	
0.25	398	251	71	
0.5	507	132	38	
1.0	499	135	38	
1.5	564	148	42	
2.0	628	176	50	
2.5	727	196	56	
3.0	768	207	59	
5.0	628	170	48	
10	372	104	30	

GLASS B	TEMPERATURE	CONDITION:
NUCLEATION	763 K	Ion exchanged in KCl/argon gas at a flow rate of 400 litres per hour. Fibres exposed to the vapour for 30 minutes.
CRYSTALLIZATION	798 K	

TIME (Hours)	MEAN TENSILE STRENGTH (MN/m^2)	STANDARD DEVIATION OF STRENGTH	95% CONFIDENCE LIMITS OF THE MEAN	WEIBULL MODULUS
0	1264	361	103	3.7
0.25	901	243	69	
0.5	530	143	41	3.4
1.0	495	134	38	
1.5	558	145	41	3.9
2.0	661	172	49	
2.5	771	193	55	4.6
3.0	840	218	62	
5.0	825	206	59	5.6
10	582	146	42	5.7

ELASTIC MODULUS OF FIBRES

GLASS A

*Denotes fibres too fragile to test

TIME (MINUTES)		0	20	40	60	120	360
N = 743 K C = 773 K	Modulus of Elasticity (GN/m^2)	70.4	79.2	83.7	89.9	98.2	101.9
N= 743 K C = 798 K	(GN/m^2)	70.4	87.7	96.5	99.1	101.4	100.8
N = 743 K C = 823 K	(GN/m^2)	70.4	97.6	103.0	*	*	*
N = 753 K C = 773 K	(GN/m^2)	70.4	81.3	85.6	92.7	101.1	*
N = 753 K C = 798 K	(GN/m^2)	70.4	83.9	98.1	102.8	*	*
N = 753 K C = 823 K	(GN/m^2)	70.4	93.7	100.3	*	*	*

N = Nucleation temperature

C = Crystallization temperature

ELASTIC MODULUS OF FIBRES

GLASS A

*Denotes fibres too fragile to test

TIME (MINUTES)		0	20	40	60	120	360
N = 763 K C = 773 K	Modulus of Elasticity (GN/m^2)	70.4	78.1	88.8	97.6	*	*
N= 763 K C = 798 K	(GN/m^2)	70.4	81.2	91.4	102.9	*	*
N = 763 K C = 823 K	(GN/m^2)	70.4	85.5	*	*	*	*
N = K C = K	(GN/m^2)						
N = K C = K	(GN/m^2)						
N = K C = K	(GN/m^2)						

N = Nucleation temperature

C = Crystallization temperature

ELASTIC MODULUS OF FIBRES

GLASS B

TIME (HOURS)		0	0.25	0.5	1.5	3.0	10.0
N = 763 K C = 773 K	Modulus of Elasticity (GN/m^2)	63.6	62.9	64.1	64.9	72.6	88.4
N = 763 K C = 798 K	(GN/m^2)	63.6	64.3	64.4	74.5	87.0	92.2
N = 763 K C = 823 K	(GN/m^2)	63.6	68.6	77.9	91.1	94.6	97.6
N = 763 K C = 873 K	(GN/m^2)	63.6	79.6	87.9	94.8	95.1	96.3
N = 763 K* G = 798 K	(GN/m^2)	63.6	65	64.5	69.8	84.3	89.1

N = Nucleation temperature

C = Crystallization temperature

*Glass B fibres after ion exchange.
Argon flow = 400 l/h. Exchanged for 30 mins.

APPENDIX III

The general equation for diffusion is given by

$$\frac{\partial c}{\partial t} = \frac{\partial}{\partial x} \left(D(c) \frac{\partial c}{\partial x} \right) \qquad (1)$$

where c = concentration

x = diffusion coefficient

t = time

$D(c)$ = concentration dependent diffusion coefficient

This reduces to the following equation when the system has radial symmetry:

$$\frac{\partial c}{\partial t} = \frac{1}{r} \frac{\partial}{\partial r} (D(c)\, r \frac{\partial c}{\partial r}) \qquad (2)$$

$$= \frac{1}{r} D \frac{\partial c}{\partial r} + r D \frac{\partial^2 c}{\partial r^2} + r \frac{\partial c}{\partial r} \frac{\partial D}{\partial r} \qquad (3)$$

Now $D = D(c)$

$c = c(r,t)$

$\therefore \frac{\partial D}{\partial r} = \frac{\partial c}{\partial r} D'(c)$ where ' denotes differentiation with respect to c.

$$\therefore \frac{\partial c}{\partial t} = \frac{D}{r} \frac{c}{r} + D \frac{\partial^2 c}{\partial r^2} + \frac{\partial c}{\partial r} \frac{D}{r} \qquad (4)$$

Now at $r = 0$ $\frac{\partial c}{\partial r} = 0$,

and near $r = 0$ $\frac{\partial c}{\partial r} = (\frac{\partial c}{\partial r})_o + (\frac{\partial^2 c}{\partial r^2})_o + \ldots\ldots$

$$\therefore \frac{1}{r} \frac{\partial c}{\partial r} = (\frac{\partial^2 c}{\partial r^2})_o + \frac{r}{2} (\frac{\partial^2 c}{\partial r^2})_o$$

as $r \to 0$, $\frac{1}{r} \frac{\partial c}{\partial r} \to (\frac{\partial^2 c}{\partial r^2})_o$

at $r = 0$ equation (3) becomes:

$$\frac{\partial c}{\partial t} = 2 D \frac{\partial^2 c}{\partial r^2} \qquad (5)$$

The solution to the diffusion equation was attempted by the use of a finite difference approximation where all partial derivatives were replaced by difference approximations and equations were written down at nodal positions across the fibre. The numerical method used was the "predictor,corrector method" for non-linear parabolic equations developed by Douglas and Jones[75]. A predictor formula advances the solution from t = nk to t = $(n + \frac{1}{2})k$ where k represents a time step and is assigned a value appropriate to the physical process. After this step a correction formula advances the solution from t = $(n + \frac{1}{2})k$ to $(n + 1)k$. The fibre was divided into nodal points radially such that :

$$r + ih, \quad h = \frac{a}{m}$$

The predictor formula denoting $C_L^n = c(ih,nk)$ was derived using the following equations:

$$\frac{\partial c}{\partial t} = \frac{C_L^{n+\frac{1}{2}} - C_L^n}{(k/2)}$$

$$\frac{\partial c}{\partial r} = \frac{C_{L+1}^n - C_{L-1}^n}{2h}$$

$$\frac{\partial^2 c}{\partial r^2} = \frac{1}{h^2}\left(C_{L+1}^n - 2C_L^n + C_{L-1}^n \right)$$

These equations are substituted into (4) and (5) thus generating a set of linear algebraic equations. Applying the same reasoning a similar set of equations was derived for the corrector formula. Both were sets of tri-diagonal equations which were solved for:

$$C_0^{n+1}, \quad C_1^{n+1} \quad \ldots\ldots\ldots\ldots \quad C_{m-1}^{n+1}$$

For computational purposes the equations and diffusion coefficient were expressed in non-dimensional form:

$$r = aR$$

$$t = \frac{Ta^2}{D_{max}}$$

$$D = D_{max} \cdot d$$

where R , T are the non-dimensional radius and time and D is the non-dimensional diffusion coefficient. D_{max} is the maximum diffusion coefficient and d,a are constants. A procedure for checking the programme was to make D a constant and calculate a diffusion profile assuming constant surface concentration c_i. The results were compared with solutions given in Crank[57] pages 66,67 and a good agreement was found for this simple case.

1 492 527

PATENT SPECIFICATION

(11) 1 492 527

(21) Application No. 53270/73 (22) Filed 16 Nov. 1973
(23) Complete Specification filed 13 Nov. 1974
(44) Complete Specification published 23 Nov. 1977
(51) INT CL² C03C 21/00
(52) Index at acceptance
C1M 13E 13J 13N 13P3 13S1 13S2A D15B1 D15C D27 S9A4

(72) Inventors RONALD WILLIAM JONES and PETER WILLIAM McMILLAN

(19)

(54) GLASS CERAMIC FIBRES

(71) We, NATIONAL RESEARCH DEVELOPMENT CORPORATION, a British Corporation established by Statute, of Kingsgate House, 66—74 Victoria Street, London, S.W.1., do hereby declare the invention for which we pray that a patent may be granted to us, and the method by which it is to be performed, to be particularly described in and by the following statement:—

This invention relates to glass ceramic fibres and methods for the production thereof.

Glass fibres have found application for some years as a reinforcing and insulating material. When incorporated into certain low modulus metals and alloys however many of the glasses fail to substantially reduce the creep associated with these materials because of the low modulus of elasticity of the fibre. Attempts to produce an improvement in elastic modulus by devitrification of glass fibre have hitherto resulted only in fibres which are too fragile to provide satisfactory reinforcement.

We have now found that glass ceramic fibres can be produced which have satisfactory strength properties.

According to the present invention there is provided a glass ceramic fibre of a diameter no greater than 50 microns having a microcrystalline interior and an amorphous outer surface layer no greater than 500A in thickness; the glass ceramic fibre containing a first alkali metal ion whose concentration increases smoothly from said layer to said interior, and a second alkali metal ion so distributed that the ratio (total alkali metal ion)/(silica) is constant from said layer to said interior.

A glass ceramic fibre according to the present invention may be produced by replacing alkali metal ions in the outer surface layer of a homogeneous vitreous fibre by a different alkali metal ion so that the concentration of said different alkali metal decreases smoothly from said layer into the interior, and applying a divitrification treatment effective in the interior but not effective in the outer surface layer.

The higher "different" alkali metal composition at the surface layer is effective to raise the resistance to devitrification of said layer relative to the resistance of said interior.

Vitreous fibres i.e. parent vitreous fibres, prior to surface modification, usually have a uniform composition at the surface and interior. Parent vitreous fibres may be prepared from a wide range of glass compositions, and preferably nucleate readily without requiring a heterogeneous nucleating agent. In practice compositions contain silica in addition to one or more alkali metal oxides and may also contain other substances such as phosphorus pentoxide and zinc oxide. In general one alkali metal oxide, typically lithium oxide, predominates in the composition of the vitreous bodies.

Parent vitreous fibres may be formed from a homogeneous melt of the constituent oxides, for example, by drawing the melt through a suitable bushing.

Surface modification of a parent vitreous fibre to produce a surface modified vitreous fibre according to the present invention may be effected by methods in which the surface of the parent fibre is treated with an alkali metal compound under conditions such that ion exchange takes place and ions of a different alkali metal at the surface of the body are replaced wholly, or preferably partly, by ions of the alkali metal from the compound. In general the alkali metal which is replaced predominates in the parent vitreous fibre and clearly the concentration ratio of the replaced species metal to the replacing metal is lower in the surface layer than in the interior of the body by this surface modification. Because the concentration ratio of the different alkali metal pound is used in a melt, to elude a small ions is closer to unity in the surface layer than in the interior said layer is relatively resistant to devitrification and is preferably very resistant. Although it is preferable for only part of the alkali metal in the surface layer to be replaced, the concentration ratio of the two most significant ions in the surface layer ideally being unity (and typically within 20% of unity), total replacement is generally toler-

able provided of course that the ratio increases from the surface to the interior. In the latter case there will then be a region between the surface and the interior in which no alkali metal ion is predominant and which therefore resists devitrification. Although the concentration ratio of different alkali metal ions increases from the surface to the interior, the proportion of total alkali metal ions to silica remains constant.

If so desired, replacement may be effected by treating the surface of the fibre with a melt comprising an alkali metal compound so that ion exchange takes place, for example between lithium in the fibre and a potassium compound such as potassium nitrate. Where a melt is employed the fibre may be immersed therein. After treatment the residual alkali metal compound is washed off. It may be desirable particularly when a potassium compound is used in a melt, to include a small amount of lithium nitrate therein, to increase the rate of ion exchange. Alternatively, the fibre may be subjected to ion exchange treatment by an alkali metal compound e.g. potassium nitrate in the vapour phase e.g. in an inert gas such as argon. It will be appreciated that the selection of the metal which is to enter the surface of the parent vitreous fibre is dependent on the need for the resultant composition of the surface of the fibre to resist devitrification.

The ion exchange treatment is generally conducted close to the annealing point (usually within 20°C) of the surface modified vitreous body although higher temperatures may be employed in some cases. In general it is undesirable for the temperature at which maximum crystal growth occurs in the final surface to be reached or undue crystallization may take place therein.

As it will be appreciated, the treatments hereinbefore described impart resistance to crystallization in the surface of the parent vitreous fibre so that during subsequent devitrification the interior crystallizes while the surface layer remains relatively amorphous. It is believed that the properties of the glass ceramic fibre result from inhibition of crystal growth from the exterior towards the interior of the fibre. The surface layer of modified composition is preferably made as thin as possible so that the mechanical properties of the devitrified product are not thereby affected adversely, and must be no thicker than 500Å. It will be appreciated that after modification the surface layer is continuous with the interior of the fibre, there being no interface—because the composition changes smoothly—between the interior and said layer.

The composition in the surface layer is generally such that when, on devitrification, the rate of crystal growth in the interior is a maximum, the rate of crystal growth in the surface layer is at least an order of magnitude less than said maximum rate. The rate differential is usually much greater than this however, and the rate of crystal growth at the surface is preferably substantially zero. As the surface layer is 500Å or less in thickness, the volume fraction of crystallinity in the microcrystalline product is usually lower by a factor at least 10^3 in the surface layer than in the interior.

Devitrification of a surface modified vitroeus fibre may be effected by a two part heat treatment during the first and second stages of which nucleation and crystal growth are respectively promoted. The microcrystalline product may have a practical working strength 60% or more of the strength of the parent vitreous fibre. Generally the stength is at least 60,000 p.s.i. The modulus of elasticity of the product is in general greater than that of the parent vitreous fibre from which it is derived and is typically at least 14×10^6.

As hereinbefore indicated the glass ceramic fibre may be incorporated into low modulus materials such as metals and alloys, particularly in copper, aluminium, tin, lead, zinc and alloys based thereon, for example Babitts metal, to reduce the rate of creep. It is of particular interest as a reinforcing material for bearings. The vitrified product may also be employed as a reinforcement to other matrices such as polymers, ceramics, plastics, cement and gypsum plaster.

The devitrified fibres can also be employed as an insulating material.

The invention is illustrated by the following Examples:—

Example 1

Glass-Ceramic Fibre

A glass batch of mole percentage composition 29 Li_2O 68 SiO_2 1 ZnO 1 K_2O 1 P_2O_5 is prepared by grinding the ingredients (reagent grade) until the mixture passes through a sieve of British Standard mesh size 36.

This batch is then fired in a platinum crucible in air at 1450°C for 4 hours. It is then poured into cold water, crushed and remelted for a further 4 hours to homogenize the glass. The glass is again poured into iced water and the product crushed. The crushed glass is then transferred to a single-tip platinum bushing, the glass is remelted and glass fibre drawn at 450 r.p.m. on to a 10" diameter drum. The average diameter of the fibres as measured by optical microscopy is 32 μm.

Specimens of the glass fibre are then subjected to the following heat treatments.

A. Devitrification:

In order to produce glass ceramic fibres the properties of which can be compared with those of glass ceramic fibres according to the present invention, the above glass fibres are

subjected to a heat treatment in air by raising the temperature to 490°C and holding at this temperature for 1 hour and then further raising the temperature to 525°C and holding for 10 hours. Thereafter the fibres are cooled at the natural cooling rate of the furnace.

B. Surface Modification and Devitrification:

In order to produce glass ceramic fibres according to the present invention, the above glass fibres are subjected to a heat treatment in an atmosphere in which argon gas carries a saturated vapour of potassium nitrate over the fibres. The gas is passed over potassium nitrate which is contained in a boat and heated to 400 to 420°C. The fibres are maintained near to the potassium nitrate and maintained at a temperature close to the annealing point, which in this case is 400°C. The gas is passed over the fibres for thirty minutes at a rate of 400 litres per hour. The fibres are then subjected to the devitrifying heat treatment A. This treatment is carried out in the apparatus previously used for atmospheric treatment and the fibres are thus taken to 490°C directly after the KNO_3 vapour treatment and finally crystallized by treatment at 525°C. All fibres are cooled to room temperature at the natural cooling rate of the furnace. The fibres produced by treatments A and B are tested and the following results obtained.

(i) Mechanical strength of glass ceramic fibres produced by treatment A is in the range 47,000 p.s.i. to 100,000 p.s.i.; the mean is 54,000 p.s.i. and standard deviation 17,500 p.s.i. (estimated on a sample of 37 fibres).

(ii) Mechanical strength of glass ceramic fibres produced by treatment B is in the range 49,000 p.s.i. to 115,000 p.s.i.; the mean 87,000 p.s.i. The standard deviation is 22,000 p.s.i. (estimated on a sample of 41 fibres).

(iii) The modulus of elasticity of glass fibres prior to heat treatment is 11×10^6 p.s.i. After heat treatment A the modulus of the glass ceramic fibres is 14×10^6 p.s.i. and after treatment B the modulus of the glass ceramic fibres is 14.5×10^6 p.s.i.

The change in relative concentration of alkali metals in glass ceramic fibre produced by treatment B is determined by Flame Photometry in the following manner:—

Fibres are immersed in 1% hydrofluoric acid/water solution and slowly dissolved therein at a constant rate. By taking aliquots of the solution at intervals of time and spraying the solution into a gas flame spectra are obtained for the potassium ions measurement of the intensity of which spectra enables the concentration of lithium and potassium at different distances from the surfaces of the fibres to be determined. The intensity of the spectra is compared with the intensity obtained with standard solutions of varying potassium ion concentration. The results obtained are set out in the Table.

TABLE

Distance into the fibre from the surface (μm)	Li:K ratio
0.1	1:1
0.8	2:1
1.6	5:1
3	10:1

If desired, the relative concentration of the alkali metals may be determined by a Radioactive Tracer technique as follows:—

The fibres are first irradiated in a reactor in order to produce the radioactive isotope of potassium therein i.e. K_{42}. The fibres are then immersed in 2% hydrofluoric acid/water solution. The dissolution rate of glass fibres at this concentration of acid is almost linear with time and fibres dissolve at a rate of 0.8 m per minute. By taking aliquots at varying time intervals it is possible to measure the concentration of potassium ions at various points within the fibre. This is done by monitoring and analysing the radiation emitted by the K_{42} ions in the aliquots of solution. This gives a concentration profile from which the ratio of K^+ to Li^+ can be calculated for any distance from the fibre surface towards its centre.

Example 2

Glass Ceramic Fibre/Tin Composite

A composite is prepared by infiltration with tin of a bundle of fibres held in a mould under vacuum. The mould is immersed in molten tin and a positive gas pressure (20 p.s.i.) of argon or nitrogen is applied over the tin. The molten metal is forced into the mould and infiltrates the fibres. Prior to insertion of the fibres into the mould, they were plated with tin to increase the degree of wetting of the fibres by the molten tin. The composite has a strength 3.6 tons per square inch, 50% greater than the strength of the unreinforced metal.

Example 3

Glass Ceramic Fibre/Tin Composite

Fibres are first plated with silver by an electroless deposition method in order to make them electrically conducting. They are then electroplated with tin from an alkaline bath comprising potassium stannate after which the coated fibres are hot pressed to compact and produce a composite. The volume fraction of fibre to tin can be varied by controlling the thickness of tin coating. Compaction is con-

ducted in a die at a pressure of 4—5 tons per square inch and at a temperature close to the liquidus temperature of tin.

WHAT WE CLAIM IS:—

1. A glass ceramic fibre of a diameter no greater than 50 microns having a microcrystalline interior and an amorphous outer surface layer no greater than 500Å in thickness; the glass ceramic fibre containing a first alkali metal ion whose concentration increases smoothly from said layer to said interior, and a second alkali metal ion so distributed that the ratio (total alkali metal ion)/(silica) is constant from said layer to said interior.

2. A glass ceramic fibre as claimed in Claim 1, in which said first alkali metal ion is lithium ion.

3. A glass ceramic fibre as claimed in either of the preceding claims, in which said second alkali metal ion is potassium ion.

4. A glass ceramic fibre as claimed in any preceding claim, wherein the ratio of the concentrations of the first and the second alkali metal ions in the surface layer is within 20% of unity.

5. A glass ceramic fibre as claimed in Claim 1 and substantially as hereinbefore described with reference to Example 1.

6. A method of making a glass ceramic fibre as claimed in any preceding claim, comprising replacing the alkali metal ions in the outer surface layer of a homogeneous vitreous fibre by a different alkali metal ion so that the concentration of said different alkali metal decreases smoothly from said layer to the interior, and applying a divitrification treatment effective in the interior but not effective in the outer surface layer.

7. A method as claimed in Claim 6, in which the replacement step comprises treating the fibre with a melt comprising a compound of the different alkali metal.

8. A method as claimed in Claim 6, in which the replacement step comprises treating the fibre with a vapour comprising a compound of the different alkali metal.

9. A method as claimed in any of Claims 6 to 8, in which during the replacement step the fibre is maintained at a temperature within 20°C of the annealing point.

10. A method as claimed in Claim 6 and substantially as hereinbefore described with reference to Example 1.

11. A glass ceramic fibre made by a method as claimed in any of Claims 6 to 10.

12. A composite material comprising glass ceramic fibres as claimed in any of Claims 1 to 5 or 11.

13. A composite material as claimed in Claim 12, further comprising a metal, alloy, ceramic, plastic material, cement or plaster.

14. A bearing of a composite material as claimed in Claim 13 and comprising a metallic material.

15. A composite material as claimed in Claim 12 and substantially as described in any one of Examples 2 and 3.

16. A method of making a composite material as claimed in any of Claims 12 to 15, the method being substantially as hereinbefore described with reference to Example 2 or Example 3.

17. A composite material made by a method as claimed in Claim 16.

R. S. CRESPI,
Chartered Patent Agent,
Agent for the Applicants.

Printed for Her Majesty's Stationery Office, by the Courier Press, Leamington Spa, 1977
Published by The Patent Office, 25 Southampton Buildings, London, WC2A 1AY, from which copies may be obtained.